Optical Control of "*All Visible*" Fluoroazobenzene-Containing Architectures: From Small Molecules to 3D Networks

DISSERTATION

zur Erlangung des akademischen Grades
doctor rerum naturalium
(Dr. rer. nat.)
im Fach Chemie

eingereicht an der
Mathematisch-Naturwissenschaftlichen Fakultät
der Humboldt-Universität zu Berlin

von
M. Sc. Fangli Zhao

Präsidentin der Humboldt-Universität zu Berlin
Prof. Dr.-Ing. Dr. Sabine Kunst

Dekan der Mathematisch-Naturwissenschaftlichen Fakultät
Prof. Dr. Elmar Kulke

Gutachter/innen: 1. Prof. Dr. Stefan Hecht
2. Prof. Dr. Matthias Ballauff

Tag der mündlichen Prüfung: 13. 02. 2018

Die vorliegende Arbeit wurde in der Zeit von Dez 2013 bis März 2017 am Institut für Chemie der Humboldt-Universität zu Berlin unter der Anleitung von Prof. Stefan Hecht, Ph.D. angefertigt..

Acknowledgement

I would like to express my gratitude here to some people for their help throughout the time of my PhD study. Firstly, I would like to give my special and sincere thanks of gratitude to Dr. David Bléger and Professor Stefan Hecht who have been always supportive of my research goals and helped me in matters of knowledge and technology to pursuit these goals. I am especially indebted to Dr. David Bléger, my supervisor and mentor, he has provided me extensive personal and professional guidance during the whole time of my studies as well as during the completion of this thesis and taught me a lot about both scientific research and life in general! I would also like to thank Prof. Stefan Hecht for his support and guidance in all stages of my studies. He has shown me, by his broad knowledge, skills and especially his enthusiasm for science, how a good scientist should be.

Special thanks to Dr. Lutz Grubert for his contribution to the first project (*i.e.* electrochemical experiments in section 3). I would also like to acknowledge Dr. Aurelio Bonasera and Dr. Ulrich Noechel (Helmholtz-Zentrum Geesthacht Zentrum für Material- und Küstenforschung) for their technical help for the hydrogel project.

I am thankful to all members of the 'Hecht group' with whom I have had the pleasure to work during my studies. Specifically I would like to mention my lab mate Christopher Knie for translating the abstract of the thesis into German as well as my 'lunch group' members: Sebastian Fredrich, Dr. Aurelio Bonasera, Dr. Dennis Chung-Yang Huang and Dr. Virginia Valderrey for their suggestions for the thesis and the joy we have had in the past years. I am also very grateful to Ms. Daniela Voigtländer and Ms. Claudia Rothkirch for their kind help in administrative events.

A very special gratitude goes to the Deutsche Forschungsgemeinschaft (DFG) for providing the funding: this work would not have been possible without its financial support.

Nobody has been more important to me in the pursuit of my studies than members of my family. I would like to thank my parents, brothers and sister, whose love and support are always with me in whatever I pursue. Last but by no means least, I wish to thank my loving and supportive partner, Janko Weßlowsky, for his love, understanding, encouragement and hard German lesson during the completion of this thesis, particularly for the time in Germany.

It is really great sharing the time with him!

Abstract

Ortho-fluoroazobenzenes represent one of the most interesting family of visible-light-responsive azobenzenes. Since the first report by our group in 2012, they have been intensively studied at the molecular level, for biological applications, and in bulk materials, due to their outstanding photo/electrochemical properties. Typically, *ortho*-fluorinated azobenzenes can isomerize in both directions using visible light with high photo-conversions, and the *Z*-isomers exhibit superior thermal half-lives (up to 2 years).

In this work, two projects based on our recently acquired knowledge of fluorinated azobenzenes are presented. First, exploiting complementary absorption profiles and ease of electrochemical isomerization, a mixed azobenzene dimer, whose four isomers can be orthogonally addressed was prepared. It was investigated from its photo-isomerization, thermal relaxation, and electrochemical isomerization aspects. Second, we prepared a photo-responsive hydrogel via covalently cross-linking a poly(ethylene glycol) (PEG)-based precursor with a fluorinated azobenzene forming a 3D polymer network. As a result, the gel's mechanical properties could be tuned reversibly due to the azobenzenes' isomerization triggered by visible light irradiation.

Kurzzusammenfassung

Ortho-Fluorazobenzole stellen eine der interessantesten Familien von Azobenzolen dar, die mit sichtbarem Licht geschaltet werden können. Seit ihrer ersten Erwähnung durch unsere Gruppe im Jahr 2012 wurden sie aufgrund ihrer hervorragenden photo/elektrochemischen Eigenschaften intensiv auf molekularer Ebene, für biologische Anwendungen und in Volumenmaterialien untersucht. Typischerweise können *ortho*-fluorierte Azobenzole in beide Richtungen mit sichtbarem Licht und hohem Photoumsatz geschaltet werden. Außerdem weisen die *Z*-Isomere überlegene thermische Halbwertszeiten (bis zu 2 Jahre) auf.

In dieser Arbeit werden zwei Projekte vorgestellt, die auf unseren kürzlich erworbenen Kenntnissen über fluorierte Azobenzole basieren. Zunächst wurde ein gemischtes Azobenzoldimer dargestellt, welches komplementäre Absorptionsprofile sowie die leichte elektrochemische Isomerisierung ausnutzt und dadurch dessen vier Schaltzustände orthogonal adressiert werden können. Dieses wurde bezüglich seiner Photoisomerisierung, thermischen Relaxation und seines elektrochemischen Schaltverhaltens untersucht. Anschließend haben wir ein 3D-Polymernetzwerk durch kovalente Vernetzung einer polyethylenglykol(PEG)-basierten Vorstufe mit einem fluorierten Azobenzol hergestellt, was zur Bildung eines photoempfindlichen Hydrogels führte. Als Folge davon konnten die mechanischen Eigenschaften des Gels durch Bestrahlung mit sichtbarem Licht und der dadurch ausgelösten Azobenzol-Isomerisierung reversibel beeinflusst werden.

Table of Contents

1. Introduction

In nature, plenty of materials and systems have the ability to reversibly adjust their structures and properties in response to environmental stimuli. This includes for example mimosa pudica, which defend themselves by folding leaves inward when touched or shaken,[1] and also chameleons, which are capable of changing their skin colors for camouflage, socializing signaling, and in reactions to temperature and other conditions. Other examples include the catalytic action of enzymes that can be altered by temperature and pH,[2] heat-shock response in bacteria,[3] and many more. These exotic phenomena from nature inspire and promote researchers to develop and explore man-made molecular systems which can be switched "on" and "off" at will with external stimuli for specific uses.

Comparing with many other forms of external inputs that can influence the properties of molecular systems and materials, light as a clean, abundant and energy-efficient power source, is of significant interest to scientists, as it can be utilized in a remote manner and offers precise control over wavelength, intensity, as well as duration. For all these reasons, light has been widely used as a driving force in life sciences[4,5] and materials science.[6] Among different class of photo-responsive compounds, photochromic molecules (also referred to as photoswitches), which undergo reversible switching between two or more states with the stimulation of light, have shown their great advantages. In most cases, they switch from a stable state to a metastable state under irradiation with ultraviolet (UV) light, and convert back to the original state either thermally or irradiation with visible light. The two isomers often differ dramatically in many properties, such as absorption spectra, redox potentials, end-to-end distances, emissive behaviors, and dipole moments.

Among several well-established photoswitches,[7–9] azobenzenes are one of the most popular members. They have relatively high quantum yields of isomerization allowing them to reversibly isomerize over many cycles upon exposure to light of appropriate wavelength. The *E*/*Z* isomerization results in significant structural, chemical, and physical changes between the *E* and *Z* isomers, making it a component of choice for numerous molecular devices[10–12] and functional materials.[13–15] Although a large number of azobenzenes have been explored for diverse applications, there are still inevitable drawbacks that limit their use

for certain purposes. For example, the $E \longrightarrow Z$ isomerization often relies on UV light, which could limit its biocompatibility. Besides, the photoconversions are typically incomplete in both directions due to the overlapping absorption bands. Also, *Z* isomers often show limited thermal stability. In order to overcome these limitations, considerable work towards developing advanced azobenzenes has been carried out.[16] In particular, the development of (thermally) bi-stable azobenzene, whose $n \longrightarrow \pi^*$ bands of both *E* and *Z* isomers are separated in the visible region, has gained significant attention.[17–22]

In this context, our group[22,23] has prepared remarkable *ortho*-fluoroazobenzenes that show distinct $n \longrightarrow \pi^*$ absorption bands of *E* and *Z* isomers in the visible region. Thereby isomerization, which is addressed by visible light only, can be achieved in both directions with near quantitative photoconversions. Importantly, the *Z* isomers display superior thermal half-lives (up to 2 years at room temperature in solution). Our recent investigation of electrochemical reductive isomerization of *Z*-fluoroazobenzenes[24] (see section 2) offers another efficient pathway to activate the isomerization process, further increasing the opportunity of fluoroazobenzenes, in particular for applications where orthogonal activation modes are necessary. Thus far, a wide variety of applications based on the fluorinated azobenzene moiety has been reported by us[25,26] and others.[27–30]

In the present work, based on the recently revealed properties of fluoroazobenzenes we explored new applications by incorporating *ortho*-fluoroazobenzenes into more complex molecular systems and materials. Inspired by the current interest in the fabrication of "smart" materials able to perform specific tasks or complex work on demand, we first developed multi-state switches by connecting *ortho*-tetrafluoroazobenzenes (F4-azo) with parent azobenzenes via proper design (see section 3), in which all the individual states can be selectively addressed using orthogonal inputs.

Secondly, we prepared polymeric networks by incorporating F4-azo derivatives into a PEG-based hydrogels via "click" chemistry (see section 4). In this work, the elastic moduli of the gels were measured and evaluated. The mechanical property of the resulting hydrogels, which is a key parameter especially when hydrogels are used as biomedical materials, can be tuned reversibly upon exposure to green and blue light, *i.e.* without the use of damaging UV light. The thermal dynamic properties of F4-azos within the polymeric networks were

also investigated.

In order to fully understand the work presented above, readers will be guided in the following section first with an introduction of relevant theoretical background of azobenzenes, especially fluoroazobenzenes, as well as hydrogels.

2. Theoretical background

2.1 Azobenzene

2.1.1 General properties of azobenzenes

Since Hartley discovered *Z*-azobenzene in 1937,[31] considerable work has placed azobenzenes among the best characterized photoswitches. Azobenzenes can be readily synthesized and the photo-switching properties are easily modified by altering substituent patterns. Light-induced *E*/*Z* isomerization events occur with relatively high quantum yields and minimal photo-bleaching. In general, the *E* form with a near linear conformation is the thermally stable state, which can switch to the metastable *Z* form upon UV irradiation (see Fig. 2.1).[32] The *Z* form adopts a bent conformation with the two phenyl rings twisted out of plane around 56° relative to the azo group,[33] and it can revert to *E* form thermally or after visible-light irradiation. The *E* form has a near zero dipole moment, while the *Z* form has a dipole moment of 3 Debye. Additionally, the end-to-end distance of each isomer, *i.e.* the distance between the carbons at the *para* positions of the phenyl rings, is also quite different (9 vs 5.5 Å).[34] The absorption spectrum of *E* form shows an intensive band in the UV region around 320 nm due to the $\pi \longrightarrow \pi^*$ transition, and a weak band in the visible region around 440 nm resulting from the $n \longrightarrow \pi^*$ transition. On the other hand, the *Z* form has a more intense $n \longrightarrow \pi^*$ band (also near 440 nm), and a blue-shifted $\pi \longrightarrow \pi^*$ band at 280 nm. The photo-isomerization and the resulting dramatic structural, physical and chemical changes enable its use as a photoswitch, especially in biomolecules to control biological environments[35,36] and in supramolecular materials to convert light into mechanical energy.[37,38]

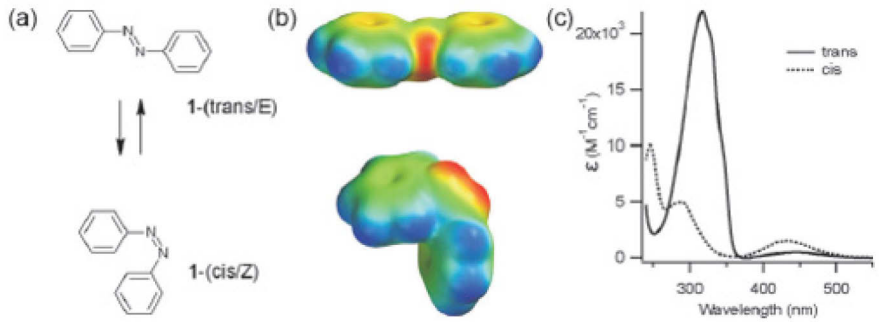

Fig. 2.1 (a) and (b) Structures of *E* and *Z* isomers of azobenzene. Space filling models are colored by electrostatic potential (red - negative to blue - positive). (c) Electronic absorption spectra of the *E* and *Z* isomers of azobenzene dissolved in ethanol.[32]

As stated in the introduction, azobenzenes also exhibit some considerable drawbacks. First of all, the absorption spectra of *E*- and *Z*-azobenzene are substantially overlapping, as a consequence incomplete photo-switching is observed and irradiation produces a photostationary state (PSS) in common azobenzenes with 80% for the $E \longrightarrow Z$ isomerization and 70% for the $Z \longrightarrow E$ isomerization.[39] This drawback can be amplified in some systems, where the remaining *E*-isomer still dominates the properties of the material, resulting in undesired effects. Secondly, UV light is often needed to trigger the $E \longrightarrow Z$ isomerization, which is especially not desirable for in *vivo* manipulation where cells and tissues could be harmed. Longer wavelengths of light (ideally between 650 nm and 950 nm, the so-called "biological window") may be preferable, which can penetrate cells and tissues more easily.[40] Furthermore, thermal $Z \longrightarrow E$ relaxation can occur completely in short time producing 100% of *E*-isomer, which in some cases may not be desired. For example, in the context of photo-controlling biomolecules, continuous irradiation with high dosage of light would be needed to compete the thermal relaxation.

2.1.2 Visible light responsive azobenzenes

For the above reasons, considerable research has been carried out to improve the properties of azobenzenes, and in particular the development of azobenzenes that can be addressed by visible light only via modifying the substituents patterns has recently achieved

significant progress.[16]

Basically, the strategies involve either shifting the π ⟶ π* band to longer wavelength or splitting the n ⟶ π* bands of the *E*- and *Z*- isomer, which normally overlap in the visible region. Red-shifted absorption can typically be achieved by creating a push-pull system with electron donating groups on one side of the azo unit and electron withdrawing groups on the other side, leading to a red-shifted π ⟶ π* band which substantially overlaps with the n ⟶ π* band. However, push-pull azobenzenes have very short-lived *Z* isomers.[41] As a result, the photo-isomerization cannot be observed, unless using ultrafast spectroscopy apparatus. Short lived *Z* isomers are problematic in some cases, *e.g.* if one wants to accumulate large fraction of *Z* isomers. Therefore, the strategy offering bi-stable photoswitches via separation of n ⟶ π* bands of *E*- and *Z*-isomer has attracted much interest, and typically three approaches can be adopted.

C2 bridged azobenzenes

The first example was reported in 2009 by Siewersten and co-workers,[17] which is a C2 bridged azobenzene (see Fig. 2.2 a). By bridge-linking in the *ortho*-positions, the distorted nonplanar geometries separate the n ⟶ π* bands of *E*- and *Z*-isomer by 100 nm, which allows for switching in both directions (385 nm *Z* ⟶ *E*, 520 nm *E* ⟶ *Z*) with almost complete photoconversions (100% *Z* ⟶ *E*, 92% *E* ⟶ *Z*). It is noted that the thermally stable state in this structure is *Z* form, because of the strain induced by the bridge in the *E* form, which is opposite to common azobenzenes. The thermal half-life of the *E* isomer in this configuration is relatively short, which is calculated to be 4.5 hours at 28.5 °C in hexane for **C2-bridged azo**.

Woolley's group[42] further modified the structure by attaching bis-*p*-amido substituents or bis-*p*-amino substituents (see Fig. 2.2 b, **bis-*p*-amido-azo** and **bis-*p*-amino-azo**), to allow conjugation to biomolecules. The molecule **bis-*p*-amino-azo** shows significant absorbance of the *E* form in the red region (600 nm), which can fully convert to *Z* form under irradiation of red light, indicating good biocompatibility. Hammerich *et al.*[43]recently reported similar compounds by incorporating heteroatoms, *i.e.* oxygen or sulfur (see Fig. 2.2 b, **S-hetero-azo** and **O-hetero-azo**), into the bridge linker. The structures generate broad and more

bathochromic-shifted n ⟶ π* bands with a maximum absorption at 525 nm which extends up to 700 nm, allowing to switch efficiently (> 99%) from the *E*- to the *Z*- isomer upon irradiation with far-red light (660 nm). Importantly, the thermal half-life of ***E*-S-hetero-azo** is extended to 3.5 days, much longer than the parent **C2-bridged azo** ($\tau_{1/2}$ = 4.5 h). The synthetic procedure of these compounds is also shorter and more reliable.

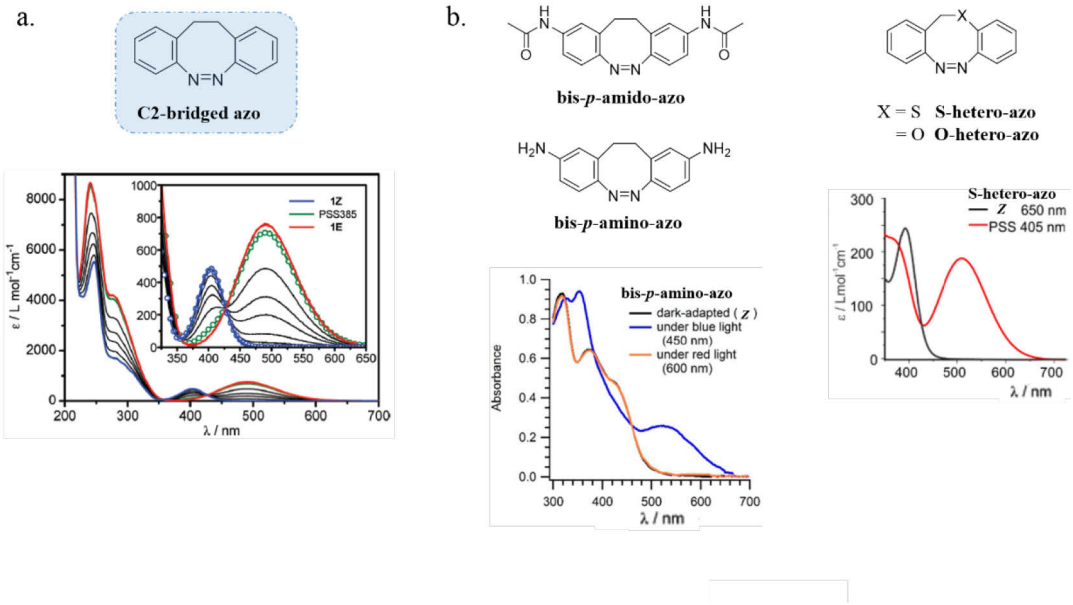

Fig. 2.2 a) Original bridged azobenzene and corresponding UV/vis spectrum. b) *para*-Amino-substituted and heteroatom-substituted bridged azobenzenes with corresponding UV/vis spectra.[42,43] In all cases, *Z*/*E* isomerization can be trigged by visible light.

Tetra-*ortho*-methoxy azobenzenes

Another design was reported by Woolley's group,[18] which took a somewhat different approach to separate the n ⟶ π* bands of *E* and *Z* isomers. Through introducing four methoxy groups in the *ortho*-positions of the azo band (Fig. 2.3 a), the photo-switching can also be achieved upon irradiation with visible light (530 nm for *E* ⟶ *Z*, 450 nm for *Z* ⟶ *E*) with high photoconversions (80% *E* ⟶ *Z*, 85% *Z* ⟶ *E*). The electron-donating methoxy groups result in the blue-shifting of the π ⟶ π* transition and red-shifting of the n ⟶ π* transition of the *E* form, compared to parent azobenzene. They concluded that this is most likely due to the twisting of the *E* form due to electronic repulsion between the methoxy

groups with the N lone pairs on the azo group, while the geometry of the *Z* form disrupts this repulsion. In addition, the *Z* isomer of the **tetramethoxy-azo** shows good thermal stability with a half-life of 14 days at room temperature in DMSO. Later on, the same group developed similar azobenzene derivatives with tetra-*ortho*-substituents as photo-switching building blocks for incorporation into biomolecules, in order to manipulate biological environment with visible light (Fig. 2.3 b), such as tetra-*ortho*-chloro compounds,[19,44] tetra-*ortho*-thioester compounds,[45] as well as tetra-*ortho*-methoxy azobenzenes with strong electron donating *para* substituents.[21,46]

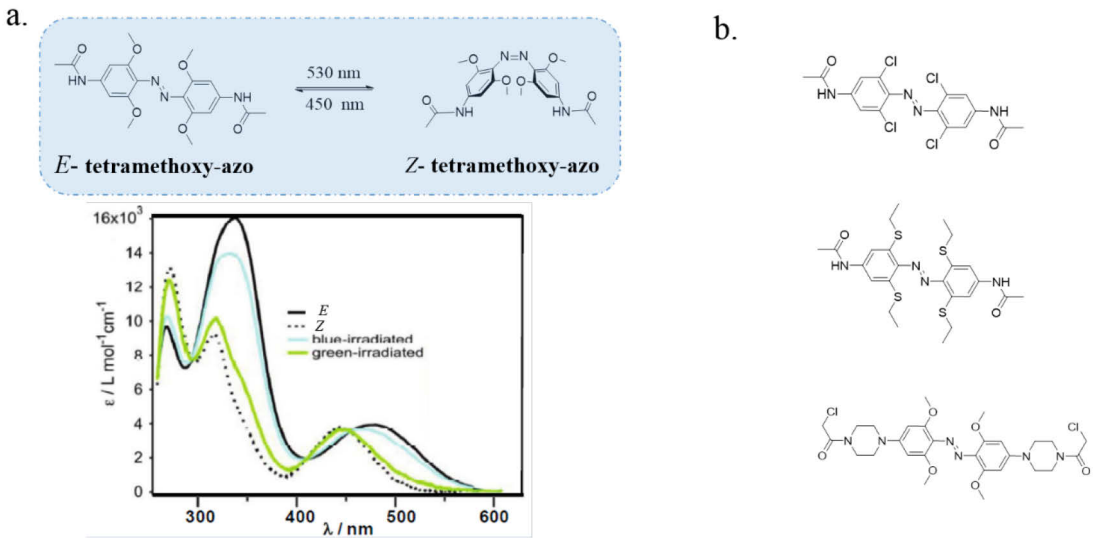

Fig. 2.3 a) Photo-isomerization and UV/vis absorption spectrum of tetra-*ortho*-methoxy azobenzene induced by visible light. b) Other examples of tetra-*ortho*-substituted azobenzene derivatives from Woolley's group.[18–21]

Ortho-Fluoroazobenzenes

More recently, our group reported a similar approach to realize the separation of n ⟶ π* bands by functionalizing azobenzene in *ortho* positions with fluorine atoms, whose *E* and *Z* isomers display distinct n ⟶ π* transitions (see Fig. 2.4 a, 42 nm separation for compound **F4**).[22] This separation allows to selectively address both isomers using blue and green light, respectively, causing *E*/*Z* isomerization with nearly quantitative photoconversions (up to

90% for $E \longrightarrow Z$, 97% for $Z \longrightarrow E$ for compound **F4-diester**). Moreover, the *Z*-isomers exhibit remarkably long thermal half-lives (ca. 700 days at room temperature in DMSO for compound **F4**). The separation is further extended (50 nm for **F4-diester**) through introducing electron withdrawing groups (EWGs) in *para*-positions, due to the synergic inductive effects from fluorine atoms and EWGs, while inversely the separation is reduced to 22 nm for **F4-diamino** because the electron donating groups, *i.e.* amino groups, counteract the inductive effect of fluorine atoms. Additionally, since fluorine atoms are rather small groups, the planarity of the *E* isomer is preserved (see Fig. 2.4 b), unlike the azobenzenes mentioned above, with bulky methoxy groups or bridge linker in which the *E* forms are strongly distorted. The planarity of this moiety is particularly of interest for certain applications in which an efficient conjugation along the π-system is required,[47] or that involve assemblies based on π, π-stacking.

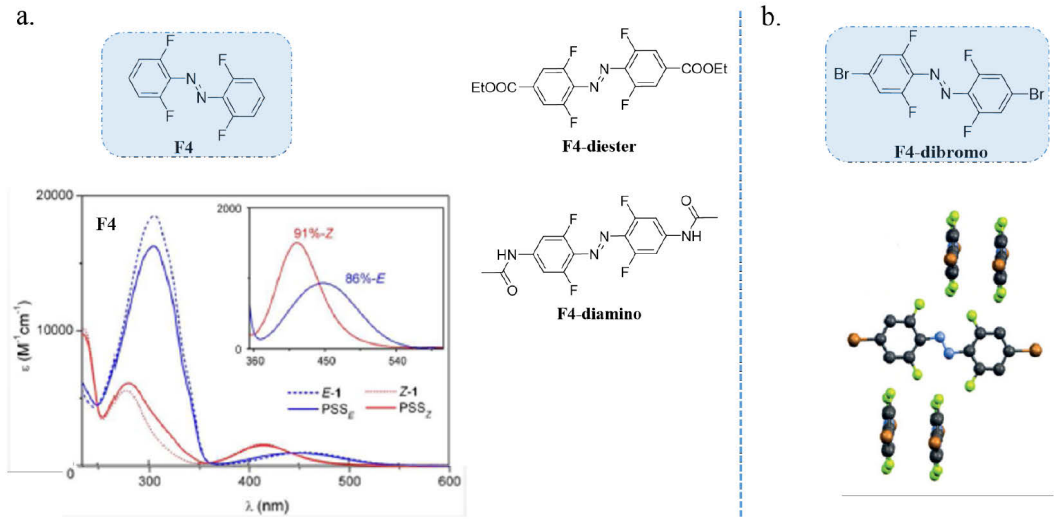

Fig. 2.4 a) *ortho*-tetrafluoroazobenzenes and UV/vis spectrum of compound **F4** with its PSS mixtures upon irradiation with visible lights (λ > 500 nm or λ = 410 nm**)**.[22] b) X-ray crystal structure of **F4-dibromo**, highlighting the planarity of the molecule.[23]

Subsequently, we carried out a comprehensive study on the effect of substitution on the key photo-chemical properties of *ortho*-fluoroazobenzenes. Three series of fluoroazobenzenes were synthesized varying the position, number, and nature of electron withdrawing groups,

structures of partial compounds are shown in figure 2.5.[23] In summary, introducing fluorine substituents in the *ortho* positions leads to an effective n ⟶ π* bands' splitting of the *E* and *Z* isomers, and as a consequence the *E*/*Z* isomerization can be trigged solely upon exposure to visible light with higher overall quantum yields. For example, the quantum yields for the *E* ⟶ *Z* isomerization following n ⟶ π* excitation (510 nm) were calculated to be around 0.3 in acetonitrile for both **F4** and **F2-asym**, higher than the values of around 0.2 obtained through π ⟶ π* transition (340 nm). This is due to the excitation through the S_1 state, *i.e.*, n ⟶ π* excitation, which is more efficient than that through S_2 state (π ⟶ π* excitation).[48] Introducing electron withdrawing groups (see Fig. 2.5 **F4-diester**, **F4-diamide** and **F4-dicyano**) in the *para* positions can further extend the splitting of the n ⟶ π* bands, while electron donating groups in the *para* positions narrow down the separation. Owing to the electron withdrawing effect of fluorine atoms, the energy of the n orbital of the *Z* form is remarkably lowered, thus all the *ortho*-fluoroazobenzenes described here display longer thermal half-lives compared with non-substituted azobenzene.

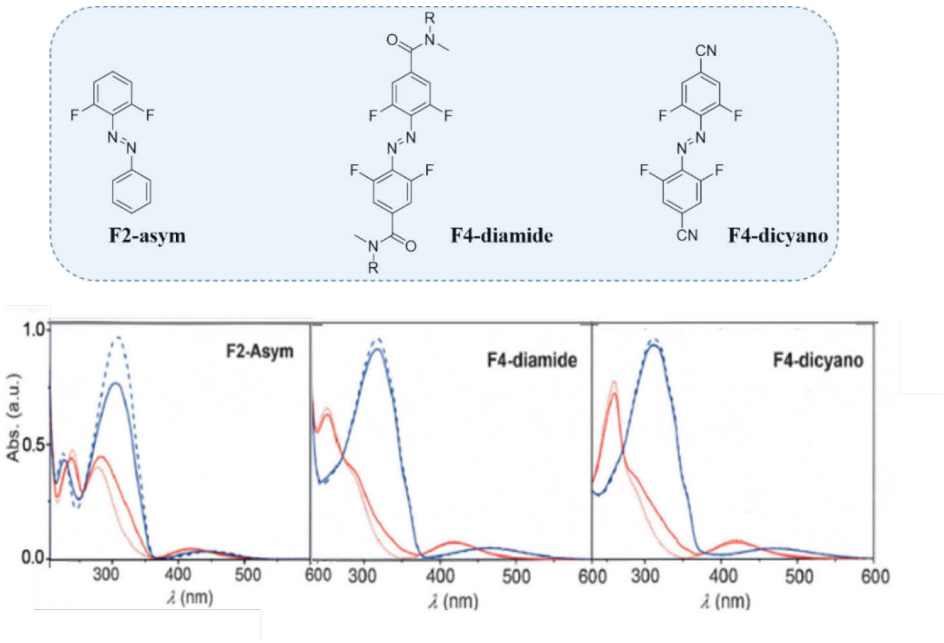

Fig. 2.5 Structures of **F2-asym, F4-diamide** and **F4-dicyano** as well as corresponding UV/vis spectra (dotted line: pure isomers, full lines: PSS mixtures upon irradiation with blue or green light).[23] All these compounds can perform *E*/*Z* isomerization upon exposure to visible light and display long thermal half-lives.

Other approaches

In the course of making long wavelength switching molecules, recently some new photoswitches such as BF2-adducts (see Fig. 2.6) have been reported.[49,50] The coordination of BF2 with an azo group's lone pair leads to a reversal of the positions of n ⟶ π* and π ⟶ π* bands, while the π ⟶ π* bands of *E*- and *Z*- isomers are well separated in the visible region, thus allowing to switch in both directions using visible light (see **BF2-azo** in Fig. 2.6, left, 570 nm for *E* ⟶ *Z*, 450 nm for *Z* ⟶ *E*) with high quantum yields ($\phi_{E\rightarrow Z}$ ~0.48, $\phi_{Z\rightarrow E}$ ~ 0.67). Introducing electron donating groups, *e.g.* methoxy or amino group (see Fig. 2.6, right) in *para* position on the phenyl ring further pushes the π ⟶ π* bands to longer wavelength.[50] Functionalizing with *para*-methoxy group (see ***para*-methoxy-BF2-azo)** not only shifts the activation wavelength to the red region, but also induces lager separation of the π ⟶ π* bands compared to **BF2-azo**, allowing for more efficient isomerization. Besides, the thermal relaxation of *Z* isomer is barely affected compared to **BF2-azo** ($\tau_{1/2}$ = 12.5 h), with a thermal half-life of 10.4 h calculated at room temperature in degassed methylene chloride. In the case of ***para*-amino-BF2-azo**, the activation wavelength is shifted to 680 nm with a tail extending to 760 nm. It enables isomerization using near infrared light (NIR, 710 nm), which could be very beneficial for the manipulation of biological processes. However, the thermal isomerization barrier is strongly lowered by the electron donating effect, as the thermal half-life of *Z*- ***para*-amino-BF2-azo** was determined to be 250 s only.

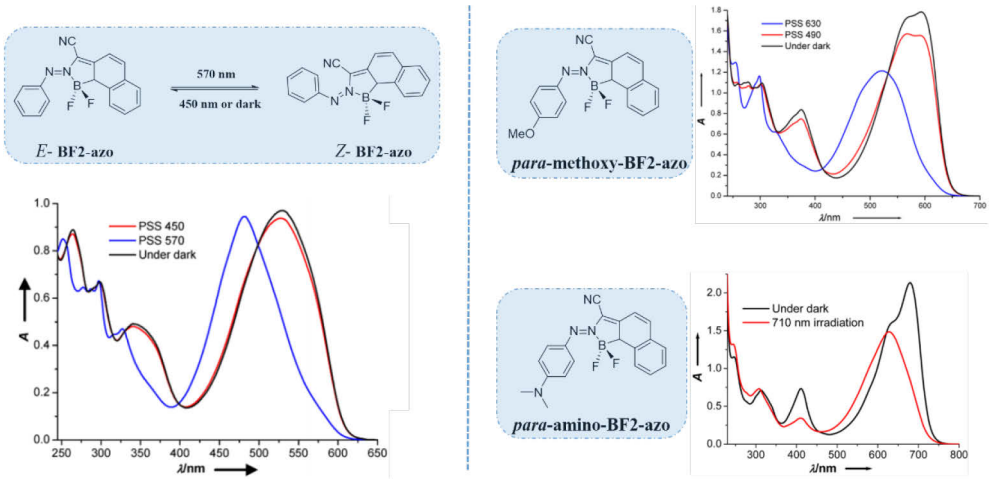

Fig. 2.6 Left: *all visible* **BF2-azo** and its UV/vis spectra.[49] Right: red-shifted *para*-substituted BF2-azos with corresponding UV/vis spectra.[50]

2.1.3 Molecular orbital theory of *ortho*-tetrafluoroazobenzenes

The properties of *ortho*-tetrafluoroazobenzens with spectral separation in the visible region as well as enhanced thermal stability of the *Z* isomers can be reasonably explained within the framework of molecular orbital (MO) theory (see Fig. 2.7), which has been described in our previous work.[22] In azobenzene (Fig. 2.7 top), due to the distorted planarity and reduced π-conjugation, both the HOMO (n) and LUMO (π*) levels in the *Z* form are higher than in the *E* form. The HOMO energy of the *Z* isomer was calculated to be -5.71 eV, being 0.41 eV higher as compared to the *E* isomer with E_{HOMO} = -6.12 eV, the LUMO of the *Z* isomer was placed at -1.94 eV compared to -2.17 eV for the *E* isomer. Because of the coincidental similar shifts of n- and π*-orbital energies in the *Z* isomer, the n ⟶ π* excitation energies are quite similar for both *E* and *Z* isomers. Therefore, there is no obvious separation of the n ⟶ π* bands in the absorption spectra of azobenzene.

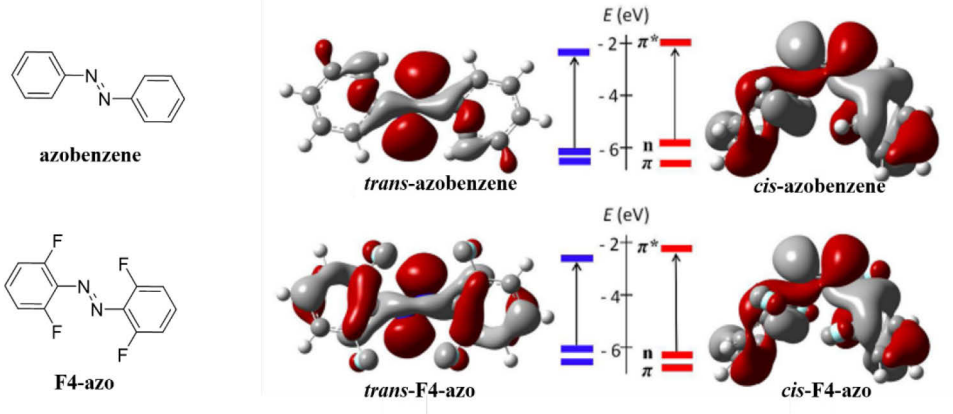

Fig. 2.7 Energetic diagram of the π, n, and π* orbitals of azobenzene (top) and F4-azo (bottom), and representation of the n-orbitals (HOMOs) calculated at the B3LYP/6-31G (d) level (arrows highlight n ⟶ π* transitions).

In the **F4-azo** (see Fig. 2.7 bottom), however, introducing fluorine atoms in the *ortho* positions, all the molecular orbitals in both *E* and *Z* isomers are lowered (besides the n orbital of the *E* isomer which is slightly higher, E_{HOMO} = -6.03 eV) compared to the corresponding molecular orbitals in azobenzene. The LUMO energy of *E* isomer is calculated to be -2.39 eV, and the LUMO/HOMO energies of *Z* isomer are -2.26 eV and -6.22 eV, respectively. The

energy decrease is especially strong for the n orbital of the *Z*-**F4-azo** (0.51 eV lower than the n orbital of *Z*-azobenzene, even 0.19 eV lower than the *E*-**F4-azo**). As a consequence, the n ⟶ π* excitation energy of the *Z*-**F4-azo** increases resulting in blue-shift of the n ⟶ π* band ($\lambda_{n\text{-}\pi^*}$ = 414 nm in acetonitrile) compared to parent azobenzene ($\lambda_{n\text{-}\pi^*}$ = 456 nm), while the n ⟶ π* band of the *E* isomer barely changes ($\lambda_{n\text{-}\pi^*}$ = 456 nm), *i.e.* the n ⟶ π* bands of the two isomers in **F4-azo** are effectively separated. Therefore, isomerization with visible lights in both directions was achieved, which produced PSSs containing 91% of *Z*-**F4-azo** with green light (> 500 nm) and 86% of *E*-**F4-azo** with blue light (410 nm). It was also shown in our investigations that introducing electron withdrawing groups (*e.g.* ester groups) in the *para* positions of the phenyl rings, in combination with the *ortho*-fluorine effect, could further increase the separation of the n ⟶ π* bands, and oppositely the separation is lowered by introducing electron donating groups. Moreover, the activation energy for the thermal *Z* ⟶ *E* isomerization is remarkably increased (117 kJ/mol) compared to the reported value for non-substituted azobenzenes (ca. 100 kJ/mol).[51]

2.1.4 Electrochemistry of fluoroazobenzenes

Besides light, electrons are another alternative driving force often used for triggering the conversion of photoswitches with high efficiency and minimum interference with the surroundings. Photochromic molecules and systems change not only the optical properties but also the electrical properties.[7] The difference in the electronic levels between the two isomers generated from the interconversion of a photoswitch, such as diarylethenes[52,53] and spiropyrans,[54] has made them ideal conjugated molecules for the development of optically gated electronic devices. In this context, considerable work in the investigation of the electrical properties of azobenzenes has also been carried out,[55–61] but some critical aspects remained unclear.

From previous investigations, we know that the electrochemical reduction of azobenzene is reversible following two sequential one-electron reductions,[55] which generates the same species from both the *Z* and *E* isomers.[56] In our recent work,[24] we further detailed a comprehensive study of the electrochemical switching behavior of azobenzene using a variety of experimental techniques. More than one dozen of azobenzene compounds were

investigated in this work, where we clarified a general phenomenon that the $Z \longrightarrow E$ isomerization can be trigged reductively using a catalytic amount of electrons, quantitatively generating the thermodynamically favored *E* isomer. This electrochemical switching process is highly efficient and is independent of spectral overlap and quantum yields, *i.e.* the isomerization can be achieved independently from the intrinsic photo-chemical properties of the azobenzene molecules.

Rapid thermal $Z \longrightarrow E$ isomerization was found in all cases before reaching the cathodic peak potential of the *E* isomer, most likely following a pathway of fast radical chain reaction (Fig. 2.8 left). Upon initiation by reducing a small amount of *Z* isomer, the formed $Z^{\bullet-}$ isomers rapidly isomerize to the radical anions of *E* isomer ($E^{\bullet-}$), followed by an electron transition from the $E^{\bullet-}$ to another neutral *Z* isomer to generate the thermal stable *E* isomer and the newly formed $Z^{\bullet-}$ propagating the chain. This result was supported by computational evaluation of the activation barriers for both the charge-neutral azobenzene and the corresponding radical anion (Fig. 2.8 right). As shown in the figure, the energy of the transition state for the isomerization of the radical anion ($\Delta G^{\ddagger}$ = 19.6 kcal/mol) is much lower as compared to the charge-neutral case ($\Delta G^{\ddagger}$ = 37.4 kcal/mol). This dramatically decreased thermal activation barrier results in the extremely rapid and irreversible isomerization of the radical anion ($Z^{\bullet-} \longrightarrow E^{\bullet-}$), the rate ($k_{iso}$ = 3.3 × 10^{8} s^{-1}) in the case of azobenzene was accelerated by 13 orders of magnitude as compared with that of thermoneutral $Z \longrightarrow E$ isomerization (k_{Δ} = 1.9 ×10^{-5} s^{-1}) at room temperature.

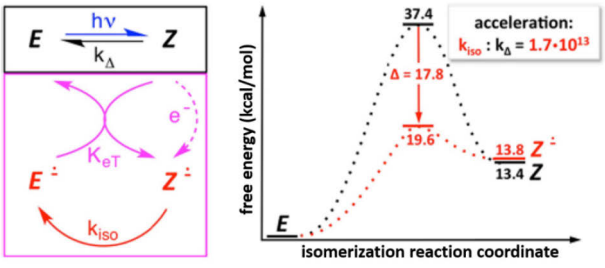

Fig. 2.8 Proposed mechanism and evaluation of the activation barriers for the electrocatalytic isomerization of *Z*-azobenzenes.[24]

In this work, several other fluorine-substituted azobenzenes were studied, which show

additional interesting electrochemical behaviors besides the ones mentioned above. Azobenzenes with fluorine substituents are easier to reduce compared with native azobenzene (see Fig. 2.9 compound **1**), *i.e.* the reduction potentials are more positively shifted, owing to the strong I-effect of fluorine atoms. The reduction potential varies strongly depending on the substitution patterns. Introducing two fluorine atoms symmetrically around the azo bond (*i.e.* one on each phenyl ring, see compound **2**) in the *ortho* positions already leads to a positive shift of 300 mV, while adding further fluorines to the *ortho* or *meta* positions have only a marginal effect (see **3** and **4**). Interestingly, with four fluorines on the *ortho* positions, *i.e.* compound **4**, the cyclic voltammetry shows clearly two nearly reversible one-electron transitions, which is not often observed of the second oxidation wave due to the unstable property of the dianion,[62] indicating stabilized electrical property by the fluorines. Placing fluorines only on one side of the azo bond (compound **5**) induces a slight shift only (positive shift of 130 mV compared to **1**). This difference is mainly due to the slightly non-symmetric twist of one phenyl ring resulting from the one side substituted fluorine atoms. This effect can be countermined by substitution symmetrically on both of the phenyl rings (see **2** and **4**). Notably, substitution on the *para* positions with ester groups (see compound **6**) causes a significant positive shift (around 700 mV) in contrast to compound **1**, because the coordination of the inductive effect of the ester groups and fluorines further shifts the reduction potential to much lower LUMO level (-2.99 eV *vs*. **1** with -2.17 eV, and **3** with -2.39 eV).[22] The remarkable electrochemical properties of fluoroazobenzenes may be leveraged to create complex systems activated by orthogonal stimuli (see section 3).

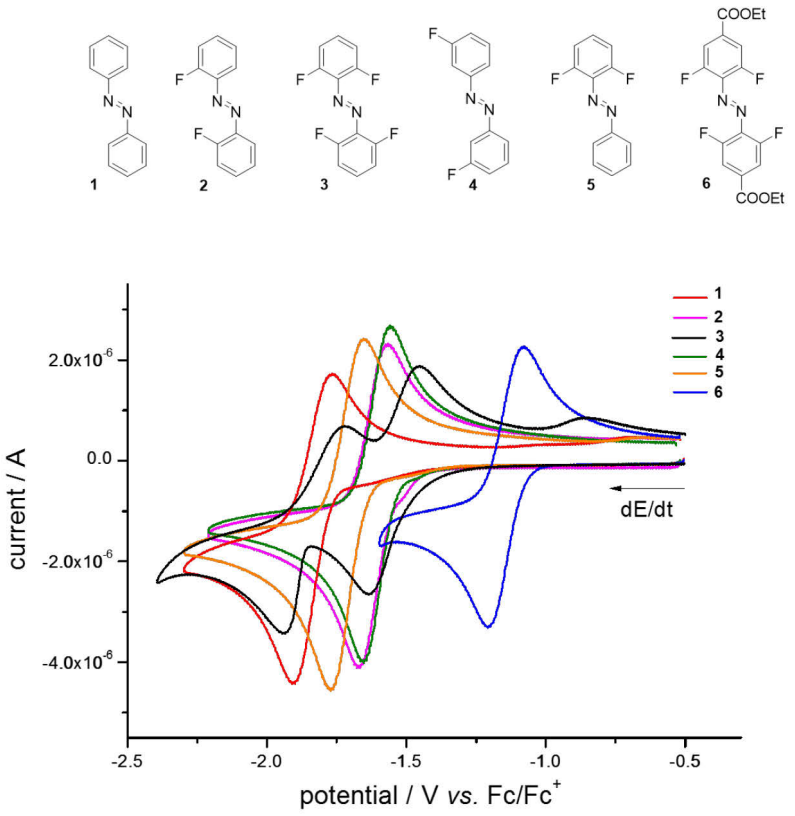

Fig. 2.9 Structures of selected fluorozaobenzene derivatives and corresponding cyclic voltammograms.[24]

2.1.5 Applications of *ortho*-fluoroazobenzenes

The benefits of visible light include a large window of available wavelengths, good penetration in tissues, and its harmless character. For these reasons, in addition to their superior thermal stability, fluoroazobenzene derivatives have been used as functional moieties for a variety of applications, such as the design of new photoswitches, the fabrication of advanced materials, as well as the manipulation of biological systems.

F-azos for the design of new photoswitches

In 2015, our group[25] successfully synthesized a bi-stable azobenzene which can undergo sensitized two-photon-triggered isomerization by covalently linking a two-photon-absorbing triarylamine to a thermally stable *ortho*-fluoroazobenzene (see Fig. 2.10). This strategy allows the use of low energy NIR-photons (750 nm) combined to the high spatial 3D resolution of

two-photon activation. The one-photon-induced $E \longrightarrow Z$ isomerization with visible light (500 nm) quantitatively generates the *Z* isomer, which displays a superior thermal half-life of more than 500 days.

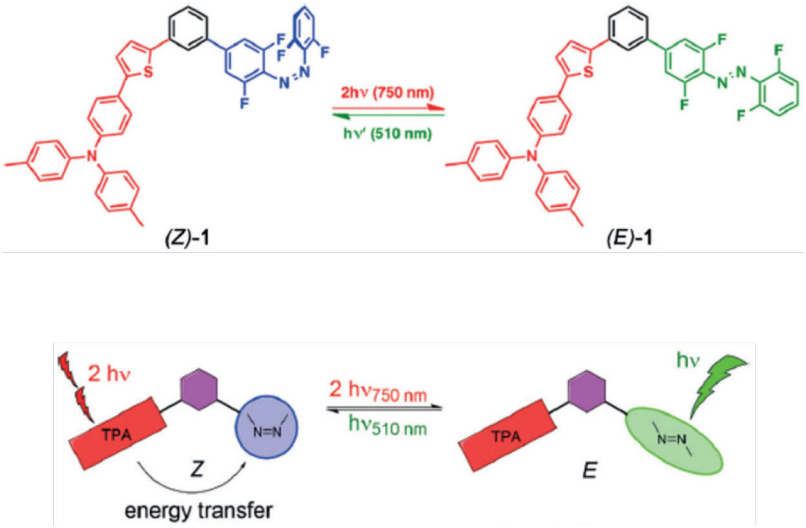

Fig. 2.10 Triarylamine–azobenzene and illustration of the operating principle based on two-NIR photon sensitized *Z*⟶*E* photo-isomerization and one-visible-photon direct $E \longrightarrow Z$ photo-isomerization of *ortho*-fluorinated azobenzene.[25]

F-azos in the fabrication of advanced materials

Nearly at the same time, our group and collaborators from Delft University[26] reported visible-light-responsive metal-organic-frameworks (MOFs) through incorporating *ortho*-fluoroazobenzene derivatives into Al and Zr frameworks (see Fig. 2.11). The MOFs exhibit different architectures that strongly influence the isomerization of fluoroazobenzenes inside the voids. Al-based nodes has congested 1D channels that hinder the efficient isomerization. In contrast, the framework built up with Zr provides enough space that allows the switch to isomerize freely within the pores. Upon irradiation these two frameworks show distinct photochromism and gas-adsorption capacities. Notably, it was proved that in the case of the Zr-framework, which exhibits good *Z*/*E* photoconversions, the $E \longrightarrow Z$ isomerization triggered by green light is more efficient (higher PSS) than that trigged by UV light.

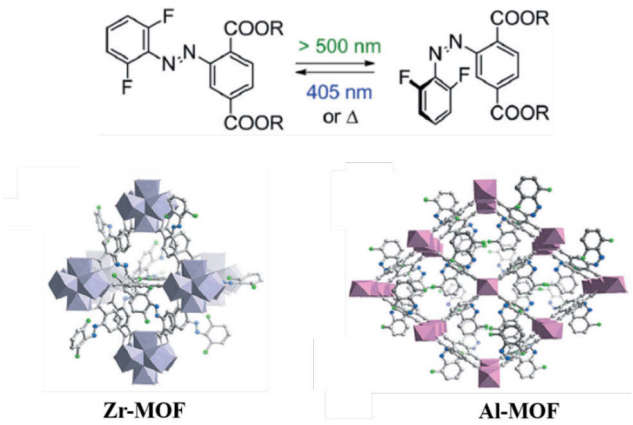

Fig. 2.11 Molecular structure of the MOFs' linker and representation of the proposed frameworks' structures: left, view of the octahedral supercages of Zr-MOF. Right, the Al-MOF structure with disordered F-azo-groups located in the pores of the framework.[26]

Fluoroazobenzenes have also been used for the construction of visible-light-responsive liquid crystalline (LC) polymer networks (see Fig. 2.12 left).[27] An *ortho*-fluoroazobenzene moiety was incorporated into a nematic polymer network, where the molecules aligned in the polymer film in a splay-orientated manner. This design enables the polymer film to perform continuous chaotic oscillatory motion upon exposure to sunlight or irradiation with a combination of green and blue lights.

Using similar materials, Katsonis' group[28] prepared a liquid crystalline film with a twist-oriented organization in the presence of a chiral dopant (see Fig. 2.12 right). The main differences compared to our design are: i) *para*-electron-donating methoxy groups instead of electron-withdrawing ester groups, ii) more flexible methacrylate (not methyl methacrylate) groups, and iii) twisted rather than splayed design of the films. Through adjusting the cross-linking density and optimizing the molecular orientation in the film, long-lived photo-mechanical deformation in the liquid crystalline polymer network (> 8 days) were obtained, attributed to the remarkable thermal stability of the fluorinated azobenzene.

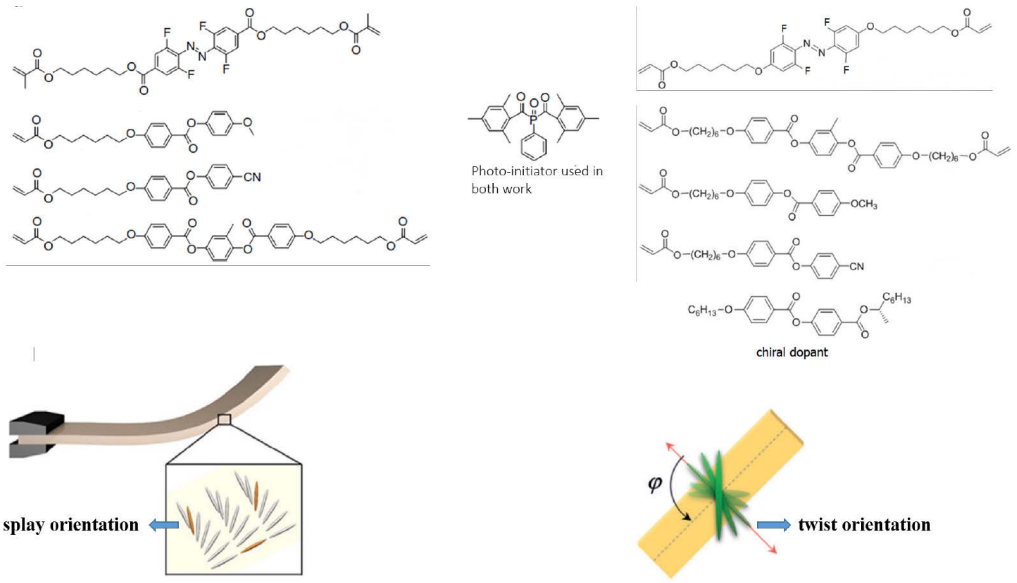

Fig. 2.12 Chemical structures of components used for preparing the nematic liquid crystalline networks and corresponding schematics of the liquid crystalline films with splay- (left)[27] and twist- (right) organization.[28]

F-azos for biological applications

Inspired by our investigations, in 2015 Wang *et al.*[29] prepared proteins with visible light controlled functions (see Fig. 2.13). They genetically incorporated a pentafluoro azobenzene (**F-PSCaa 1**) into proteins via the expansion of the genetic code, the *para* fluorine was then substituted by the nearby cysteine's thiol to generate a bridge in situ. The bridge is switchable in response to visible light (540 nm for $E \longrightarrow Z$ and 405 nm for $Z \longrightarrow E$ isomerization). In consequence, the conformation and binding of proteins could be regulated by the isomerization of the azobenzene bridge.

A new application of fluoroazobenzene in biological systems was recently reported by Trauner and Barber.[30] They prepared a tetra-*ortho*-fluoroazobenzene-containing molecule, which can activate/deactivate the potassium channel accompanied the isomerization of fluoroazobenzene. The utility of visible light provides a useful research tool for further investigation in living animals/humans.

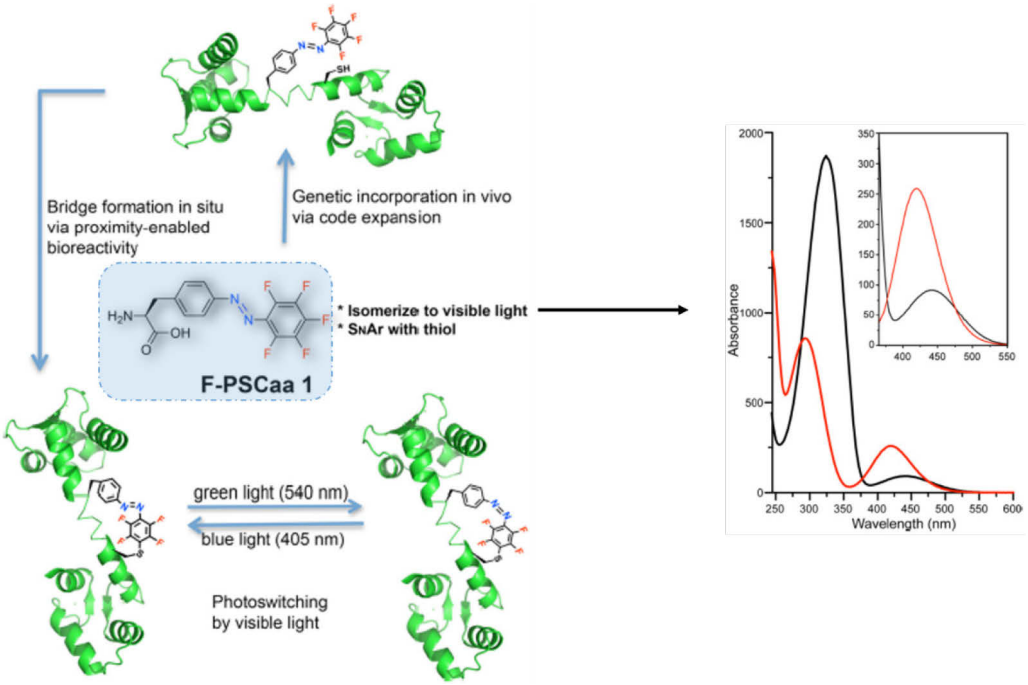

Fig. 2.13 The process of in situ formation of an azo-bridge on proteins controllable by visible light and UV/vis spectrum of **F-PSCaa 1** after illumination with green (540 nm, red curve) and blue (405 nm, black curve) light.[30]

In summary, the successful use of fluoroazobenzenes in several reports by us and others confirmed their practical values. With the rapid development of materials science, we believe that more promising work based on this moiety will emerge in the near future.

2.2 Hydrogels

2.2.1 Introduction

Hydrogels are three-dimensional hydrophilic polymer networks with high water content, which can be formed from monomers or macromonomers via covalent cross-linking (chemical gels) or from small molecules that self-assemble into macrostructures through non-covalent interactions (physical gels).[63–66] A representative flexible hydrogel network is illustrated in figure 2.14.

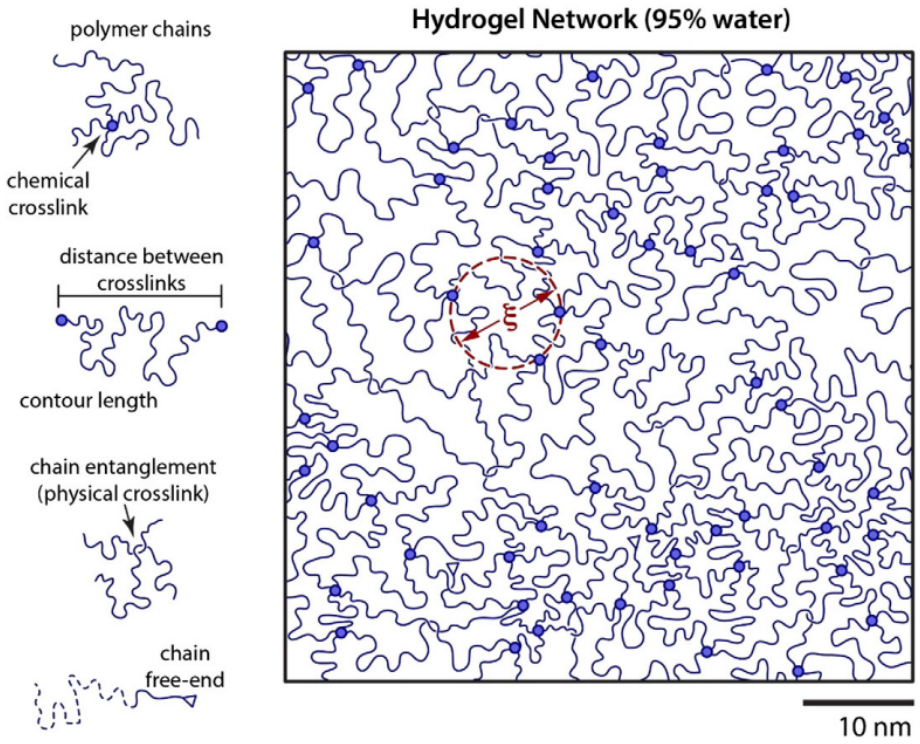

Fig. 2.14 Illustration of a semi-dilute flexible polymer network, with minimal coil overlap and a persistence length on the order of nanometers. The mesh size (ξ) is approximately 10 nm.[67]

The ability of hydrogels to absorb water arises from either hydrophilic functional groups attached to the polymer backbone or by the hydrophilicity of the backbone itself, while their resistance to dissolution arises from cross-links between network chains, in which water can be trapped within the pores without flowing freely like in solutions. However, water exchange can occur while the soft and rubbery consistence is retained, resembling living tissues. The properties of hydrogels, such as inherent structures, mesh size, swelling rate, mechanical

strength and permeability, can be significantly different depending on the method of preparation. Due to the ease of preparation and the above-mentioned properties including high water content, porosity, and biocompatibility, as well as facile tunability of chemical structures, hydrogels are materials of choice for several biomedical applications. Thus far, they have been successfully used for drug delivery, cell encapsulation and tissue repair.[68–72]

Hydrogels can be divided into many different kinds of categories depending on diverse parameters, such as preparation method, material structures (natural or synthetic), charge content (neutral, anion, or cation) among many others.[70] For example, based on the mechanisms of network formation, including covalent cross-linking and non-covalent interactions (such as hydrogen bonds, hydrophobic interactions, π - π interactions, van der Waals forces, and electrostatic interactions), hydrogels can be simply divided into physical gel and chemical gel. Alternatively, hydrogels can also be classified as natural gel and synthetic gel depending on the compositions of the building blocks. Finally, classification can be made as well according to the pore size: nanogel (nanometers) and microgel (micrometers).

2.2.2 Huisgen 1, 3-dipolar "click" cycloaddition in hydrogel synthesis

A wide variety of methodologies (including physical and chemical cross-linking strategies) have been developed to prepare hydrogels. However, click chemistry has appeared as a most important tool to fabricate hydrogels for fulfilling various purposes. Click chemistry provides extremely selective and orthogonal reactions that proceed in mild conditions with high efficiency. Since the first click hydrogels were reported by Hilborn in 2006,[73] numerous functional hydrogels prepared with click methods have been studied and reviewed.[74–76] Click reactions used for hydrogel fabrication include copper-catalyzed azide-alkyne cycloaddition (CuAAC), strain-promoted azide-alkyne cycloaddition (SPAAC), Diels-Alder (DA) reaction, and thiol-ene chemistry, among others. Here we only discuss CuAAC and SPAAC, the two methods applied in this thesis.

Copper-catalyzed azide–alkyne cycloaddition

Copper-catalyzed azide–alkyne 1,3-dipolar cycloaddition (CuAAC) (see scheme 2.1) produces molecules covalently linked via 1,2,3-triazole, is a very effective tool for the facile

construction of simple to complex architectures. It gained increasing popularity for hydrogel fabrication because the reaction is highly specific, quantitative, and tolerant to a variety of functional groups under physiological conditions.[77,78]

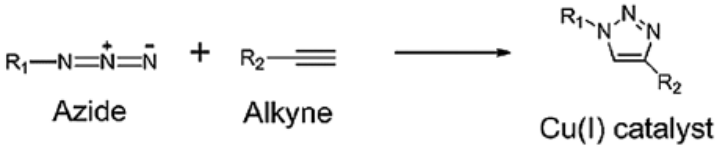

Scheme 2.1 Cu(I)-catalyzed azide-alkyne [3+2] cycloaddition (CuAAC).

The active form in the catalytic process is Cu(I), and there are three common protocols for click conjugation: (1) direct use of a Cu(I) source (*e.g.* CuBr, CuI), (2) alternative generation of Cu(I) by the reduction of a Cu(II) intermediates (*e.g.* $CuSO_4$, $Cu(OAc)_2$), and (3) direct oxidation of the element Cu (0). All three protocols are widely used, but the method (2) which generates Cu(I) in situ using Cu(II) salts is known to be more practical since the catalytic system is unaffected by oxidizing and aqueous conditions. It should be noted that copper can generate biologically detrimental reactive oxygen species when used with reductant (*e.g.* sodium ascorbate), which can limit its utility for biological studies.[79,80] However, this can be circumvented by means of photo-induced reduction of Cu(II) salts.[81]

The CuAAC reaction is considered to be a stepwise process following a concerted mechanism.[82–84] According to the most recent study, two catalytic pathways, dominated mainly by the bis-copper complex pathway, have been proven to be involved in the catalytic processes (see Fig. 2.15).[85] As shown in the figure, at the commencement of the reaction, Cu(I) and terminal alkyne form a mono-copper acetylide (**1Cu**), **1Cu** further reacts rapidly with another molecular catalyst offering a cationic dinuclear complex $\mathbf{1Cu_2}$. Subsequently, the active $\mathbf{1Cu_2}$ and azide form the intermediate 3,5-bis(metallated) triazole $\mathbf{2Cu_2}$. Lastly, protodemetallation, which arises from the reaction with the terminal alkyne, generates the disubstituted 1,2,3-triazole product and bis-copper complex $\mathbf{1Cu_2}$, leaving out complex **1Cu** from the catalytic cycle. The other pathway, which is catalyzed by the mononuclear counterparts **1Cu** and **2Cu** (see Fig. 2.15), has been proven to be very slow [k_{obs} ($\mathbf{1Cu_2}$)/k_{obs} (**1Cu**) > 94], hence the bis-copper pathway is kinetically favored.

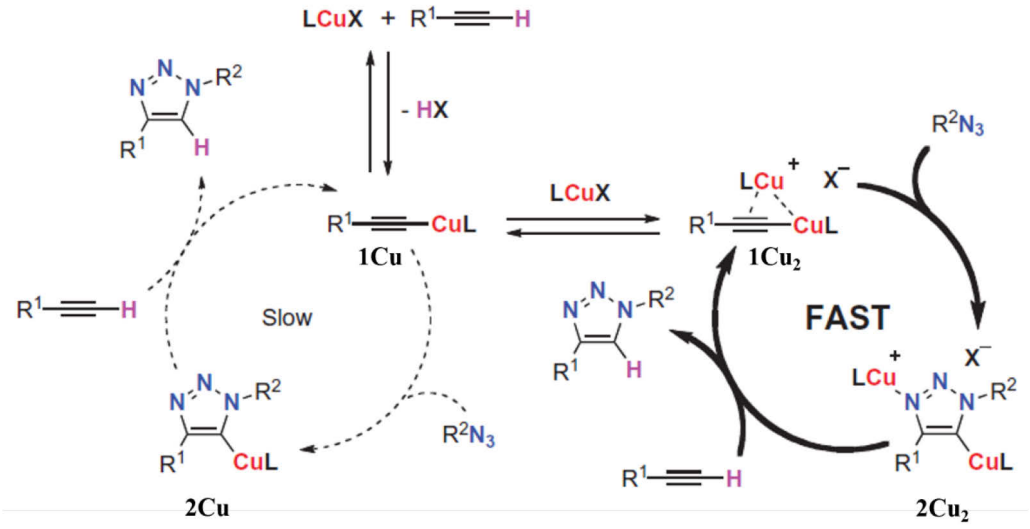

Fig. 2.15 Bertrand's conclusive mechanism of CuAAC: bis-copper complexes (**1Cu$_2$**, **2Cu$_2$**) dominated two-pathway processes.[85]

Although the versatile CuAAC reaction has been widely exploited, there are some drawbacks that cannot be neglected, especially in the context of biological applications. Namely, potential cytotoxicity of copper ions and reactive oxygen species generated by copper ions might lead to structural damage of biomolecules such as proteins, nucleic acids, polysaccharides, and lipids.[86]

Strain-promoted azide-alkyne cycloaddition

In order to reduce the risk of transition metal related toxicity issues, Cu-free click strategies have been recently developed.[87–91] In the strain-promoted azide-alkyne cycloaddition, as the name implies, the reaction's driving force results from the ring-strain (see cyclooctyne structures in scheme 2.2). The bond angle of the sp-hybridized carbons in cyclooctynes is around 160°, which is distorted toward the transition state of the cycloaddition reaction, thus leading to a dramatic rate acceleration.[92]

The reactivity of cyclooctyne can be altered via modulation of electronic properties (*e.g.* with fluorine atoms, see **DIFO** in scheme 2.2) or strain-energy (such as **DIBO**, **DIBAC**,

BARAC in scheme 2.2). The first cyclooctyne **OCT** (see scheme 2.2) prepared by the Bertozzi group specifically as a bioorthogonal reagent, displays vastly accelerated reaction kinetics compared to the linear alkynes.[93,94] Later, they proved that the reaction rate can be enhanced through introduction of electron-withdrawing fluorine atoms (**DIFO**) in the propargylic position.[95] It was shown that the rate of **DIFO** was 60 times faster than **OCT**, but its water-solubility is less than ideal. In addition, the synthesis is also rather challenging. However, dibenzo-functionalized analogues such as **DIBO**,[96,97] **DIBAC**[98] and **BARAC**[99] are relatively easier to synthesize and can be substituted at various aryl positions to enhance kinetics or solubility. Most importantly, dibenzocyclooctynes such as **DIBAC** and **BARAT** react with azides even faster than **DIFO**.[100]

Due to the high efficiency and bioorthogonality of SPAAC, it has found widespread applications such as biomolecule labeling,[101–103] surface modification,[104,105] PEGylation of proteins[98] and *in vivo* imaging.[95,106] The first SPAAC hydrogel was reported by the Anseth group in 2009.[107] They fabricated a cytocompatible hydrogel via functionalizing a macromolecular precursor with the **DIFO** moiety.[107] The macromolecular precursor reacted with four-arm PEG-azide for direct encapsulation of cells within hydrogels which can be degraded by metalloproteinase enzyme.

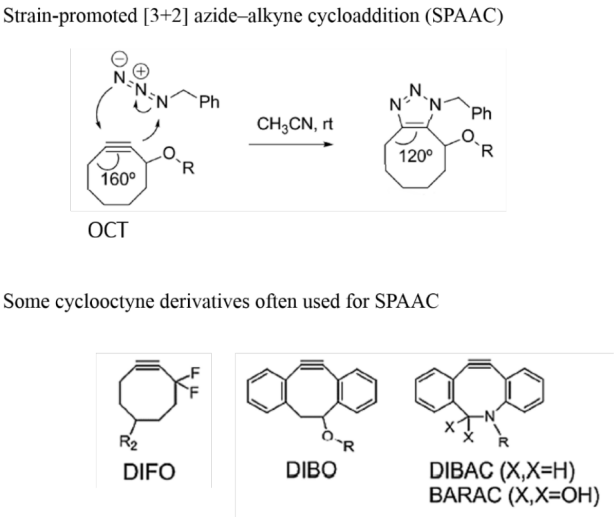

Scheme 2.2 Strain-promoted azide-alkyne cycloaddition and developed cyclooctynes for SPAAC.

2.2.3 Photo-responsive hydrogels

The first time that hydrogel was utilized as soft contact lens materials which interfaced with human body can be traced back to 1960.[108] Since then, hydrogels have emerged as promising materials in many fields and reviewed from different points of view.[72,75,109,110] With the development of materials science, hydrogels which can respond or adapt to external stimuli or changes in their environment have gained increasing interest and have been the focus of recent research. Stimuli-responsive abilities enable hydrogels to be used as "smart" materials, whose properties (stiffness, hydrophobicity, and mesh size) can be tuned on demand. These dynamic hydrogels are particularly investigated for drug delivery applications.

Numerous stimuli-responsive hydrogel systems have been developed until now, the stimuli involved including temperature,[111,112] pH,[113,114] electronic fields,[115] magnetic fields,[116] and light.[117] Among these external inputs, light assuredly is an attractive option since most light-induced processes can be carried out rapidly under aqueous conditions, and can be controlled remotely via adjusting wavelength, intensity and duration of irradiation. Therefore, the properties of hydrogel can be manipulated spatially and temporally with great ease and convenience in a non-invasive manner.

Photo-responsive hydrogels commonly are composed of a polymeric network and a photo-responsive moiety, the latter normally works as the functional part. Photo-responsive molecules can be incorporated into hydrogel systems as cross-linkers or pendant groups, while upon irradiation the photo-active hydrogels show changes in their physical or/and chemical properties. Three types of photo-induced reactions are typically used: degradation, dimerization, or (reversible) isomerization.

Photo-degradation

Light-induced degradations are irreversible processes which can be used to create "one-time" responsive materials. The most common photo-labile groups used for hydrogel formation are *o*-nitrobenzyl derivatives (see Fig. 2.16 top), which exhibit high photolytic efficiencies. Photo-cleavage occurs upon exposure to UV light or via two-photon absorption,[117,118] generating 2-nitrosobenzaldehyde and a carboxyl acid derivative. The rate of degradation can be tuned via altering substituents and positions on the phenyl ring.[119]

Cross-linking *o*-nitrobenzyl moieties into hydrogel networks allows to spatiotemporally regulate the resulting materials' properties. Thus, it has been widely used as functional groups for preparing photo-degradable polymers for diverse biological applications, such as uncaging of proteins,[120] cleaving of peptides from a solid support[121] and controlling cell adhesion.[122,123] Anseth's group[124] has reported a photo-degradable hydrogel by introducing a modified *o*-nitrobenzyl moiety into the backbone of a poly(ethylene glycol) (PEG) macromonomer. In that way, the gel's physical and chemical properties can be tuned dynamically and externally, which offers a dynamic environment for cell cultures.

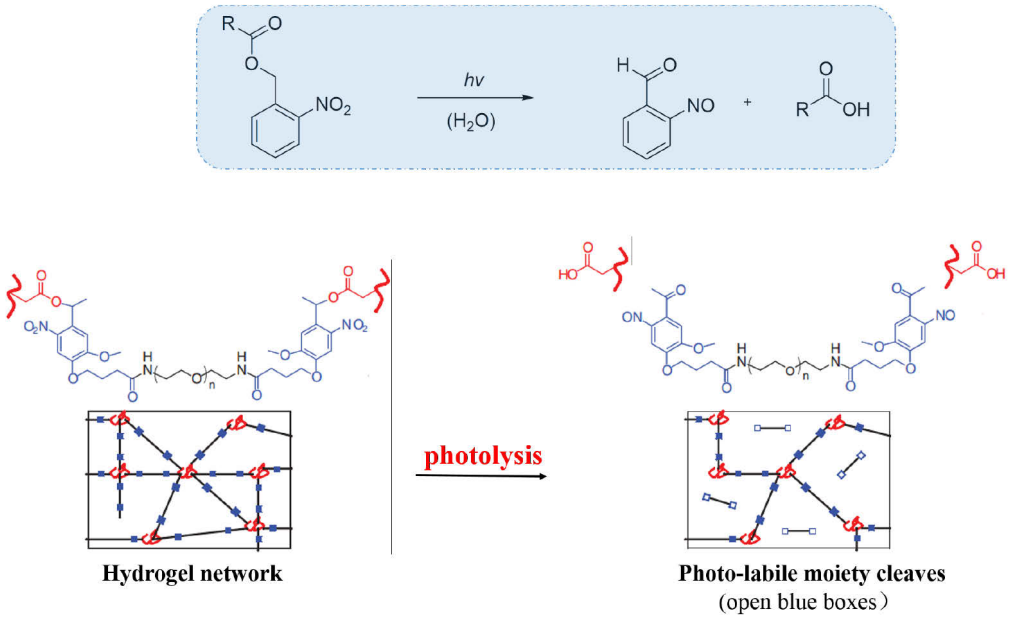

Fig. 2.16 Top: photo-cleavable *ortho*-nitrobenzylester used for the construction of irreversible photo-degradable hydrogels. Bottom: an example of PEG-based hydrogel network connected by an *ortho*-nitrobenzylester derivative. Upon irradiation, the photo-labile moiety cleaves and degrades the physical structure of the hydrogel.[124]

Other photo-cleavable molecules such as triphenylmethane,[125] azosulfonate[126] and pyrenylmethyl ester[127] have also been used as functional building blocks for hydrogel formation.

Photo-dimerization

Coumarin (see Fig. 2.17 top) is a molecule often used as a reversible cross-linking moiety to control sol-gel processes and regulate swelling properties of hydrogels.[128–130] The molecule is known to photo-dimerise when irradiated with light > 280 nm, while cleavage of the dimer is triggered with light < 260 nm.[131,132] For example, when coumarin groups were introduced into polyoxazoline, photo-coupling and photo-cleavage reactions could be carried out under irradiation with light of 319 nm and 253 nm, respectively.[133] Gelation occurs via dimerization, while the hydrogel turns into a fluid polymeric solution after the reverse cleavage reaction. Coumarin has also been used to strengthen the mechanical property of hydrogels by post-gelation photo-dimerization.[134] As shown in figure 2.17, a coumarin-functionalized peptide low molecular weight gelator (LMWG) first forms a self-assembled fiber under appropriate condition. Irradiation of the fiber with 365 nm leads to the covalent dimerization of coumatin molecules within the neighboring fibers, as a consequence the gel's stiffness is increased.

Besides coumarin, many other functional groups undergoing reversible dimerization have been used for the preparation of hydrogels with photo-tunable abilities, such as cinnamylidene acetate,[135] anthracene,[136] nitrocinnamate[137,138] and poly(cinnamic acid).[139]

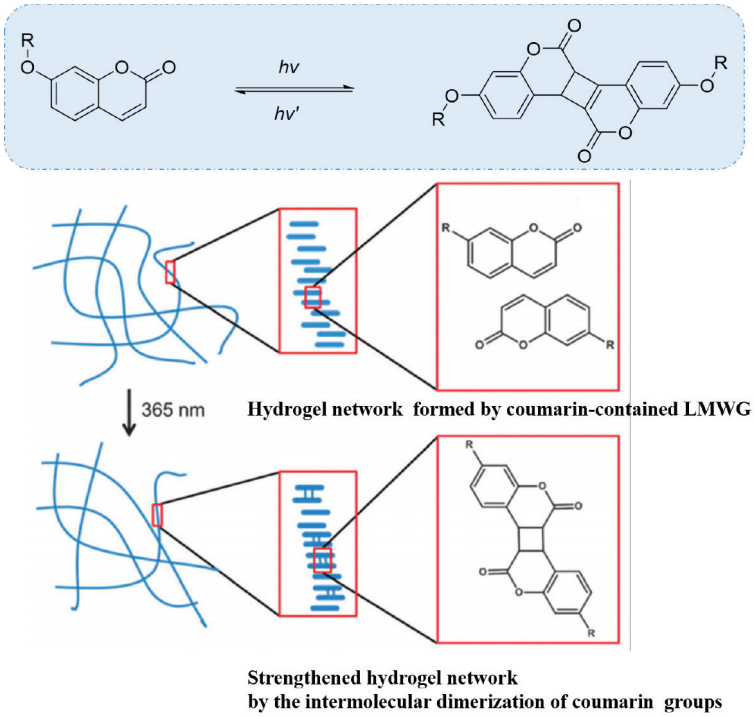

Fig. 2.17 Top: Coumarin undergoes reversible photo-dimerization/cleavage upon irradiation with appropriate wavelengths of light (320 nm for the coupling, 250 nm for the cleavage). Bottom: a non-covalent hydrogel network formed by the coumarin-containing LMWG. After irradiation with UV light, the stiffness of the hydrogel was increased due to the dimerization of the neighboring coumarin molecules within the fibers.[134]

Photo-isomerization

The advantages of photo-isomerization processes are reversibility and hence repeatability. They can be divided into two major classes: electrocyclization and *Z*/*E* isomerization. Spiropyrans are one type of photo-responsive groups that are often used as functional groups for constructing and modifying properties of hydrogels, which follows the process of electrocyclization. The closed-ring spiropyran (**SP**, see Fig. 2.18) isomer is neutral and hydrophobic, while the UV light generated open-ring merocyanine (**MC**, see Fig. 2.18) isomer is zwitterionic and hydrophilic. The process can be converted back thermally or using visible light irradiation. These two species have vastly different physico-chemical properties making the molecule far more than just a simple photoswitch. A broad range of stimuli can be used to induce its reversible isomerization which include not only light, but also temperature, pH value, solvent polarity, metal ions and redox potential. Owing to this versatility,

spiropyrans have been widely used as building blocks to manipulate properties of hydrogels in diverse forms, including incorporation into peptides,[140] polymers,[141] as well as low-molecular-weight gelators.[142]

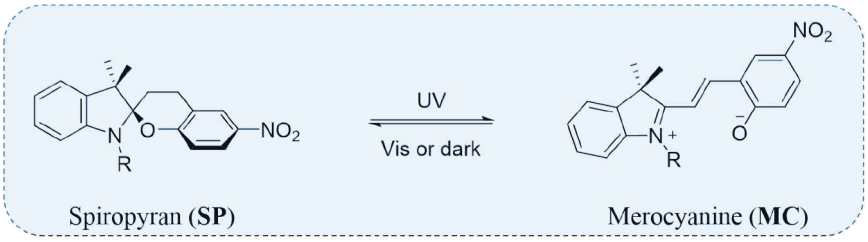

Fig. 2.18 Spiropyran undergoes electrocyclization isomerization process between a thermally stable hydrophobic closed **SP**-form and a metastable hydrophilic open **MC**-form.

For example, due to their different water-affinity, spiropyrans are often used to alter the dimensionality of a gel (extension/shrinkage via swelling/deswelling).[143] Schiphorst *et al.* prepared such hydrogels containing spiropyrans (see Fig 2.19). The hydrophilic protonated **McH**$^+$ isomer uptakes water, while the hydrophobic **SP** isomer releases water, therefore allowing repeatable swelling and deswelling of the material. This allows the hydrogels to be implemented as light-responsive valves in microfluidics. Additionally, the **SP** form has a twisted structure due to the perpendicular connection between the indoline moiety and the chromene moiety, while the **MC** form adopts a plana geometry. It has been found that the planar **MC** form has a strong tendency to aggregate driven by intermolecular π stacking, while the non-planar **SP** form does not aggregate.[144–146] This property is often used in spiropyran-containing hydrogel systems to control sol-gel processes.[142]

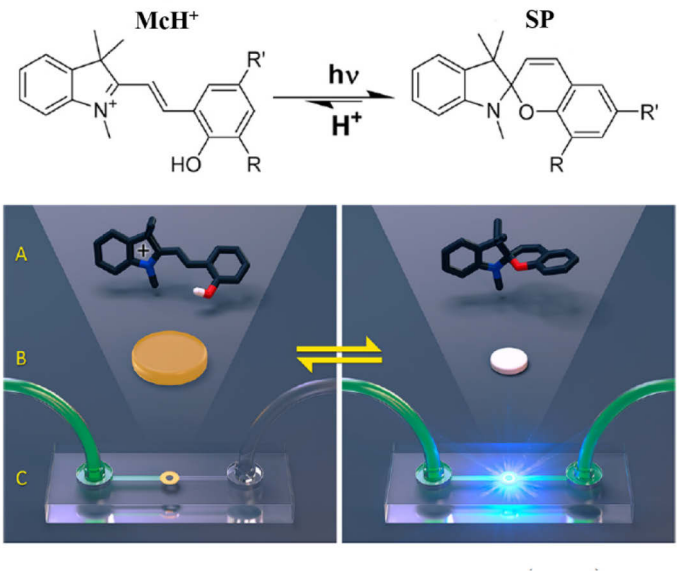

Fig 2.19 Isomerization of a protonated merocyanine (**McH+**) and the spiropyran (**SP**) form (A) with the corresponding effect on the size of a hydrogel by irradiation with light (B), implemented as photo-responsive valve in microfluidics (C).[147]

Azobenzene might be one of the most widely used compounds in hydrogel systems which utilize *Z/E* processes to perform light-induced reactions. This popularity is mainly due to the great differences in structures, polarities and hydrophobicities of the *Z* and *E* isomers. In addition, the properties of azobenzene can be manipulated easily via altering the substitution pattern on the benzene rings. Thus, they are often used as cross linkers or pendent groups for constructing photo-responsive hydrogels through covalent incorporation into polymer networks to modify hydrogels' properties on demand (see table 2.1).[148–150] Additionally, leveraging hydrophobicity effects, azobenzenes can be used with cyclodextrins[151–153] to control sol-gel processes and to adjust cross-linking densities via the formation of inclusion complexes, or act as low-molecular-weight gelator to induce sol-gel phase transitions.[154–158] A representative hydrogel system consisting of azobenzene and cyclodextrin is shown in figure 2.20.[71] The *E*-azo isomer can form tight complex with cyclodextrin via host-gust interactions, leading to the formation of hydrogel networks. Upon irradiation with UV light, the planar *E* isomer was converted to the kinked *Z* isomer, which tends to dissociate from the complex, inducing the hydrogel network to collapse into a fluid solution. The sol ⟶ gel process can be triggered reversibly by visible light irradiation. In this

work, a protein was encapsulated into the hydrogel system, and spatially-temporally controlled release of the protein was achieved via manipulating the gel ⟶ sol process.

Table 2.1 Photo-modulations of azobenzene-containing hydrogels.

Chemical design	Photo-induced effect	Mechanism
Physical gel	- Phase transition (sol-gel)	- Disruption of π-stacking[154–158]
		- Dissociation of inclusion complex[151–153]
Chemical gel	- Contraction/expansion	- Disruption of π-stacking[150]
	- Stiffening/softening	- Other structural disturbance[159]

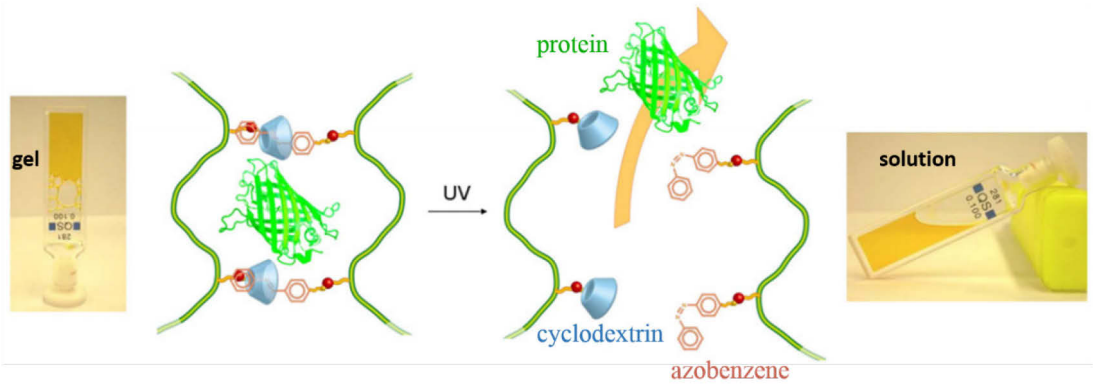

Fig. 2.20 Schematic representation of protein photo-release from a hydrogel composed of *E*-azobenzenes and cyclodextrin modified dextrans. Upon UV light irradiation azobenzene moieties isomerize from *E* to *Z* configurations, resulting in the dissociation of crosslinking points, further allowing the entrapped protein to migrate into the media. Pictures show the gel and sol states.[71]

In addition to azobenzenes, other molecules undergoing *Z*/*E* isomerization (such as stilbenes[160] or fumaric amides[161]) are also used for modifying gels' properties. However, because of their lower photo-stability, they are not used as often as azobenzenes.

3. Orthogonal switching in four-state azobenzene mixed-dimers*

3.1 Introduction

Light-induced molecular switches, which undergo interconversion between two isomers in response to optical stimulation still remain a hot topic in scientific research, due to their broad application as functional building blocks for creating "smart" materials.[9,18,162,163] In light of the rapid development in this field, much research in recent years has focused on the development of multi-component photochromic molecular systems that integrate several switches in one single molecule. Potential applications include molecular-level information processing and storage,[164,165] as well as the ability to perform more complex tasks. In a multi-state photochromic system, molecular switches isomerizing between two states without directionality are typically not able to perform continuous work.[166,167] On the other hand, if more than two states can be selectively addressed, sequential reversal to the initial state following a different path—*i.e.* directionality—is reachable, allowing more complex tasks to be performed and do useful work at all scales.

Considerable achievements towards fabricating addressable multi-switching systems have been obtained over the last decades. The photoswitches used in those systems include nearly all known organic photochromic compounds, such as diarylethenes,[168,169] stilbenes,[170] spiropyrans,[171,172] dihydropyrenes[173,174] and azobenzenes.[175] Azobenzene-based multi-state photo-switching systems are advantageous due to the large geometrical changes associated with *E/Z* isomerization, which is especially desirable for inducing large photo-mechanical movements in polymers[176–178] or to control biological environment.[35]

However, the design of the multi-state photochromic compounds which can be addressed efficiently, that is to say using different inputs generating distinguishable responses simultaneously, is still a very challenging task.[179] Different strategies can be followed for linking photoswitches depending on their chemical structure(s) (identical or not) and the type of connection (electronically coupled or decoupled). In order to optically address all isomers selectively, one approach consists in connecting two identical photoswitches in direct electronic conjugation. In such dimers, the first isomerization creates an isomer with new

* Parts of this chapter have been published in "F. Zhao, L. Grubert, S. Hecht, D. Bléger, *Chem. Commun.* **2017**, *53*, 3323-3326."

spectral features, potentially allowing the use of a different color of light for the second isomerization. This approach produces 3-state compounds; however, their photo-isomerization ability might be dramatically impaired, as generally observed in photoswitches with extended π-systems.[51,180] For example, in the **bis-*p*-azo** (see Fig. 3.1), where the two photochromes share a central phenyl ring, only a small amount of *EZ* isomer is formed and *ZZ* isomer is almost completely absent upon irradiation.[180] Similar behaviors were also observed in dithienylethene (DTE) dimers.[181,182] As shown in figure 3.1, in the **DTE-dimer**, where the subunits can be seen as being separated by a double bond, only the mono-closed system could be accessed due to intramolecular energy transfers.[181]

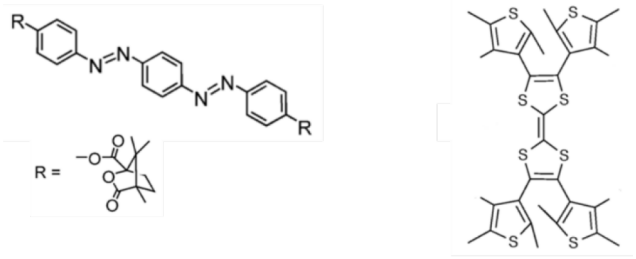

Bis-*p*-azo **DTE-dimer**

Fig. 3.1 Examples of dimers with identical subunits showing partial photochromism. [180,182]

Although the photo-switching efficiency in these symmetric dimers can be maintained for example in azobenzene-dimers by connecting the subunits in an electronically decoupled manner (*i.e.* via aliphatic chains or via perpendicular or cross-conjugated π-systems, see Fig. 3.2), selective addressability of all isomers precluded.[51,183] A judicious strategy for preparing compounds with more than two selectively addressable states and whose photo-switching efficiency is preserved is hence the covalent connection of photoswitches that have different molecular structures and are electronically decoupled from each other (*e.g.* by introducing dihedral angle, see Fig. 3.2).[184] Importantly, the spectral features of the two photochromic units must be at least partly complementary, *i.e.* their absorption bands should not completely overlap. This point is rather challenging as most (not to say all) photoswitches isomerize upon exposure to UV light, and finding enough non-overlapping absorption bands is hardly possible. The use of an additional trigger orthogonal to light can hence be beneficial.

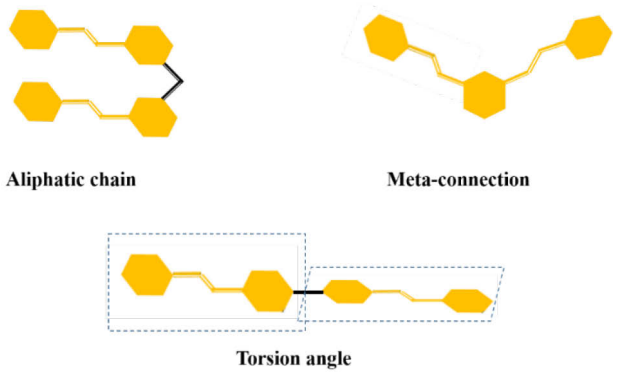

Fig. 3.2 Three connection methods for azo-dimers to maintain their photo-switching efficiency: via aliphatic chain, *meta*-connection and dihedral angles.

In this chapter, we present our strategy to connect *all-visible ortho*-tetrafluoroazobenzenes[22] to parent azobenzenes to generate 4-state compounds, whose isomers can be orthogonally addressed using different wavelengths of light or electrons. Photon/electron-induced isomerization were systemically studied by means of UV/vis spectroscopy, cyclic voltammetry, controlled-potential coulometry, and spectroelectrochemistry. Thermodynamic properties are also discussed at the end of this chapter.

3.2 Design and strategies

Photo-spectral compatibility of the subunits in multiple photoswitches is one of the crucial conditions to achieve independent addressability.[184] For this reason, we assumed that *ortho*-fluoroazobenzene derivatives (**F4**, **F4-ester**, see Fig. 3.3 left) with a parent azobenzene (**diMe**, see Fig. 3.3 left**)** would be photo-chromically compatible pairs, due to the distinct $n \longrightarrow \pi^*$ absorption bands of the *E* and *Z* isomers of *ortho*-tetrafluoroazobenzenes in the visible region, which are at least partly complementary with the parent azobenzene (see UV/vis spectra of **diMe** and **F4** in Fig. 3.3). However, this partial complementarity is not sufficient to address all 4 states independently (see Fig. 3.3 right, there is no wavelength to selectively form ZE_{F4}) because of the overlapping absorption bands of the two subunits in the UV region. Based on the knowledge of the peculiar electrochemistry of azobenzenes (see

details in section 2.1.4 Electrochemistry of fluoroazobenzenes**)**, we assumed that the fourth state ZE_{F4} could be obtained by electrocatalytic reductive isomerization, which has been shown to be independent of the intrinsic photochemical properties (separation of the absorption spectra, quantum yields) of azobenzenes. This reasoning proved successful in the case of dimer **2** (*vide infra*, section 3.6 Electrochemical studies). Ester group introduced in *para* position further separates the n ⟶ π* absorption bands (from $\Delta\lambda_{n\rightarrow\pi^*}$ = 40 nm for **F4** to 45 nm for **F4-ester**)[23] and most importantly increases the electron affinity of the azo-moiety, a crucial feature for the orthogonal isomerization of compound **2**.

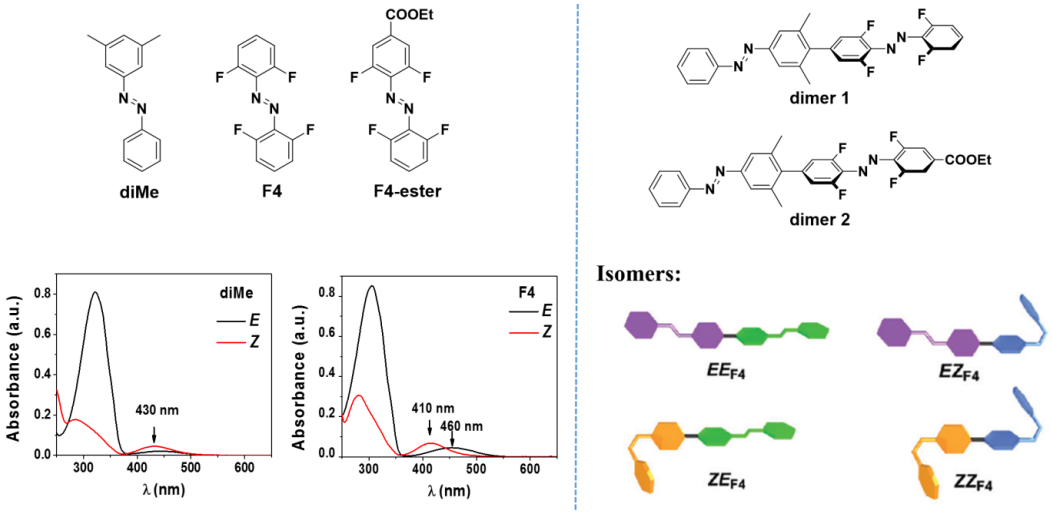

Fig. 3.3 Left: Model compounds (**diMe**, **F4** and **F4-ester**) and UV/vis spectra of **diMe** and **F4** in acetonitrile at 25 °C, c = 2.4 x 10^{-5} M. Right: molecular structures of dimer **1-2** and their corresponding four isomers.

Another important aspect to hold full addressability is the way to connect the subunits into the multiphotochromic system.[179] It is known that to keep the photo-switching efficiency in such complex systems, electronic conjugation must be precluded by connecting the photoswitches through a long liner aliphatic chain,[184,185] linking them via *meta* connection,[180,186] or introducing large dihedral angles between the moieties.[51] Besides the concern of addressability, we decided to prepare a rod-shaped mixed compound in which azobenzenes are directly connected to the *para* positions in a linear fashion (see structures of dimers **1-2**). *Ortho*-methyl groups help azobenzene units isomerizing independently within

the structure, while the rigidity and linearity of the structures are preserved. Such architectures are particularly favorable for the preparation of optomechanical systems,[187,188] which recently has been proved useful for visualizing polymers that move at surfaces upon photo-isomerization[189] and display appealing phenomena such as cooperativity or amplification when assembled into fibres[27] or crystalline thin films.[190]

3.3 Synthesis

The synthetic protocols are shown in scheme 3.1. The synthesis of model azobenzenes (**F4** and **F4-ester**) has been described in our previous studies.[22,23] Target dimers **1** and **2** were synthesized by Suzuki coupling from the corresponding bromo and pinacol ester mono-azobenzene derivatives (compounds **3**, **4**, **8** and **9**). *Para*-bromo anilines **1** and **5** were obtained via bromination with N-bromosuccinimide in good yields, followed by oxidation with Oxone® to form nitrosoarenes **2** and **6**. Since nitrosoarenes are typically unstable they were used in the next step without isolation. *Para*-bromo azobenzenes **3**, **8** and **9** subsequently obtained by condensation (Mills reaction) between the nitrosoarenes and the corresponding aniline derivatives. Note that nitrosoarene **6** is not stable in acetic acid, therefore **8** and **9** were prepared under an optimized condition in a solvents mixture (toluene/ acetic acid/trifluoroacetic acid). Compound **3** was further borylated via a Pd(0)-catalyzed coupling reaction to yield pinacol ester **4**. Dimers **1** and **2** were finally obtained via Suzuki reaction with **8** and **9**, respectively. Model compound **diMe** was prepared using the same procedure as for **3**. The detailed synthetic methods as well as corresponding characterizations are shown at the end of the chapter in the experimental section.

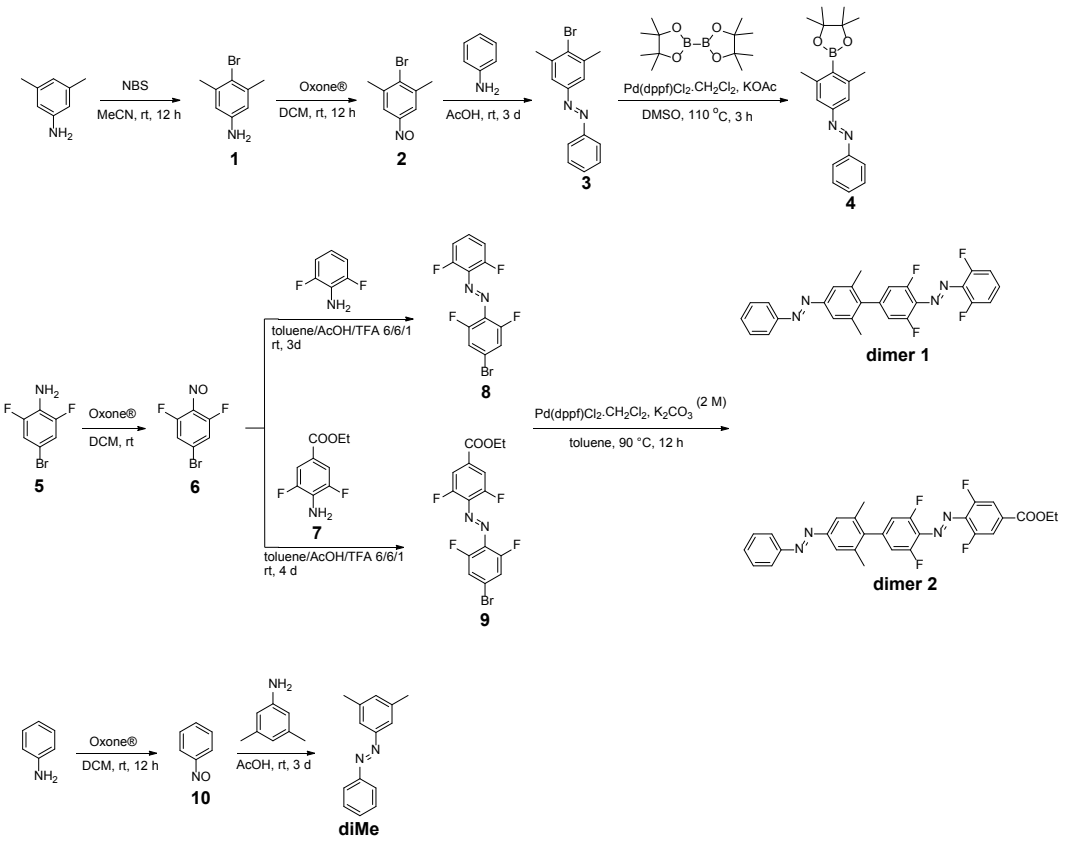

Scheme 3.1 Synthetic protocols for dimers **1-2** and model compounds.

3.4 Photo-isomerization studies

Using UV/vis spectroscopy, we investigated the photo-isomerization behavior of the dimers. Given the spectral complementarity between **diMe** and **F4**, **F4-ester** in the visible region, we envisioned that selective photo-isomerization could be achieved with at least three of the four isomers. To test this hypothesis, firstly we studied the mixture solutions of model compound **diMe** in combination with **F4** or **F4-ester**. The UV/vis spectra (see Fig. 3.4 top) and the corresponding compositions at the PSS (table 3.1) indicate that the *E*/*Z* isomerization of *ortho*-tetrafluoroazobenzenes in the mixtures can be controlled in both directions with good selectivity upon exposure to green (> 500 nm, 91% for **F4**, 95% for **F4-ester**) or blue (410 nm, 82% for **F4**, 90% for **F4-ester**) light, while the *Z* isomers of both fluorinated and parent azo-moieties are simultaneously produced upon irradiation with UV (350 nm) light. No wavelength could be found to selectively produce the *E* isomer of the fluorinated azobenzenes while keeping **diMe** in the *Z* form, however, this problem can be circumvented in dimer **2** by applying electric charges at carefully chosen potential (*vide infra*).

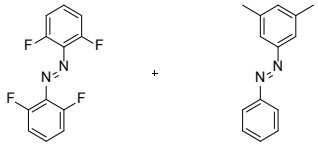

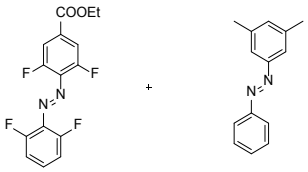

λ (nm)	PSS ratios (%)			
	E (**F4**)	*Z* (**F4**)	*E* (**diMe**)	*Z* (**diMe**)
350	8	**92**	15	**85**
> 500	9	**91**	**78**	22
405	**82**	18	**88**	12

λ (nm)	PSS ratios (%)			
	E (**F4-ester**)	*Z* (**F4-ester**)	*E* (**diMe**)	*Z* (**diMe**)
350	10	**90**	15	**85**
> 500	5	**95**	**78**	22
405	**90**	10	**85**	15

Table 3.1 PSS ratios of mixtures of model compounds: (**F4** + **diMe**, left) and (**F4-ester** + **diMe**, right) in acetonitrile at 25 °C. PSS compositions were determined by UPLC analysis using integration of the UV signal at either 442 nm (isosbestic point of **F4**) or 271 nm (isosbestic points of **F4-ester** and **diMe**).

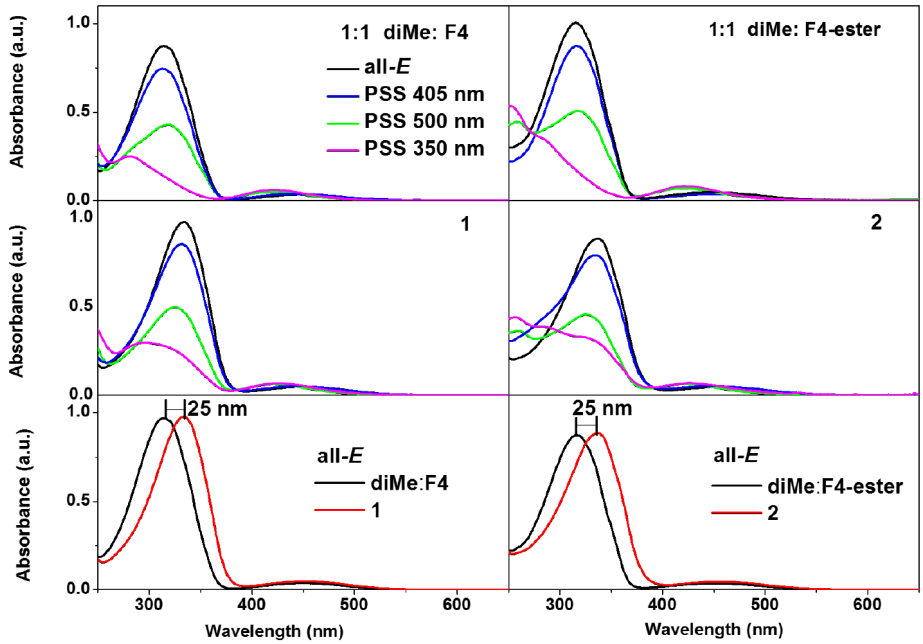

Fig. 3.4 UV/vis spectra of the mixtures of model compounds (top), dimers **1-2** (middle) and red-shift in dimer **1-2** (bottom, $\Delta\lambda_{\pi\rightarrow\pi^*}$ = 25 nm in both cases) compared to corresponding mixtures in acetonitrile at 25 °C.

Irradiation wavelength (nm)	PSS ratios (%)							
	EE_{F4}		EZ_{F4}		ZE_{F4}		ZZ_{F4}	
	1	**2**	**1**	**2**	**1**	**2**	**1**	**2**
350	6	18	10	15	10	13	**74**	**54**
405	**71**	**88**	11	8	15	4	3	0
500	3	7	**79**	**70**	0	2	18	21

Table 3.2 Compositions of dimers **1-2** at the PSSs in acetonitrile at 25 °C as determined by ^{1}H-NMR (see details in 3.9 Experimental part).

Subsequently, we investigated the switching behaviors of mixed dimers **1-2** using the same conditions as that for the mixtures (see Fig. 3.4 middle and table 3.2). The selective switching of the azobenzene moieties are somehow retained in both cases. Upon exposure to blue, green, and UV light, the three isomers EE_{F4}, EZ_{F4}, and ZZ_{F4} of dimers **1-2** could be obtained with good to high selectivity (71-79 % for **1** and 54-88 % for **2**), regardless of the initial distribution of the four isomers. The PSS ratios are in good agreement with those measured for the mixtures of the corresponding model compounds, expect for the PSS at 350 nm of **2**, which contains a lower overall amount of *Z* form compared to the **diMe**:**F4-ester** mixture (total amount of *Z* isomer of 68% for **2** *vs.* 87% for **diMe**:**F4-ester**). This trend is confirmed by comparing the absorbance spectra of the dimers with those of the corresponding mixtures (see Fig. 3.4 bottom). Moreover, for both dimers the $\pi \rightarrow \pi^*$ bands are ca. 25 nm red-shifted compared to the mixture of corresponding model compounds, indicating only partial electronic decoupling.

3.5 Thermal isomerization studies

The thermal half-lives of each unit within the dimers could be determined independently. Due to the partial electronic decoupling, as well as the big different stabilities of the *Z* isomers of isolated (*i.e.* not in the dimers) azobenzenes and *ortho*-tetrafluoroazobenzenes (a few days *vs.* up to 2 years), it appeared reasonable to simplify that around room temperature the $Z \rightarrow E$ isomerization kinetics is dominated by the dimethylazobenzene, whereas after a few hours at high temperatures, *i.e.* after almost all *Z*-dimethylazobenzenes isomerized, the kinetics will be dominated by the fluoroazobenzenes. Both sets of collected data (35-55 °C *vs.* 80-100 °C) fit

first-order exponential decays (see section 3.9 Experimental part Fig. 3.13-3.23), with thermal half-lives (at room temperature) in the order of hours for the classical azobenzene segments and days for the fluorinated moieties (see Table 3.3). Interestingly, the thermal half-lives of each photochromic unit are lowered by approximately a factor of 2 in the corresponding dimers. This decrease could arise from our experimental approximations, or more likely by the un-achieved electronic decoupling of the switches. Nevertheless, the fact that the calculated thermal half-lives of both units in the dimers have the same order of magnitude than those independently observed in solution validates our simplification.

Compound	$\tau_{1/2}$	
	diMe moiety (in hours)	**F4**/**F4-ester** moiety (in days)
diMe	109	-
F4	-	700
F4-ester	-	160
1	58	353
2	35	73

Table 3.3 Thermal half-lives of the *Z* isomers at 25 °C in DMSO as determined by UV/vis spectroscopy (see details in 3.9 Experimental part).

3.6 Electrochemical studies

Cyclic voltammetry and electrocatalytic *Z* → *E* isomerization

In order to induce the formation of the last isomer (ZE_{F4}) that could not be selectively obtained by light, we used the ability of *Z*-azobenzenes to reductively isomerize.[24,56] It is known from our previous studies that fluoroazobenzenes are more electron deficient than dimethylazobenzene, they can be reduced at lower potentials (absolute value). Hence, we speculated that selective electron-induced $ZZ_{F4} \rightarrow ZE_{F4}$ should be feasible in these dimer systems with carefully chosen reduction potentials.

To better understand the electrochemical reduction of the dimers, first of all, we investigated the cyclic voltammetric behavior of the model compounds (see Fig. 3.5). Voltammograms show typical behavior of azobenzenes with two distinct cathodic peaks ascribed to the two one-electron reduction processes. The reduction peaks of **F4** (see

Fig. 3.5 b) presented at -1.63 V and -1.94 V are a consequence of the formation of the radical anion and dianion, respectively, and the followed two reversal anodic peaks corresponding to the oxidations of the reduction products. Interestingly, the second oxidative peak, which is usually unobservable in azobenzenes due to a decomposition of the dianion,[62] can be seen clearly in the voltammogram of **F4**, suggesting that the radical dianion is stabilized by fluorine atoms. Nevertheless, it is not the case in **F4-ester**, for which only one reversible one-electron transfer (see Fig. 3.5 c, red dashed curve) with a cathodic peak at -1.38 V was observed. The absence of the anodic wave correlated to the oxidation of the second reduction peak (E_{r2} = -2.06 V) indicates an irreversible reaction, which limits the cycle to the first reduction. Most importantly, the different values of the first reduction potentials for **diMe** (-1.94 V), **F4** (-1.63 V) and **F4-ester** (-1.38 V) confirm that the fluorine-substituted azobenzenes are easier to reduce, and indicate that selective reductive isomersization of the *Z* isomer of fluorinated azobenzene in the dimers should be feasible.

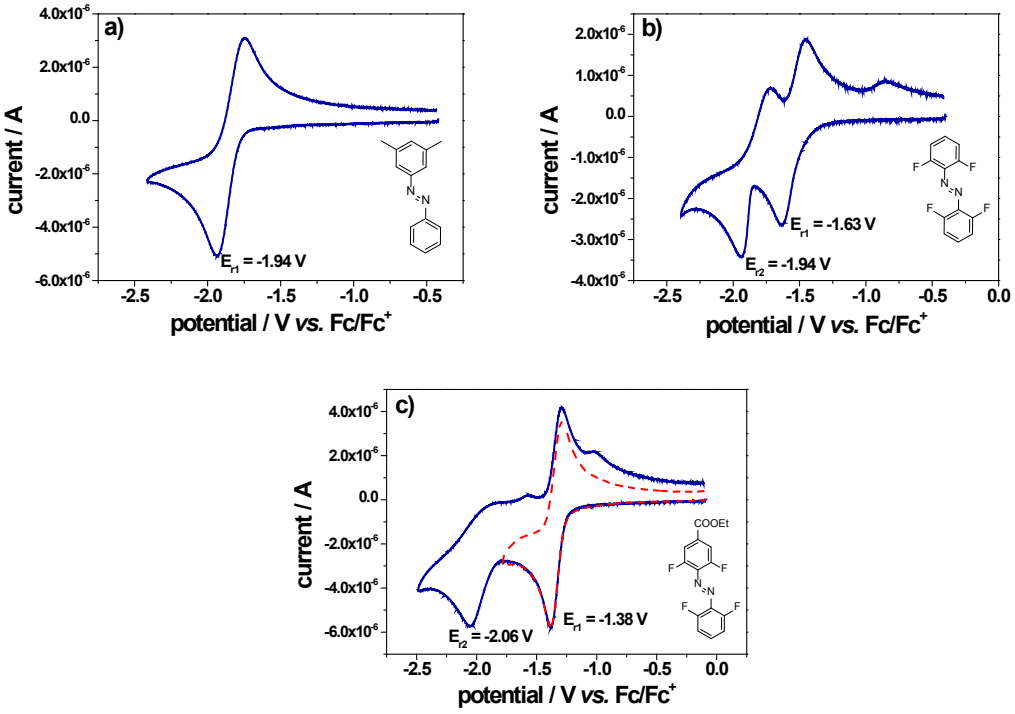

Fig. 3.5 Cyclic voltammograms of a) **diMe**, b) **F4**, and c) **F4-ester**. The red dashed curve corresponds to the reversible 1-electron process. All the solutions were prepared at a concentration of 1 x 10^{-3} M in acetonitrile (HPLC-grade, dried over calcium hydride and distilled) containing 0.1 M Bu_4NPF_6, Pt-electrode (d = 1 mm), Fc/Fc^+ as external standard, dE/dt = 1V s^{-1}.

Subsequently, the cyclic voltammetry experiments for dimers **1**-**2** were carried out with a ZZ_{F4} isomer enriched solution, as shown in Figures 3.6 a and b, respectively. The potential was measured from 0 to -2.0 V and back to 0 V. Based on our previous study (details described in section 2.1.4 Electrochemistry of fluoroazobenzenes), we know that the electron induced $Z \rightarrow E$ isomerization follows a rapid catalytic process. As soon as sufficient *Z*-configured radical anions are formed, they immediately catalyze and drive to completion the $Z \rightarrow E$ isomerization, therefore the reduction waves of the *Z* isomers cannot be differentiated from those of the *E* isomers.[24] As a consequence, the observed reduction waves in fact belong to the *E*-isomers. In the case of **1**, two reversible reduction waves appear at E_{r1} = -1.63 V and E_{r2} = -1.94 V, corresponding to the first reduction of **F4** and the concomitant second reduction of **F4** and first reduction of **diMe**. In the case of **2**, two successive reduction

waves are observed at E_{r1} = - 1.35 V and E_{r2} = -1.85 V, corresponding to the first reduction of **F4-ester**, and the concomitant first reduction of **diMe** and second reduction of **F4-ester**, respectively. The quasi-reversible process seen in the voltammogram of **2** arises from the nonreversible second reduction of **F4-ester**. Importantly, the *para*-ester group in dimer **2** increases the separation of the reduction potentials.

Solutions enriched in ZZ_{F4} were then placed in a coulometric cell and subjected to a carefully chosen reduction potential (E_{r0} = -1.3 V for **1** and -1.1 V for **2**) sufficient to induce the first reduction events of the Z_{F4} units. To better observe the species generated during the course of reduction, liquid chromatography was used for monitoring the process (see Fig. 3.6 c-d, Fig. 3.7). Note that the chromatograms do not reflect the exact composition of the solutions, as no isosbestic point can be used for integrating the peaks in the case of such mixtures containing four isomers. The processes were finished after injecting 5 mol% of electrons (calculated on the basis of the initial total concentration of EE_{F4} prior to UV light irradiation), confirming the auto-catalytic nature of the electron-induced $Z \rightarrow E$ isomerization in **1**-**2**. However, from the UPLC analytical results (Fig.3.6 c and d, Fig. 3.7 a and b), the eventual compositions recorded after finishing the injection of electrons at E_{r0} are quite different. In the case of **1**, all isomers convert back to EE_{F4}, ending up in a solution containing exclusively this isomer (Fig. 3.6 c, Fig. 3.7 a), whereas in **2** only the *Z*-fluoroazobenzenes isomerize leaving the *Z*-dimethylazobenzene moieties unaffected (Fig. 3.6 d, Fig. 3.7 b), similar like in the case of the mixture (Fig. 3.7 d). The lack of selectivity in the electron-induced isomerization of **1** can be likely explained by the rather small difference in reduction potential $\Delta E_r = E_{r1} - E_{r2}$ = 0.3 V, indicating comparable LUMOs energies. Electron transfer might then occur from $E_{F4}^{\bullet-}$ to both neutral Z_{F4} and Z_{diMe} and hence the propagation takes place within both moieties, *i.e.* the catalytic cycle is not selective. On the other hand, for **2** the difference ΔE_r = 0.5 V is large enough to prevent electron transfer between these two moieties, *i.e.* $E_{F4}^{\bullet-} + Z_{diMe} \rightarrow E_{F4} + Z_{diMe}^{\bullet-}$ is impossible and the catalytic cycle proceeds exclusively within the fluorinated moiety. As a result, starting from a solution enriched in ZZ_{F4} as obtained upon exposure to UV light (*i.e.* containing 54 % of ZZ_{F4}, see Table 3.2), one ends with a solution comprising 67 % of ZE_{F4}-**2** and 33 % of EE_{F4}-**2**.

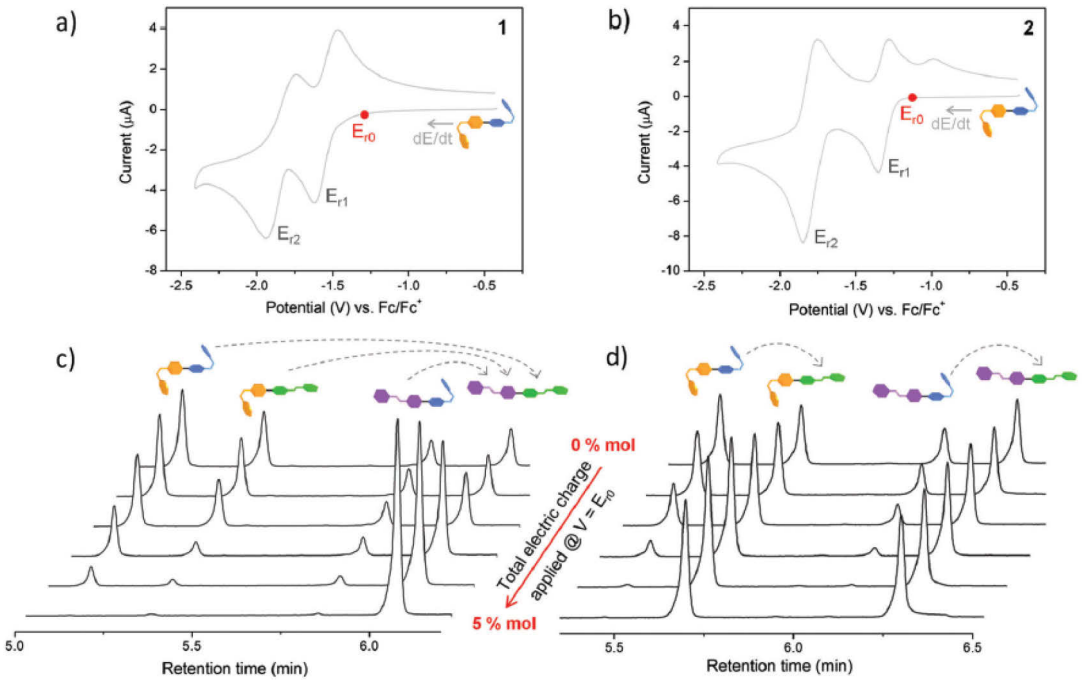

Fig. 3.6 Electron-induced $Z \rightarrow E$ isomerization in four-state switches **1**-**2**. Cyclic voltammograms of 10^{-3} M solutions of **1** (a) and **2** (b) pre-irradiated at 365 nm to enrich the solution in the ZZ_{F4} isomer. Time evolution of 1.5 x 10^{-5} M solutions of ZZ_{F4}-riched **1** (c) and **2** (d) upon potentiostatic coulometry at V = E_{r0}, as recorded by liquid chromatography (diode array detector). After applying a cumulated electric charge corresponding to 5 mol% of the initial concentration, the solution of **1** contains only EE_{F4}, whereas in the solution of **2** only the fluorinated moiety isomerized.

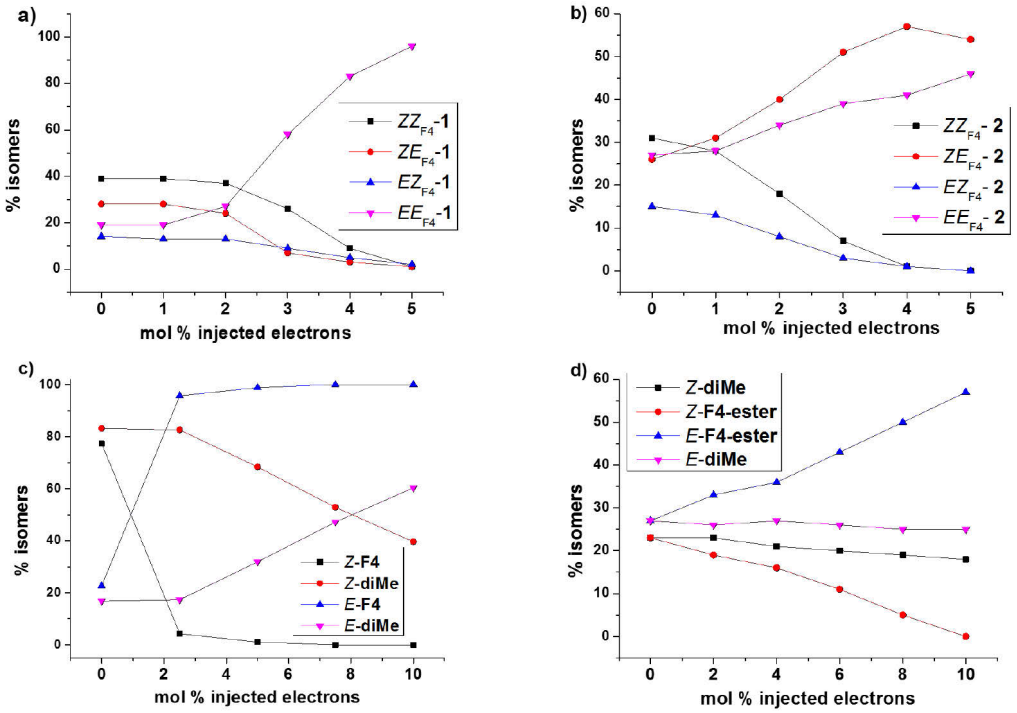

Fig. 3.7 Changes of the isomer ratios during the cathodically initiated $Z \longrightarrow E$ isomerization at E_{r0} calculated by UPLC analysis. a) dimer **1**, b) dimer **2**, c) mixture of **diMe**/**F4**, d) mixture of **diMe**/**F4-ester**.

Using the same conditions, cathodically initiated $Z \rightarrow E$ isomerization was also performed with the corresponding mixture solutions (see Fig. 3.7 c and d). In opposition to what we observed for dimer **1**, when a UV light pre-irradiated mixture solution of model compounds **F4** and **diMe** subjected to the same potential as that used for **1** (E_{r0} = -1.3 V), the reduction is mostly selective, *i.e.* at the end of the process only a few % of Z_{diMe} isomerized back while Z_{F4} was quantitatively converted to the *E*-isomer (see Fig. 3.7 c). This partial selectivity is certainly concentration dependent and might be lost at high concentration. For the mixture of **diMe**/**F4-ester**, unsurprisingly, selective isomerization of $Z_{F4\text{-ester}}$ with quantitative conversion was achieved via applying the same amount of electrons as that used for **2** (E_{r0} = -1.1 V). Nevertheless, in both cases more electrons are necessary for isomerizing the mixtures than that used for dimers. The process was finished after injecting around 10% of elections, indicating intramolecular electron transfer occurred in dimers.

3.7 Spectroelectrochemical studies

Optical absorption spectroscopy was also used as an alternative method during the cyclovoltammetry measurements in order to investigate the composition changes during the redox processes (see Fig. 3.8 and 3.9). The solutions were first irradiated with UV light in order to enrich them in *ZZ*-states. The reduction potential was applied at a speed of 10 mV/s and the corresponding UV/vis spectra were recorded every 10 mV.

In the case of **1**, upon increasing the reductive potential the spectra undergo a dramatic increase in the $\pi \rightarrow \pi^*$ band as well as a concomitant red-shift in the $n \rightarrow \pi^*$ band (see Fig. 3.8 a). The spectral change clearly shows that *ZZ*-enriched $\longrightarrow$ EE_{F4} isomerization already takes place at a potential of -1.20 V and has completed at the potential of -1.35 V (red-dot range in cyclic voltammogram) far before reaching the potential of the cathodic peak, which is in good agreement with the previous observation made by UPLC. The reductive isomerization is confirmed in the isolated UV/vis spectra highlighted within figure 3.8 a, where the spectra observed after reduction (red curve) and initial pure *EE* isomer (blue curve) are identical. Further increase of the reductive potential (blue-triangle in Fig. 3.8 b) leads to a strong decrease in the absorbance of the $\pi \rightarrow \pi^*$ band corresponding to the formed EE_{F4} isomer and apparition of new red-shifted bands at 416 nm and 510 nm attributed to the formation of the radical anion $EE_{F4}^{\bullet -}$, which is confirmed by the identical spectra of that observed in the direct reduction of EE_{F4} as shown in 3D spectroscopy (see Fig. 3.8 c and d). After completion of the redox cycle (0 V $\rightarrow$ -1.60 V $\rightarrow$ 0 V), the final spectra show that the EE_{F4} isomer is recovered, indicating a reversible reductive process.

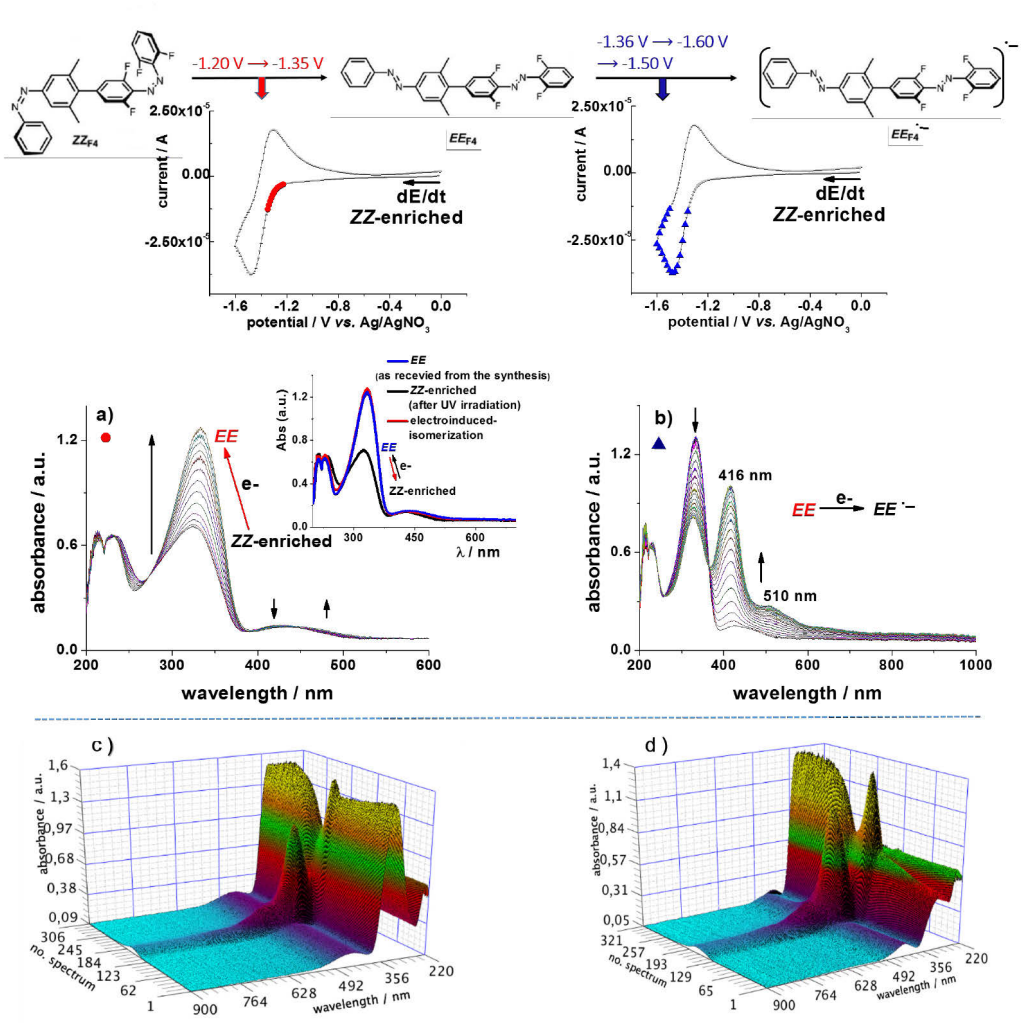

Fig. 3.8 UV/vis spectral changes during cyclovoltammetry of *ZZ*-enriched **1** solution, c = 5 x 10^{-4} M in acetonitrile containing 0.1 M Bu_4NPF_6, Pt-electrode, dE/dt = 10 mV/s.

(a) Initial quantitative *ZZ*-enriched ⟶ EE_{F4} isomerization in the range from -1.20 V to -1.35 V as well as corresponding isolated spectra of *ZZ*-enriched (black), electron-induced isomerization (red) and initial pure *EE* (blue). (b) The generation of the $EE_{F4}^{\bullet-}$ radical anion in the range from -1.36 V to -1.60 V and back to -1.50 V (blue-triangle range).

3D spectro-electrochemical plots (x, wavelength; y, time as the number of recorded spectra, from 1 to ca. 300; z, absorbance, following the cycle 0 V → -1.60 V → 0 V) of **1**

(c) starting from the *EE*-isomer and (d) starting from the *ZZ*-enriched isomer.

In the case of dimer **2** (see Fig. 3.9), electrocatalytic *Z* → *E* isomerization was also observed but the initial spectrum of the *EE*-isomer was not recovered, and *i.e.* the

ZZ-enriched ⟶ ZE_{F4} process took place selectively in the range from -0.90 V to -1.15 V. This can be seen clearly in the isolated UV/vis spectra highlighted within the figure 3.9 a, where the red curve corresponds to the species formed at the reduction potential of -1.15 V (end of the red-dot range). Its π → π* band is more intense than the starting *ZZ* – enriched solution (black curve) but weaker than the initial pure *EE* solution (blue curve), confirming that the Z_{diMe} moiety was not affected. Subsequent increase of the reductive potential (see Fig. 3.9 b) leads to the formation of radical anions mixture ($EE^{\bullet -}$ and $ZE_{F4}^{\bullet -}$). As observed in the case of dimer **1**, the process is reversible (see 3D spectra, Fig. 3.9 bottom), with the spectrum attributed to *EE* isomer being recovered at the end of the cycle from 0 V to -1.50 V and back to 0 V.

Eventually, the orthogonal isomerization was realized in dimer **2** via applying a catalytic amount of electrons.

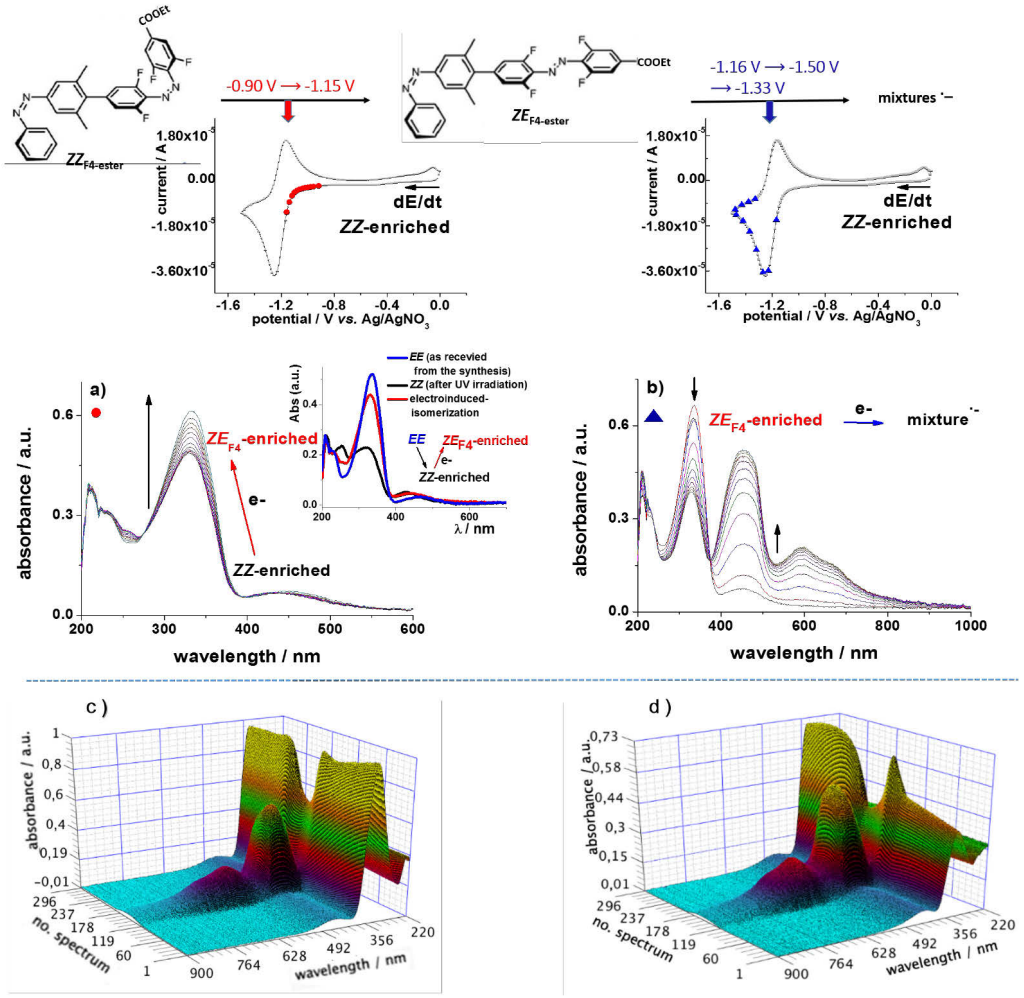

Fig. 3.9 UV/vis spectral changes during cyclovoltammetry of *ZZ*-enriched **2** solution, c = 5 x 10^{-4} M in acetonitrile containing 0.1 M Bu_4NPF_6, Pt-electrode, dE/dt = 10 mV/s.

(a) Initial quantitative *ZZ*-enriched ⟶ EE_{F4} isomerization in the range from -0.90 V to -1.15 V as well as corresponding isolated spectra of *ZZ*-enriched (black), electron-induced isomerization (red) and initial pure *EE* (blue). (b) The generation of the $EE_{F4}^{\bullet-}$ radical anion in the range from -1.16 V to -1.50 V and back to -1.33 V (blue-triangle range).

3D spectro-electrochemical plots (x, wavelength; y, time as the number of recorded spectra, from 1 to ca. 300; z, absorbance, following the cycle 0 V → -1.50 V → 0 V) of **2**.

(c) starting from the *EE*-isomer and (d) starting from the *ZZ*-enriched isomer.

3.8 Conclusion

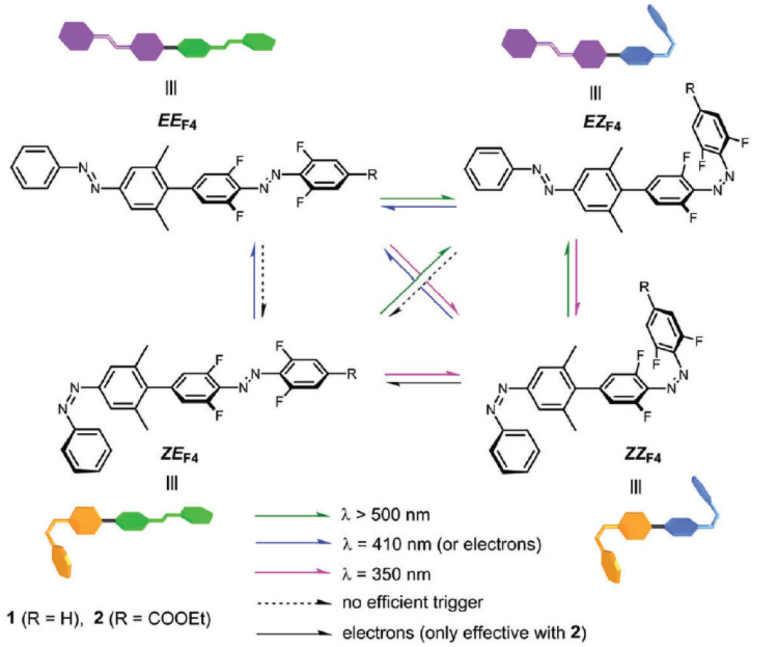

Fig. 3.10 Orthogonal switching between the four states of azobenzene-mixed dimers **1**-**2** triggered by light and electrons.

In summary, we have realized a strategy for constructing multi-photochromic systems with selective addressability (see Fig. 3.10). Owing to the (partial) orthogonality of the classical azobenzene and the fluoroazobenzene in photo- and electro-chemistry, the isomerization of each subunit in dimer **2**, whose electron affinity is enhanced by the electron-withdrawing *para*-ester group, can be controlled independently. The twisted connection arising from the dimethyl groups in this structure ensures that these two azo units remain somehow decoupled, an important condition to achieve orthogonal control in this design. Given the current interest in the development of synthetic (supra)molecular systems that exhibit directionally controlled relative motions of their components, which are useful tools for catalysis, smart materials, energy conversion and storage and medical therapy, we expect our systems to foster further research developments and be used for future practical applications.

3.9 Experimental part

General Information

Materials were purchased from commercial suppliers and used without further purification. Reactions were monitored by thin layer chromatography (TLC) carried out on silica gel plates (Merck 60F‐254) using UV light for visualization. Silica gel (Merck 60/VWR, particle size 0.040–0.063 mm) was used for column chromatography. NMR spectra were recorded on a Bruker 300 MHz (75 MHz for ^{13}C). Chemical shifts (δ) are reported in ppm from the solvent resonance as the internal standard (^{1}H-NMR: δ ($CDCl_3$) = 7.26 ppm, δ (CD_2Cl_2) = 5.32 ppm (THF-d_8) = 1.72, 3.58 ppm and ^{13}C-NMR: δ ($CDCl_3$) = 77.16 ppm, δ (CD_2Cl_2) = 53.84 ppm, (THF-d_8) = 67.21, 25.31 ppm). Data are reported as follows: chemical shift, multiplicity (s = singlet, d = doublet, t = triplet, q = quartet, m = multiplet), coupling constants (Hz) and integration. Ultraperformance liquid chromatography coupled to mass spectrometry detection (UPLC-MS) was performed with a Waters Alliance systems (gradient mixtures of acetonitrile/water) equipped with Acquity UPLC columns. The Waters systems consisted of a Waters Separations Module 2695, a Waters Diode Array detector 996, a LCT Premier XE mass spectrometer, and a Waters Mass Detector ZQ 2000.

Synthetic procedures and characterization of products

Standard procedure for oxidation of aniline to nitrosoarene derivatives

To a solution of aniline derivative (1 equiv) in DCM was added an aqueous solution of Oxone® ($KHSO_5.^1/_2KHSO_4.^1/_2K_2SO_4$, 2 equiv per amine group), DCM/H_2O:4/5. The reaction was stirred for 12 h at room temperature. The two phases were separated, the organic phase was washed with distilled water, dried over Na_2SO_4, filtered, and concentrated under reduced pressure. The resulting (nitroso) green oils are typically unstable and hence were used without further purification in the subsequent step (Mills reaction).

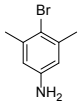

4-bromo-3,5-dimethylaniline (1): To a solution of 3,5-dimethylaniline (3.00 g, 24.79 mmol) in acetonitrile (100 mL) was added *N*-Bromosuccinimide (4.41 g, 24.79 mmol) and the solution was stirred overnight at room temperature. The reaction mixture was concentrated under reduced pressure and the residue was purified by column

chromatography (petroleum ether/ethyl acetate: 50/1 to 5/1) to give **1** as a white solid (1.64 g, 33%). ^{1}H NMR (300 MHz, CD_2Cl_2) δ ppm 6.43 (s, 2H), 3.60 (s, 2H), 2.29 (s, 6 H). ^{13}C NMR (75 MHz, CD_2Cl_2) δ ppm 146.0, 139.2, 115.8, 115.4, 24.1. HRMS-ESI: *m/z* = 200.0083 (calcd for $[M + H]^+$, 200.0075).

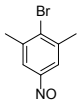

4-bromo-3,5-dimethylnitrosobenzene (2): The standard procedure for the oxidation of aniline to nitrosoarene was used with **1** (500 mg, 2.50 mmol) in DCM (20 mL) and Oxone® (3.07 g, 10.00 mmol) in H_2O (25 mL) to give **2** as a deep green liquid that was used as such in the next step.

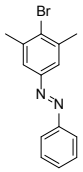

4-bromo-3,5-dimethylazobenzene (3): To a solution of **2** (535 mg) in AcOH (10 mL) was added aniline (186 mg, 2.00 mmol) and the mixture was stirred for 3 days at room temperature. The resulting solution was diluted with water (200 mL), extracted with ethyl acetate, the organic phase was dried over Na_2SO_4, filtered and concentrated under reduced pressure. The residue was purified by column chromatography (petroleum ether) to give **3** as a red solid (186 mg, 32%). ^{1}H NMR (300 MHz, $CDCl_3$) (*E*-isomer) δ ppm 7.93 (dd, *J* = 8.1, 1.8 Hz, 2H), 7.66 (s, 2H), 7.56-7.48 (m, 3H), 2.53 (s, 6 H). ^{13}C NMR (75 MHz, $CDCl_3$) (*E*-isomer) δ ppm 152.6, 150.8, 139.2, 131.1, 130.5, 129.1, 122.8, 122.2, 24.0. HRMS-ESI: m/z = 289.0338 (calcd for $[M + H]^+$, 289.0340).

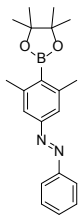

Pinacol boronic(azobenzene)ester (4): A solution of **3** (414 mg, 1.43 mmol), 4,4,4',4',5,5,5',5'-octamethyl-2,2'-bi(1,3,2-dioxaborolane) (436 mg, 1.72 mmol), $Pd(dppf)Cl_2.CH_2Cl_2$ (117 mg, 0.14 mmol), and KOAc (421 mg, 4.30 mmol) in DMSO (15 mL) was stirred for 3 hours at 110 °C. After cooling down, the solution was diluted with water (200 mL), extracted with ethyl acetate, the organic phase was dried over Na_2SO_4, filtered and concentrated under reduced pressure. The residue was purified by column chromatography (petroleum ether) to give **4** as a red solid (210 mg, 44%). ^{1}H NMR (300 MHz, $CDCl_3$) (*E*-isomer) δ ppm 7.93-7.90 (m, 2H), 7.53-7.51 (m, 3H), 7.49-7.47 (m, 2H), 2.50 (s, 6H), 1.42 (s, 12H). ^{13}C NMR (75 MHz, $CDCl_3$) (*E*-isomer) δ ppm 152.7, 143.0,

130.9, 129.1, 122.8, 120.8, 84.0, 25.0, 22.2. HRMS-ESI: m/z = 337.2112 (calcd for $[M + H]^+$, 337.2087).

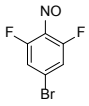

4-bromo-1,6-difluoronitrosobenzene (6): The standard procedure for the oxidation of aniline to nitrosoarene was used with **5** (1.51 g, 7.25 mmol) in DCM (20 mL) and Oxone® (8.90 g, 29.00 mmol) in H_2O (25 mL) to give **6** as a deep green liquid that was used as such in the next step.

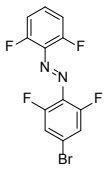

4-bromo-F_4-azobenzene (8): To a solution of **6** (1.61 g) in toluene/AcOH/TFA (6/6/1) (13 mL) was added 2,6-difluoroaniline (0.75 g, 5.80 mmol) and the solution was stirred for 3 days at room temperature. The resulting solution was diluted with water (200 mL), extracted with ethyl acetate, the organic phase was dried over Na_2SO_4, filtered and concentrated under reduced pressure. The residue was purified by column chromatography (CH_2Cl_2/petroleum ether: 1/5) to give **8** as a red solid (1.84 g, 95%). ^{1}H NMR (300 MHz, $CDCl_3$) (*E*-isomer) δ ppm 7.44-7.36 (m, 1 H), 7.27 (d, J = 8.1 Hz, 2H), 7.06 (t, J = 9.1 Hz, 2H). ^{13}C NMR (75 MHz, $CDCl_3$) (*E*-isomer) δ ppm 157.3, 153.8, 131.8, 123.9, 116.7, 116.5, 112.8, 112.5. HRMS-ESI: m/z = 332.9642 (calcd for $[M + H]^+$, 332.9650).

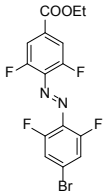

4-bromo-4'-ester-F_4-azobenzene (9): To a solution of **6** (266 mg) in toluene/AcOH/TFA (6/6/1) (10 mL) was added **7** (0.19 g, 0.96 mmol) and the mixture was stirred for 4 days at room temperature. The resulting solution was diluted with water (50 mL), extracted with ethyl acetate, the organic phase was dried over Na_2SO_4, filtered and concentrated under reduced pressure. The residue was purified by column chromatography (CH_2Cl_2/petroleum ether: 1/20) to give **9** as a red solid (60 mg, 18%). ^{1}H NMR (300 MHz, $CDCl_3$) (*E*-isomer) δ ppm 7.73 (d, J = 8.8 Hz, 2H), 7.30 (d, J = 8.2 Hz, 2H), 4.42 (q, J = 7.1 Hz, 2H), 1.43 (t, J = 7.1 Hz, 3H). ^{13}C NMR (75 MHz, $CDCl_3$) (*E*-isomer) δ ppm 156.7, 117.0, 116.7, 114.0, 113.7, 62.1, 14.2. HRMS-ESI: m/z = 404.9858 (calcd for $[M + H]^+$, 404.9862).

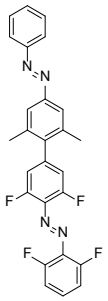

dimer **1:** To a solution of **8** (173 mg, 0.52 mmol), **4** (210 mg, 0.62 mmol), and Pd(dppf)Cl_2.CH_2Cl_2 (42 mg, 0.05 mmol) in toluene (5 mL) was added 2M aqueous K_2CO_3 (0.8 mL), and the solution was stirred overnight at 90 °C. After cooling, the solution was diluted with water (100 mL), extracted with ethyl acetate, the organic phase was dried over Na_2SO_4, filtered and concentrated under reduced pressure. The residue was purified by column chromatography (petroleum ether/ethyl acetate: 100/1 to 50/1) to give **dimer 1** as a red solid (148 mg, 62%). ^{1}H NMR (300 MHz, CD_2Cl_2) (*E,E*-isomer) δ ppm 7.96-7.92 (m, 2H), 7.71 (s, 2H), 7.59-7.51 (m, 3H), 7.49-7.39 (m, 1H), 7.16-7.09 (m, 2H), 6.97 (d, *J* = 9.3 Hz, 2H), 2.22 (s, 6H). ^{13}C NMR (75 MHz, CD_2Cl_2) (*E,E*-isomer) δ ppm 157.5, 152.6, 152.0, 136.9, 131.8, 131.1, 129.1, 122.8, 121.8, 113.7, 113.4, 112.8, 112.6, 20.5. HRMS-ESI: *m/z* = 463.1559 (calcd for $[M + H]^+$, 463.1546).

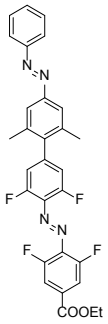

dimer **2:** To a solution of **9** (60 mg, 0.15 mmol), **4** (60 mg, 0.18 mmol), and Pd(dppf)Cl_2.CH_2Cl_2 (11 mg, 0.02 mmol) in toluene (1.5 mL) was added 2M aqueous K_2CO_3 (0.2 mL), and the mixture was stirred for 5 hours at 90 °C. After cooling, the solution was diluted with water (20 mL), extracted with ethyl acetate, the organic phase was dried over Na_2SO_4, filtered and concentrated under reduced pressure. The residue was purified by column chromatography (petroleum ether/CH_2Cl_2: 20/1) to give **dimer 2** as a red solid (46 mg, 59%). ^{1}H NMR (300 MHz, $CDCl_3$) (*E,E*-isomer) δ ppm 7.94 (dd, *J* = 8.31, 1.56 Hz, 2H), 7.73 (d, *J* = 8.8 Hz, 2H), 7.70 (s, 2H), 7.57-7.49 (m, 3H), 6.95 (d, *J* = 10.6 Hz, 2H), 4.43 (q, *J* = 11.9 Hz, 2H), 2.21 (s, 6H), 1.44 (t, *J* = 7.1 Hz, 3H). ^{13}C NMR (75 MHz, $CDCl_3$) (*E,E*-isomer) δ ppm 152.6, 152.2, 136.7, 131.1, 129.1, 122.9, 122.0, 114.0, 113.7, 113.5, 62.1, 20.8, 14.2. HRMS-ESI: *m/z* = 535.1774 (calcd for $[M + H]^+$, 535.1757).

nitrosobenzene (10): The standard procedure for the oxidation of aniline to nitrosoarene was used with aniline (1.00 g, 10.70 mmol) in DCM (40 mL) and Oxone® (9.90 g, 32.20 mmol) in H_2O (50 mL) to give **10** as a deep green liquid that was used as such in the next step.

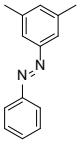

3,5-dimethyl-azobenzene (diMe): To a solution of **10** (1.15 g) in AcOH (20 mL) was added 3,5-dimethylaniline (1.00 g, 8.60 mmol) and the solution was stirred for 3 days at room temperature. The resulting solution was diluted with water (200 mL), extracted with ethyl acetate, the organic phase was dried over Na_2SO_4, filtered and concentrated under reduced pressure. The residue was purified by column chromatography (petroleum ether) to give **diMe** as an orange solid (400 mg, 22%). ^{1}H NMR (300 MHz, $CDCl_3$) (*E*-isomer) δ ppm 8.00 (d, J = 7.9 Hz, 2H), 7.64 (s, 2H), 7.60-7.49 (m, 3H), 7.17 (s, 1H), 2.47 (s, 6H). ^{13}C NMR (75 MHz, $CDCl_3$) (*E*-isomer) δ ppm 152.9, 152.8, 138.8, 132.8, 130.9, 129.1, 122.9, 120.8, 21.3. HRMS-ESI: m/z = 211.1222 (calcd for $[M + H]^+$, 211.1235).

Photo-isomerization studies

UV/Vis absorption spectra were recorded using quartz cuvettes on a Cary 50 spectrophotometer equipped with a Peltier-thermostated cell holder (temperature accuracy ± 0.1 °C). The solvents used were of spectrophotometric grade. Irradiation experiments were performed using a LOT-Oriel 1000 W medium-pressure Xe/Hg lamp equipped with band-pass filters.

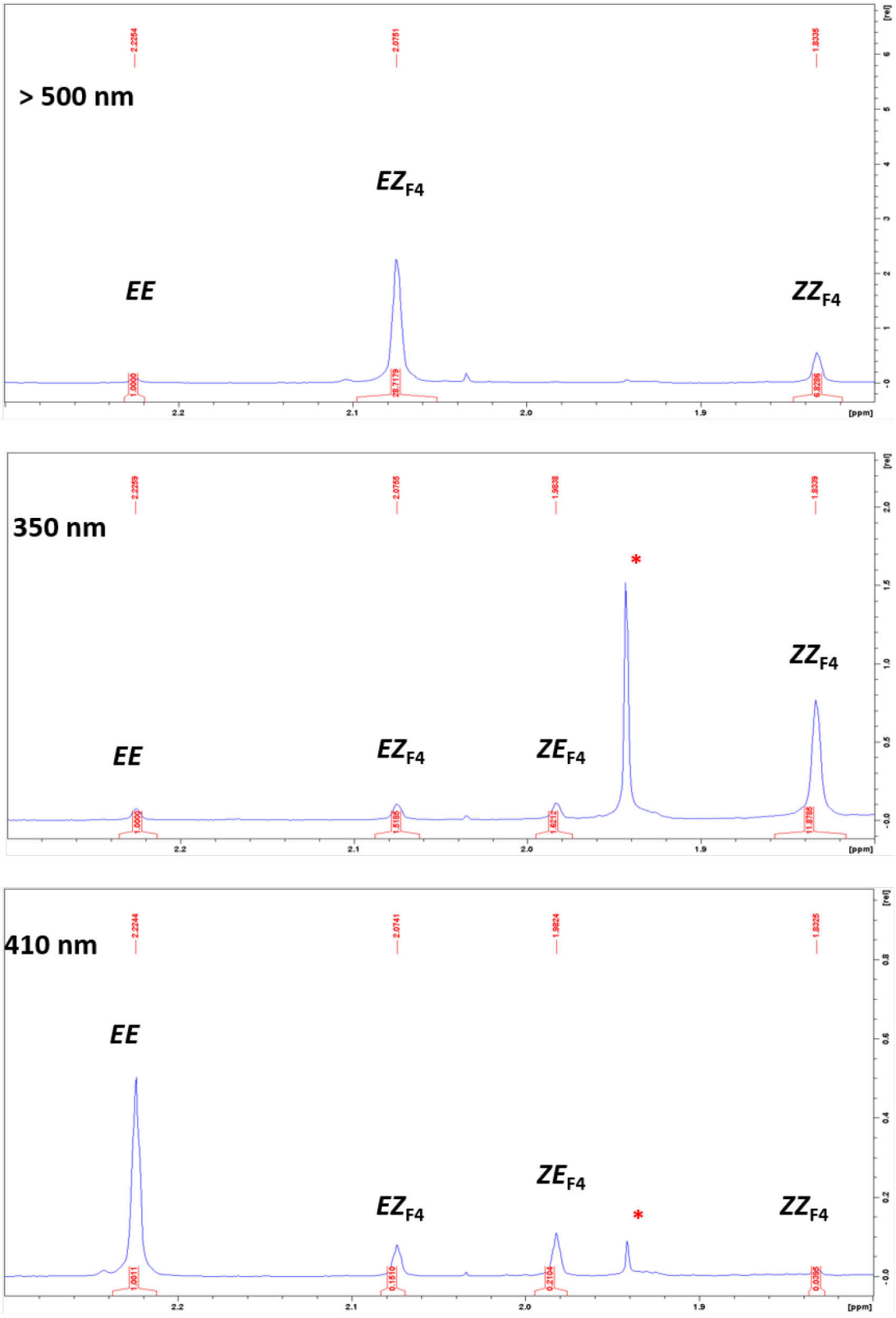

Fig. 3.11 ^{1}H NMR (aliphatic region, integration of the *ortho*-Me groups) of the PSS mixtures of dimer **1** at different wavelengths (*: MeCN). Solutions were irradiated ex-situ in MeCN, evaporated, and dissolved in THF-d_8 prior to measurement.

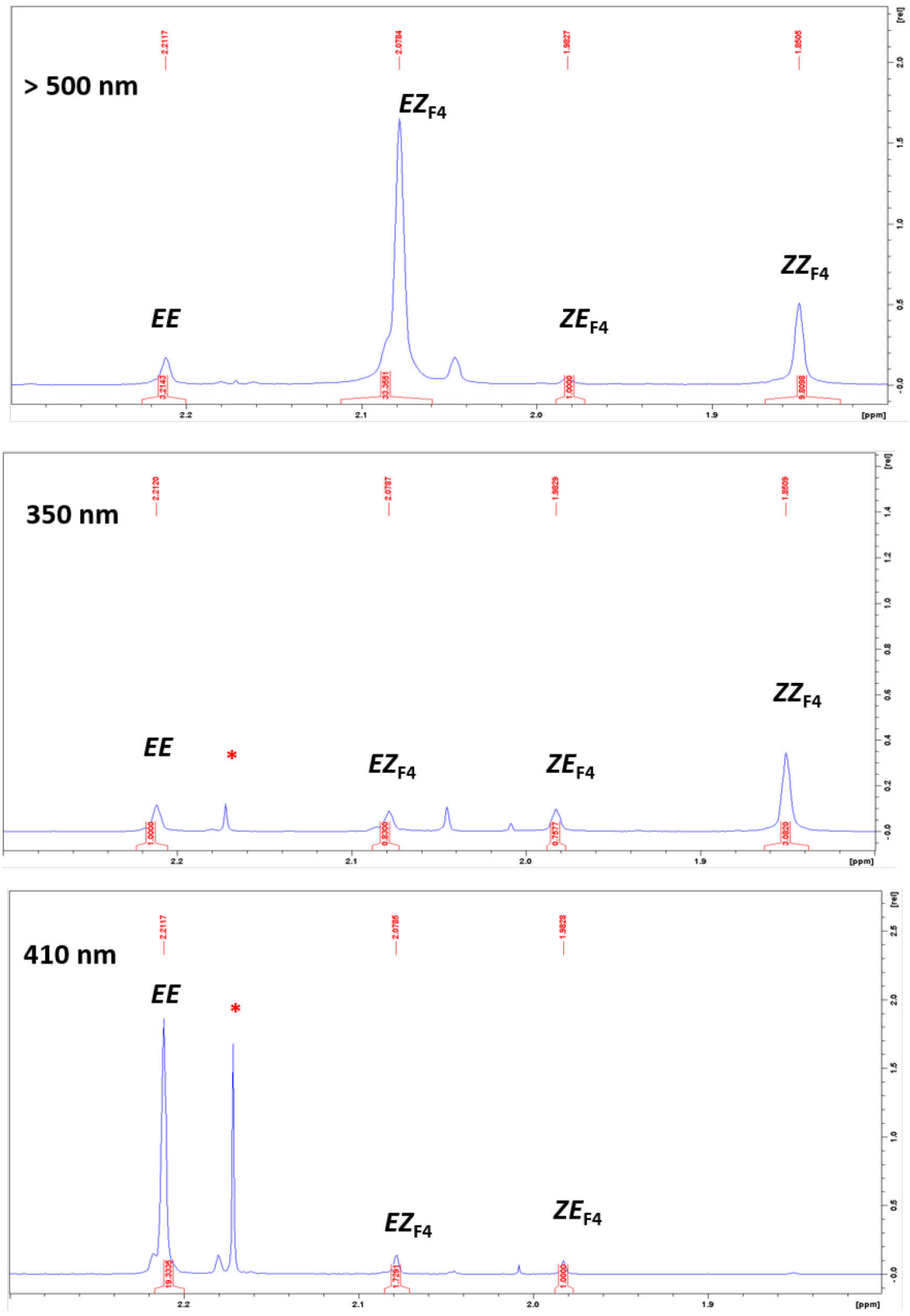

Fig. 3.12 ^{1}H NMR (aliphatic region, integration of the *ortho*-Me groups) of the PSS mixtures of dimer **2** at different wavelengths (*: acetone). Solutions were irradiated ex-situ in MeCN, evaporated, and dissolved in $CDCl_3$ prior to measurement.

Kinetics studies

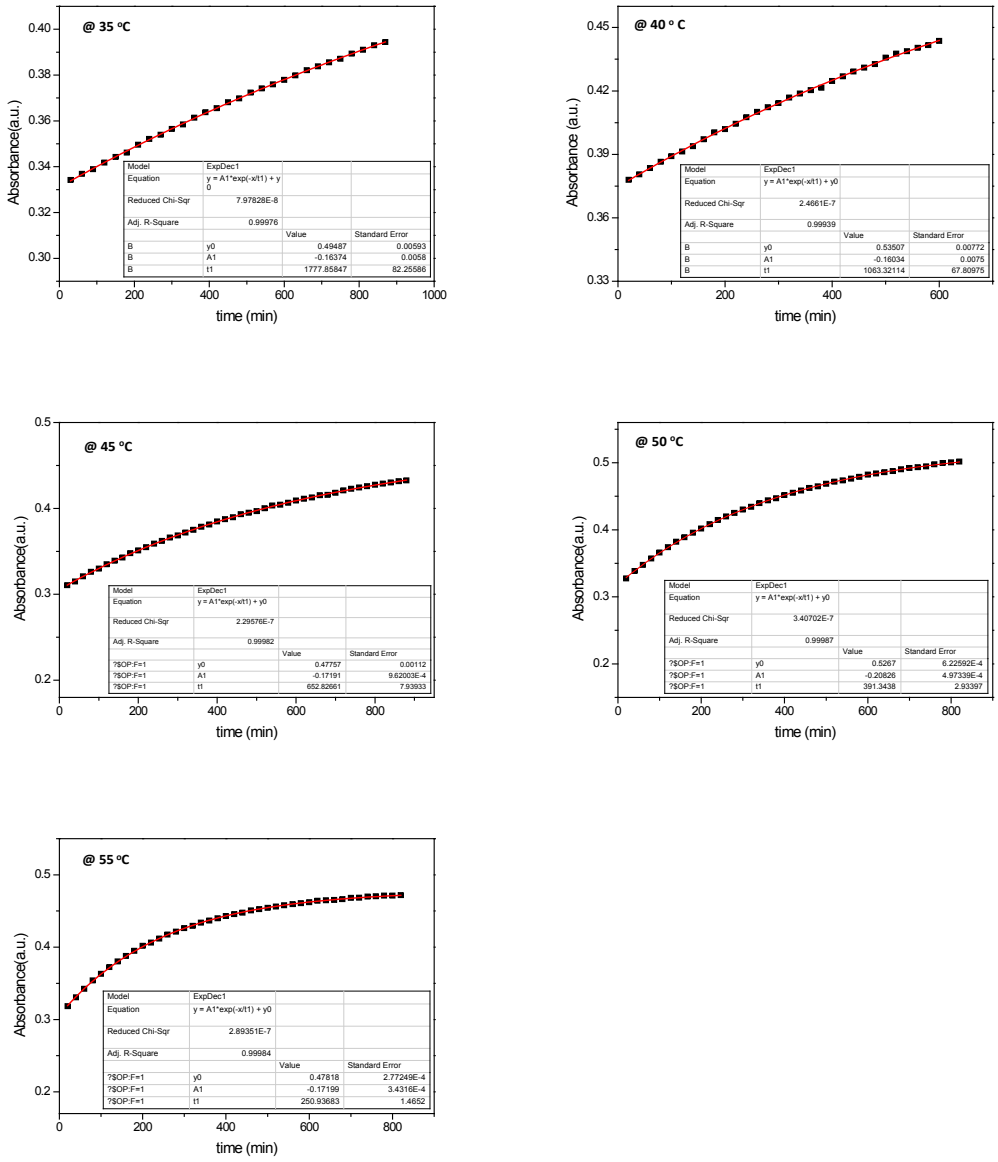

Fig. 3.13 Thermal *Z*/*E* isomerization in dimer**1** (DMSO): plots of absorbance at 335 nm (λ_{max}) versus time (minutes) at middle-range temperatures (35 °C, 40 °C, 45 °C, 50 °C and 55 °C) fitted with a first-order exponential decay.

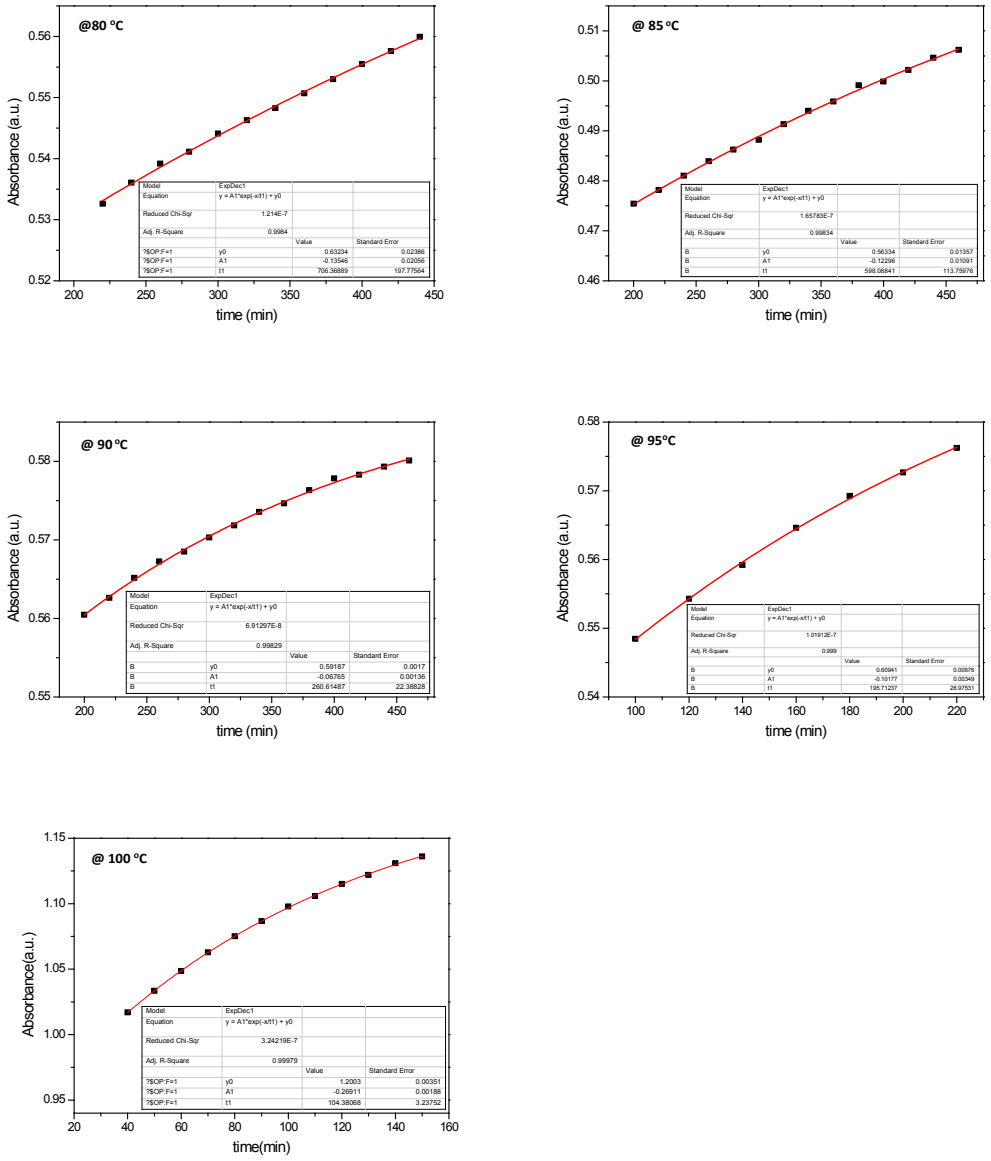

Fig. 3.14 Thermal *Z*/*E* isomerization in dimer **1** (DMSO): plots of absorbance (after removal of the first data points) at 335 nm (λ_{max}) versus time (minutes) at higher temperatures (80 °C, 85 °C, 90 °C, 95 °C and 100 °C) fitted with a first-order exponential decay.

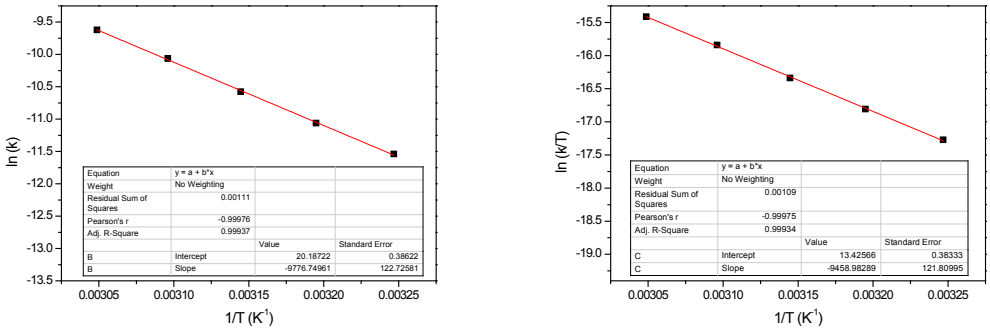

k (s^{-1})	$\tau_{1/2}$ (h)	A (s^{-1})	Ea ($kJ.mol^{-1}$)	$\Delta H^{\ddagger}$ ($kJ.mol^{-1}$)	$\Delta S^{\ddagger}$ ($J.mol^{-1}$)	$\Delta G^{\ddagger}$ ($kJ.mol^{-1}$)
3.30×10^{-6}	58	5.8×10^{8}	81	79	- 86	104

Fig. 3.15 Thermal *Z*/*E* isomerization in dimer **1** (DMSO) at middle-range temperatures (35 °C, 40 °C, 45 °C, 50 °C and 55 °C): Arrhenius plot (left), Van't Hoff plot (right), and the corresponding kinetic data and thermodynamic parameters (@ 298 K) as calculated using the Arrhenius and Eyring equations.

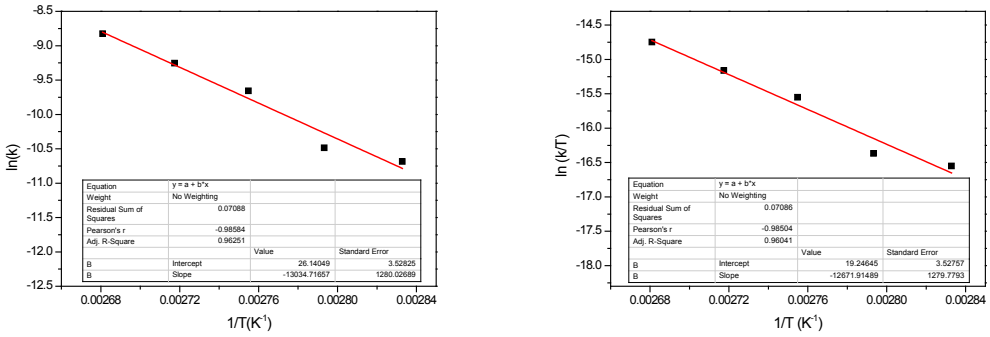

k (s^{-1})	$\tau_{1/2}$ (days)	A (s^{-1})	Ea ($kJ.mol^{-1}$)	$\Delta H^{\ddagger}$ ($kJ.mol^{-1}$)	$\Delta S^{\ddagger}$ ($J.mol^{-1}$)	$\Delta G^{\ddagger}$ ($kJ.mol^{-1}$)
2.27×10^{-8}	353	2.25×10^{11}	108	105	- 37.5	116

Fig. 3.16 Thermal *Z*/*E* isomerization in dimer **1** (DMSO) at higher temperatures (80 °C, 85 °C, 90 °C, 95 °C and 100 °C): Arrhenius plot (left), Van't Hoff plot (right), and the corresponding kinetic data and thermodynamic parameters (@ 298 K) as calculated using the Arrhenius and Eyring equations.

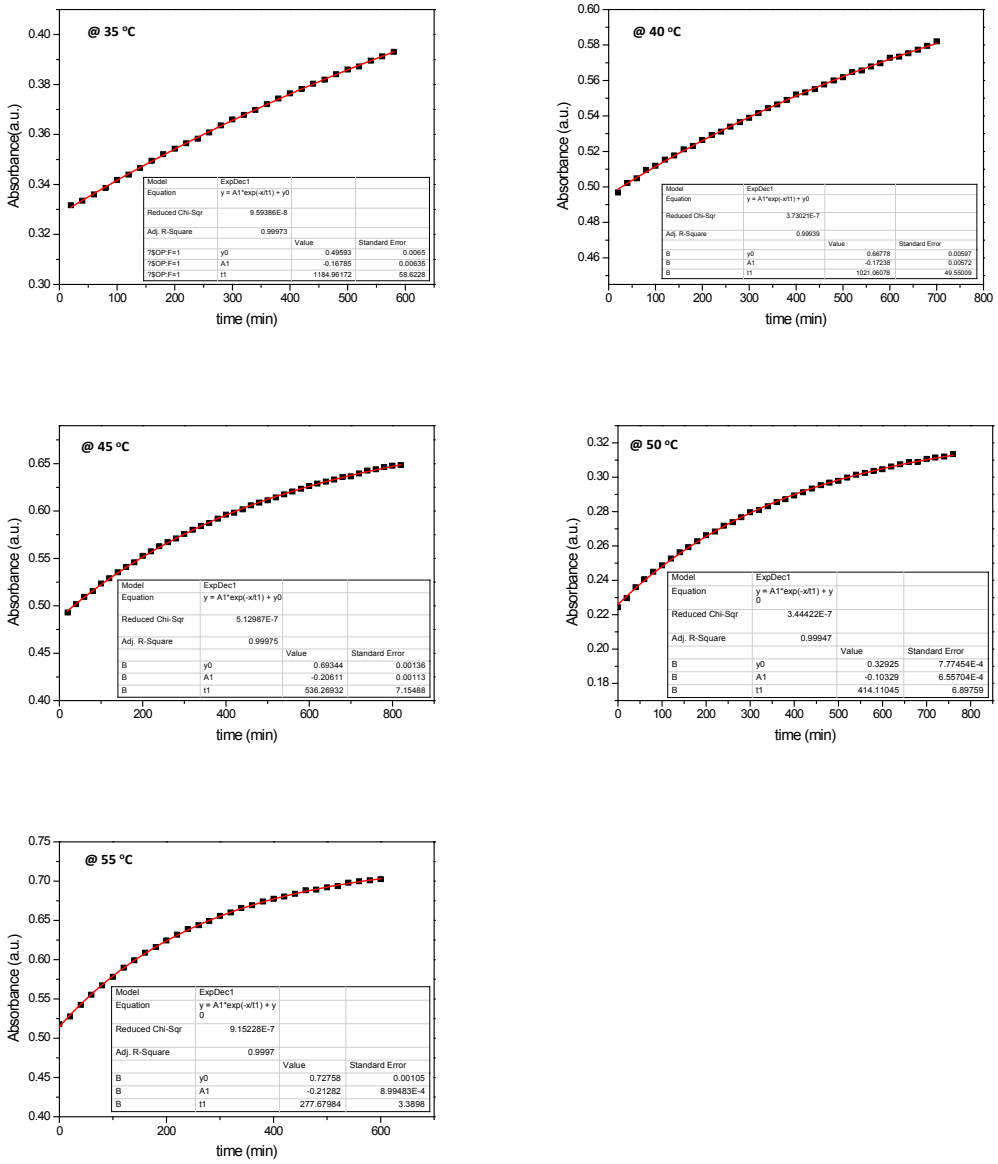

Fig. 3.17 Thermal *Z*/*E* isomerization in dimer **2** (DMSO): plots of absorbance at 337 nm (λ_{max}) versus time (minutes) at middle-range temperatures (35 °C, 40 °C, 45 °C, 50 °C and 55 °C) fitted with a first-order exponential decay.

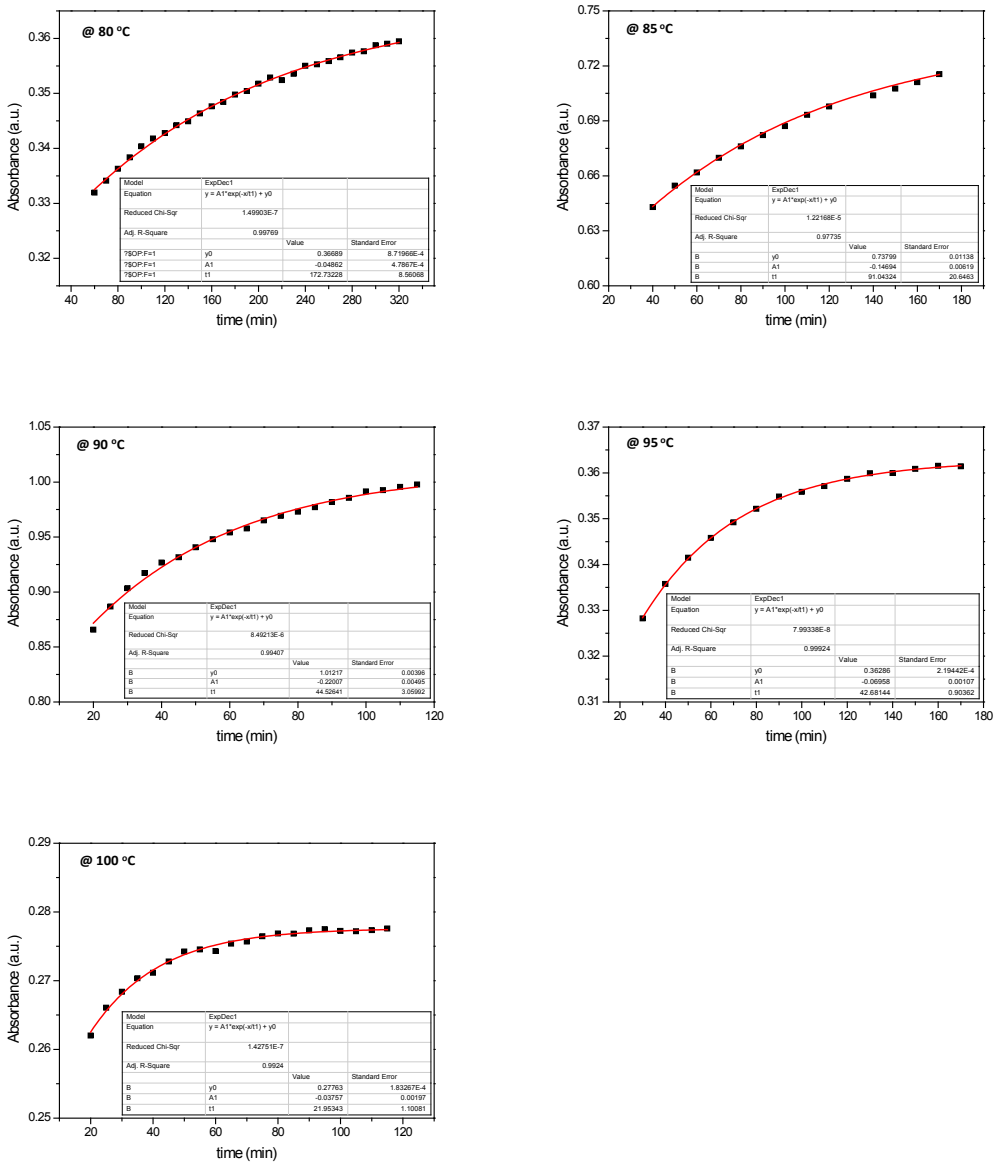

Fig. 3.18 Thermal *Z*/*E* isomerization in dimer **2** (DMSO): plots of absorbance (after removal of the first data points) at 337 nm (λ_{max}) versus time (minutes) at higher temperatures (80 °C, 85 °C, 90 °C, 95 °C, 100 °C) fitted with a first-order exponential decay.

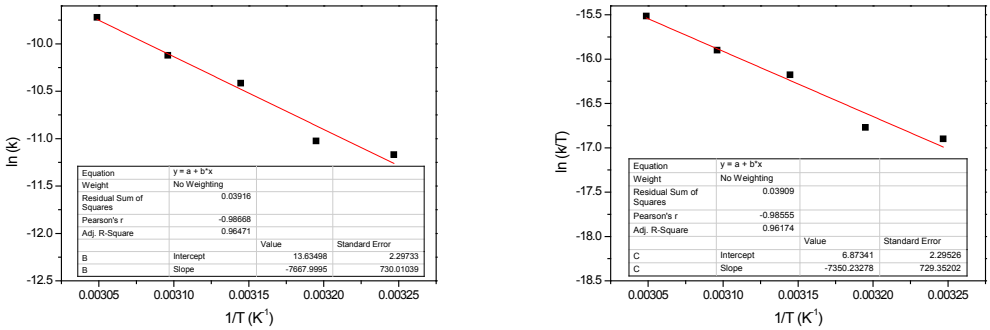

k (s^{-1})	$\tau_{1/2}$ (h)	A (s^{-1})	Ea ($kJ.mol^{-1}$)	$\Delta H^{\ddagger}$ ($kJ.mol^{-1}$)	$\Delta S^{\ddagger}$ ($J.mol^{-1}$)	$\Delta G^{\ddagger}$ ($kJ.mol^{-1}$)
5.6×10^{-6}	35	8.4×10^{5}	64	61	- 140	103

Fig. 3.19 Thermal *Z*/*E* isomerization in dimer **2** (DMSO) at middle-range temperatures (35 °C, 40 °C, 45 °C, 50 °C and 55 °C): Arrhenius plot (left), Van't Hoff plot (right), and the corresponding kinetic data and thermodynamic parameters (@ 298 K) as calculated using the Arrhenius and Eyring equations.

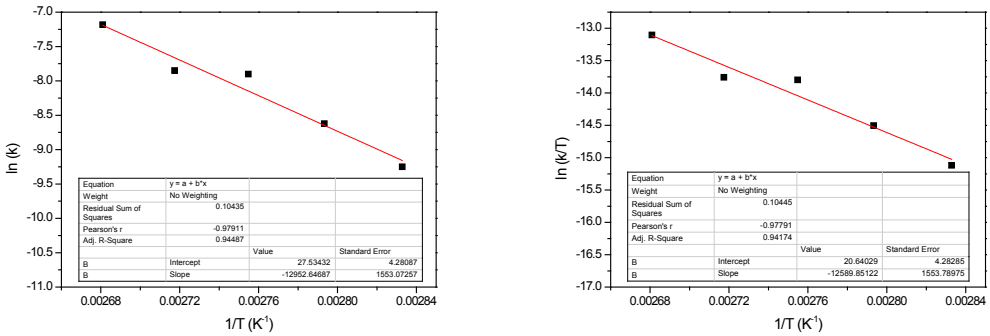

k (s^{-1})	$\tau_{1/2}$ (days)	A (s^{-1})	Ea ($kJ.mol^{-1}$)	$\Delta H^{\ddagger}$ ($kJ.mol^{-1}$)	$\Delta S^{\ddagger}$ ($J.mol^{-1}$)	$\Delta G^{\ddagger}$ ($kJ.mol^{-1}$)
1.1×10^{-7}	73	9.0×10^{11}	108	105	- 26	112

Fig. 3.20 Thermal *Z*/*E* isomerization in dimer **2** (DMSO) at higher temperatures (80 °C, 85 °C, 90 °C, 95 °C and 100 °C): Arrhenius plot (left), Van't Hoff plot (right), and the corresponding kinetic data and thermodynamic parameters (@ 298 K) as calculated using the Arrhenius and Eyring equations.

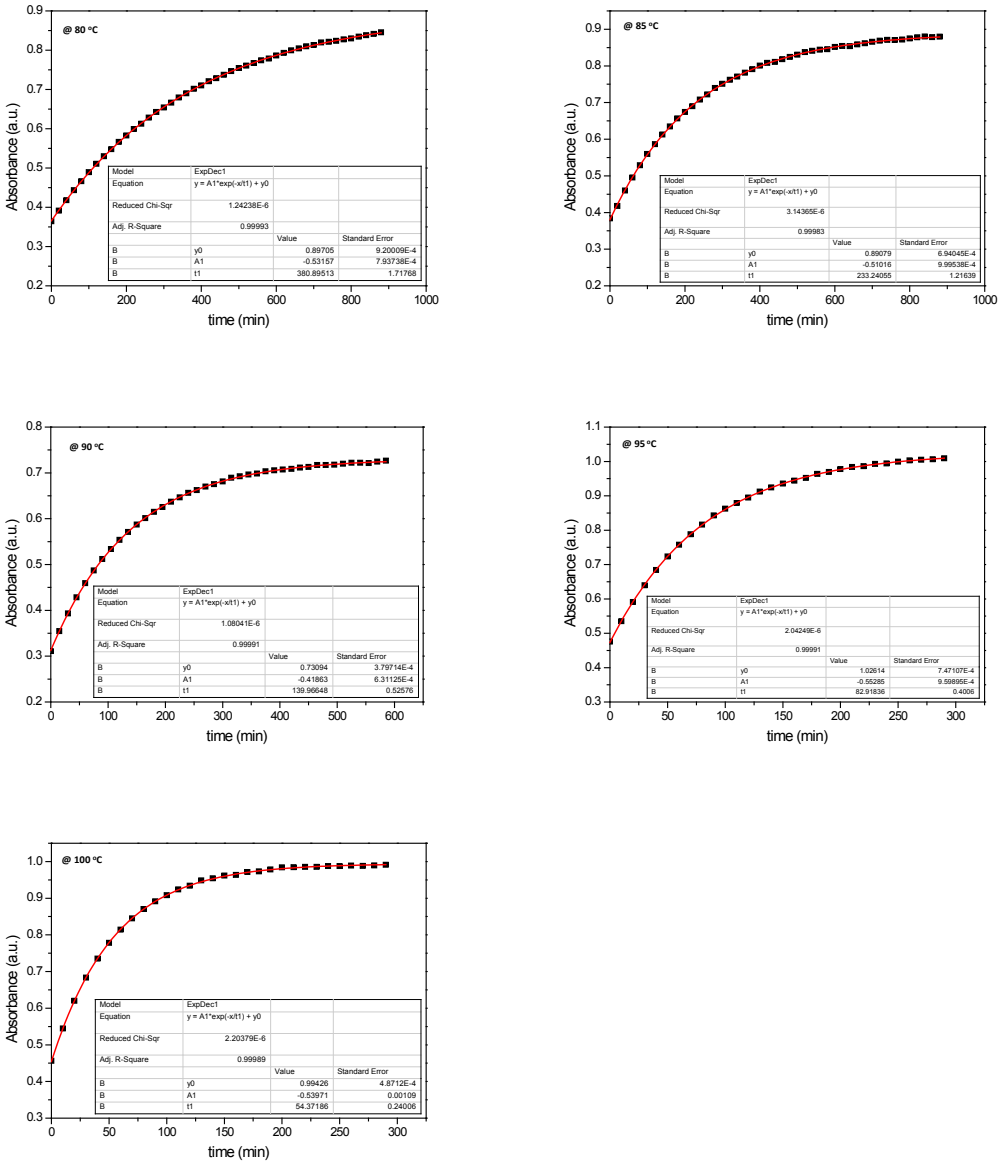

Fig. 3.21 Thermal *Z*-**F4-ester** → *E*-**F4-ester** isomerization in DMSO: plots of absorbance at 305 nm (λ_{max}) versus time (minutes) at higher temperatures (80 °C, 85 °C, 90 °C, 95 °C, 100 °C) fitted with a first-order exponential decay.

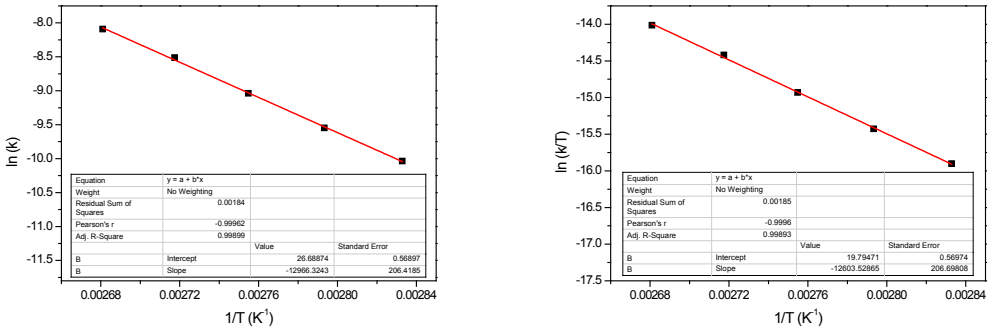

k (s^{-1})	$\tau_{1/2}$ (days)	A (s^{-1})	Ea ($kJ.mol^{-1}$)	$\Delta H^{\ddagger}$ ($kJ.mol^{-1}$)	$\Delta S^{\ddagger}$ ($J.mol^{-1}$)	$\Delta G^{\ddagger}$ ($kJ.mol^{-1}$)
5.0×10^{-8}	160	3.9×10^{11}	108	105	- 33	115

Fig. 3.22 Thermal *Z*-**F4-ester** → *E*-**F4-ester** isomerization in DMSO: Arrhenius plot (left), Van't Hoff plot (right), and the corresponding kinetic data and thermodynamic parameters (@ 298 K) as calculated using the Arrhenius and Eyring equations.

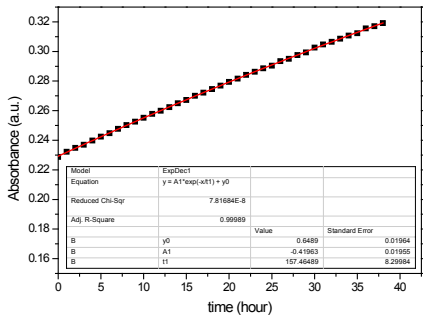

Fig. 3.23 Thermal *Z*-**diMe** ⟶ *E*-**diMe** isomerization in DMSO @ 298 K.

Cyclic voltammetry

Cyclic voltammetry was performed using a PG310 USB (HEKA Elektronik) potentiostat interfaced to a PC with PotMaster v2x43 (HEKA Elektronik) software for data evaluation. A three-electrode configuration contained in a non-divided cell consisting of a Pt disc (d = 1 mm) as working electrode, a platinum plate as counter-electrode, and a saturated calomel electrode (SCE) with an agar-agar-plug in a Luggin capillary with a diaphragm as reference electrode was used. Measurements were carried out with $1 \cdot 10^{-3}$ M solutions in 0.1 M Bu_4NPF_6 acetonitrile (HPLC-grade, dried over calcium hydride and distilled) using a scan rate of

dE/dt = 1 V s^{-1}. Data are given in reference to the ferrocene redox couple (Fc/Fc^+), which was used as external standard. Cyclic voltammograms of *Z* isomers of azobenzenes were obtained by irradiation of the electrochemical cell using a standard laboratory UV-lamp equipped with a 313 nm or 365 nm UV-tube (Vilber Lourmat, 6W).

Spectroelectrochemistry

Spectroelectrochemistry was performed using quarz cuvettes with 1 mm or 0.5 mm path length in an Avantes AvaSpec-2048x14 spectrometer combined with an AvaLight–DH-S-BAL light source. The cuvette was equipped with a Pt mesh as working electrode, a Pt wire as counter electrode, and Ag/Ag^+ (0.01 M $AgNO_3$ in 0.1 M Bu_4NPF_6 acetonitrile) as reference electrode, connected to an Autolab PGSTAT128N potentiostat from Metrohm GmbH, Germany.

$5 \cdot 10^{-4}$ M solutions of the different azobenzene derivatives in 0.1M Bu_4NPF_6 acetonitrile were placed in the cuvette, a scanning rate of 10 mV/s was used while UV/vis-spectra were recorded every 10 mV. As reference the Fc/Fc^+ redox couple was determined to have an oxidation potential of 0.12 V *vs*. Ag/Ag^+ in this configuration.

Cathodically initiated *Z* ⟶ *E* isomerization

A 0.015 mM solution in 0.1 M Bu_4NPF_6 acetonitrile (40 mL) was prepared for each sample (dimer **1-2**, mixtures of **diMe**/**F4** and **diMe**/**F4-ester**). The solutions were filled into the cathode compartment of a double H-cell, purged with argon, and irradiated with a laboratory UV-lamp (365 nm) to enrich the solutions with *Z*-isomers. A Pt-mesh was used as the cathode. The anode chamber contains the electrolyte, the electrode is a Pt-mesh as well. As a reference electrode, a standard calomel electrode was placed in the third electrode chamber. Coulometry was performed potentiostatically (Bipotentiostat PG 287 HEKA Electronics, Lambrecht Pfalz, Germany) at a working potential (E_{r0}) below the maximum peak potential followed by UPLC analysis for recording of the compositions.

4. Reversible modulation of elasticity in fluoroazobenzene-containing hydrogels using blue and green light

4.1 Introduction

Hydrogels are three-dimensional networks with high water content that have found many applications in modern medicine *e.g.* as biomedical implants, adhesives, contact lenses, or scaffolds for tissue engineering.[191] Their mechanical properties, in particular the elasticity, are essential and hence a key parameter is the shear elastic modulus (G′), with different applications requiring moduli across the 10^2 - 10^7 Pa range.[192] For instance, stem cells are known to remember past mechanical environments and differentiate depending on the elastic modulus of the substrate.[193] Hence, creating hydrogels whose elasticity can be tuned on demand is promising for inducing environmental mechanical variations that mimic the extracellular matrix (ECM) dynamics and dictate cells' fate.[72,159]

Gels are especially sensitive to their environment and can be designed to readily respond to variations in, typically, pH or temperature.[194] Depending on the molecular structure elevating the temperature can either drastically soften or harden hydrogels, due to dissociation of the network[195] or collapse transition at the critical solution temperature,[196] respectively. Light is another trigger of choice offering the advantage of precise photo-patterning[72] and allows to alter gel mechanical properties either permanently by implementing photo-cleavable groups[107] or reversibly using photochromic molecules, such as spiropyrans[147,197] or azobenzenes.[198] Following the latter strategy, non-covalent physical gels typically lead to materials with light-induced sol-gel transitions, whereas covalent chemical gels can exhibit more finely tuneable phenomena such as photo-induced motion[150,199–202] or softening/hardening.[159] For instance, Harada's group developed a poly(ethylene glycol) (PEG) network with a classical azobenzene covalently attached into the polymer backbone as shown in figure 4.1 (top).[150] This hydrogel shows expansion-contraction motions upon photo-irradiation, which is due to the *E*-azo tends to aggregate in water and function as a cross-linker, further leading to the contraction of the gel, while the aggregation dissociates with the isomerization of the azo unit from the *E*-form to the *Z*-form causing the volume of the gel to increase. The Anseth group also prepared PEG-based hydrogels that soften and stiffen via photo-isomerization of an azobenzene-containing cross-linker (see

Fig. 4.1 bottom).[159] Irradiation with light of 365 nm leads to the decrease of the gel's shear storage modulus G' (softening), which recovers its initial value after visible light irradiation (hardening). However, both cases necessitates damaging UV light.

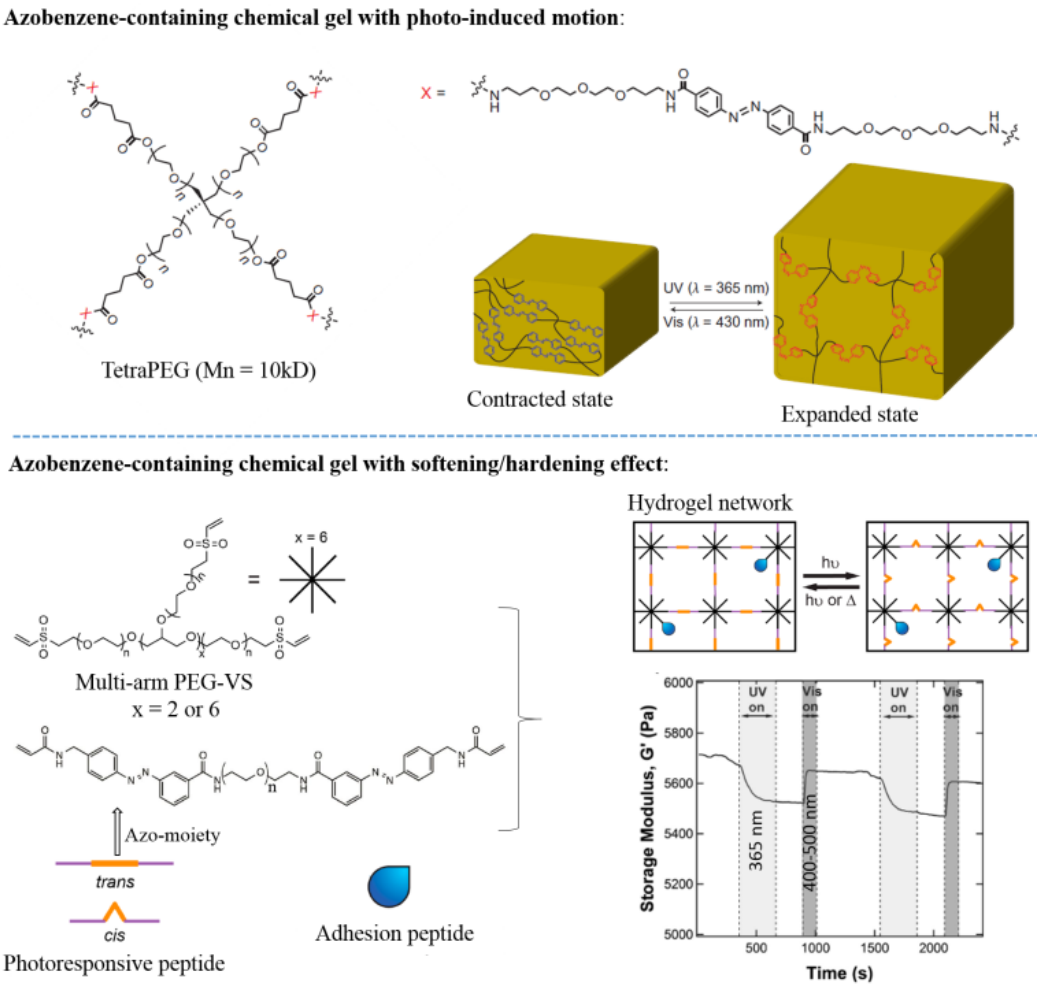

Fig. 4.1 Photo-responsive hydrogels with macro-motion (top)[150] and softening/hardening effect (bottom).[72]

The requirements of an ideal light-responsive hydrogel with tuneable elasticity acting as a scaffold for biological applications are, along cytocompatibility, reversibility, stability at moderate temperature (typically 37 °C), and operation with non-damaging visible light. In this chapter, we present a poly(ethylene glycol) chemical hydrogel incorporating *ortho*-fluoroazobenzenes as cross-linkers, which exhibits efficient optical performance, good reversible photo-modulation of elasticity and high thermal stability. PEG was used as the main structural component for hydrogel networks due to its hydrophilicity and

biocompatibility. Fluoroazobenzenes were selected as photochromic moieties due to their full addressability with visible light and very high thermal stability of the thermodynamically less stable *Z*-isomers.[22] To covalently cross-link the polymer, two synthetic methods were used in this work to construct the hydrogels: copper-catalysed azide-alkyne cycloaddition (CuAAC) and strain-promoted azide-alkyne cycloaddition (SPAAC). Nevertheless, the hydrogels synthesized by CuAAC (CuAAC hydrogel) do not display any modulus change upon stimulus of light, and the reason remains unclear. However, hydrogels prepared by SPAAC (SPAAC hydrogel) exhibit the desired photo-modulation of G'.

4.2 Results and discussion

4.2.1 CuAAC hydrogel

The CuAAC reaction is one of the most widely used "click" methods for chemical synthesis, drug discovery, bioconjugation and biochemistry due to its quick reaction rate, high efficiency and bioorthogonality (see details in section 2.2.2 Huisgen 1,3-dipolar "click" cycloaddition in hydrogel synthesis). 4-arm-PEG (Mn = 10 kDa) bearing terminal-azide groups (**tetra-N_3-PEG**) was used in this work for the hydrogel formation as shown in scheme 4.1. *Ortho*-tetrafluoroazobenzene was functionalized in both *para*-positions of the phenyl rings with a linear alkyne (see **alkyne-F4-azo**). When the two compounds are mixed together in the presence of catalytic amounts of Cu(I) in DMF, they give rise to a 1,3-dipolar cycloaddition reaction resulting in fast gelation at room temperature.

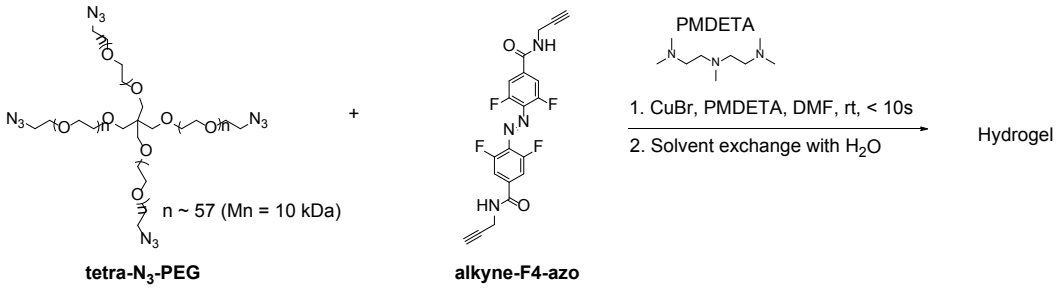

Scheme 4.1. Synthesis of CuAAC hydrogels.

4.2.1.1 Preparation of hydrogels

Gels were prepared in a round mold (diameter: 2 cm, depth: 1 mm) to fit the rheometer parallel-plate. Since **alkyne-F4-azo** is not water-soluble, the preparation of hydrogels was performed in an organic solvent (DMF), and water-swollen hydrogels were obtained by solvent-exchange against distilled water for at least three days.

The conversion efficiency of precursors into hydrogel was estimated by FTIR. The FTIR spectra were recorded with dried hydrogel samples. At first, the sample was gently cut into small pieces. Afterwards, these gel pieces were pre-dried under atmospheric condition, and further dried under vacuum for 3 days to obtain the samples. Three dry gel pieces were measured and similar results were obtained for all samples, indicating the reproducibility of the preparation method. The FTIR spectra of dry gels and **tetra-N_3-PEG** are shown in figure 4.2. The vibration band at 2109 cm^{-1} is characteristic of the azide group and was used for evaluating the conversion. Although the azide band was more intense in the spectrum of the starting material (**tetra-N_3-PEG**), a small vibration peak of N_3 was detected for the gel as well, indicating that full conversion could not be reached. Nonetheless, in consideration of the reproducible synthetic method and similar mechanical properties (*vide infra*) observed for each sample, the hydrogels were used as such for the following photo-responsive experiments.

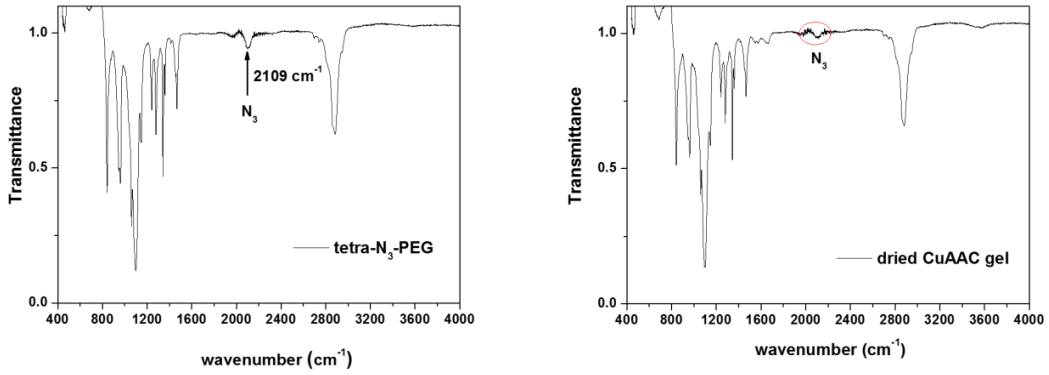

Fig. 4.2 FTIR spectra of tetra-N_3-PEG and dried CuAAC hydrogel.

4.2.1.2 Photo-isomerization of F4-azobenzene within the CuAAC hydrogels

Using UV/vis spectroscopy, we investigated the photo-isomerization behavior of the F4-azo moieties within the hydrogel network. The photochemical property of **alkyne-F4-azo** in solution was first studied. To obtain comparable results, the experiments should be carried out under the exact same conditions (*i.e.* in water). However, due to the very poor water-solubility of **alkyne-F4-azo**, acetonitrile was used instead. According to the spectra obtained for both solution and hydrogel (see Figure 4.3), no distinct difference was observed besides the absorption intensity resulting from the different concentrations. As shown in figure 4.3 (top), typical absorption spectra of fluoroazobenzenes were observed in solution. Upon irradiation with green light (> 500 nm) the absorption at 318 nm and 461 nm, which is ascribed to $\pi \longrightarrow \pi^*$ and $n \longrightarrow \pi^*$ transition of the *E*-isomer, respectively, decrease dramatically and a new peak at 420 nm arises, indicating the $E \longrightarrow Z$ isomerization process. Upon exposure to blue light (405 nm), the *Z*-isomer was quickly restored to its initial state (*i.e. E*-isomer). The reversible process produces PSSs containing 85% of *Z*-isomer with green light and 95% of *E*-isomer with blue light, as determined by UPLC (see 4.4 materials and methods).

The UV/vis spectroscopy of hydrogels was performed in a 1 mm-width quartz cuvette as shown in the bottom of figure 4.3. The hydrogel was cut into a small piece and carefully filled into the cuvette, water was then introduced into the cuvette to keep the gel in a maximum swollen state during the entire experiment. The distance between the gel sample and LED light source was kept around 10 cm to avoid heating. The UV/vis spectra of the hydrogel in the visible region show similar behaviors compared to the spectra in solution. However, due to the high concentration of photoswitches in such networks, and their high extinction coefficient in the UV region, the absorption saturated in this region and hence only the evolution of the $n \longrightarrow \pi^*$ band was monitored for the gels. A new $n \longrightarrow \pi^*$ band at 420 nm arises upon irradiation with green light, while irradiation with blue light restores the spectrum to its almost initial form (maximum at 455 nm). The reversible *Z*/*E* isomerization can be repeated for many cycles without obvious decay. Although there is no effective method to determine the PSS compositions for the bulky hydrogel, based on the very similar absorption spectra, the amount of *Z* isomer is approximated to be the same as obtained in solution (*i.e.*

near 85% of *Z*-isomer with green light *vs.* 95% of *E*-isomer with blue light).

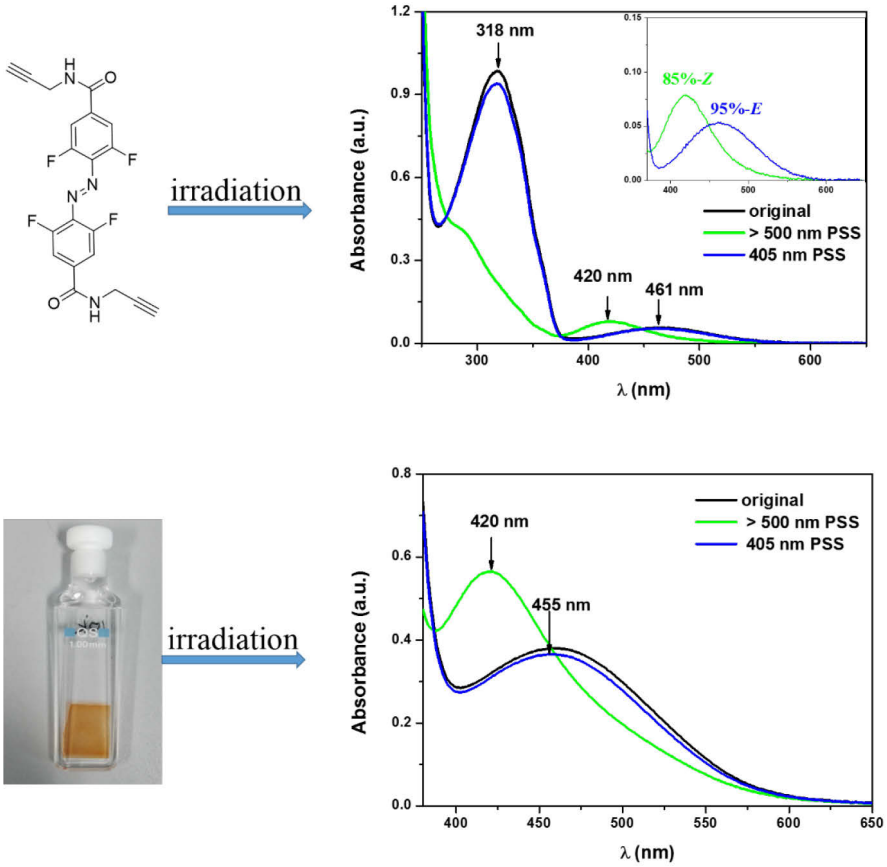

Fig. 4.3 Top: UV/vis spectrum of **alkyne-F4-azo** in acetonitrile at 25 °C, c = 10^{-5} M. Inset shows the n ⟶ π* bands and indicates the compositions (as determined by liquid chromatography) of the PSS mixtures upon irradiation with green and blue light. Bottom: UV/vis spectrum of CuAAC hydrogel (thickness = 0.5 mm) in water at 25 °C.

4.2.1.3 Rheology

Dynamic time sweep rheological experiment was conducted to monitor the response of the hydrogel's mechanical property upon exposure to light. The shear moduli were recorded after 80 minutes equilibration in water with the hydrogel loaded into the rheometer. As shown in figure 4.4, the shear elastic (also called shear storage) modulus (G') is greater than the loss modulus G", indicating that the elastic properties of the gel dominate over the viscous losses. Nevertheless, no obvious change occurs upon alternating green and blue light irradiation, although the switch exhibits very good photo-response. Even after extending the irradiation

time to 1 hour, the moduli still remain at a stable state.

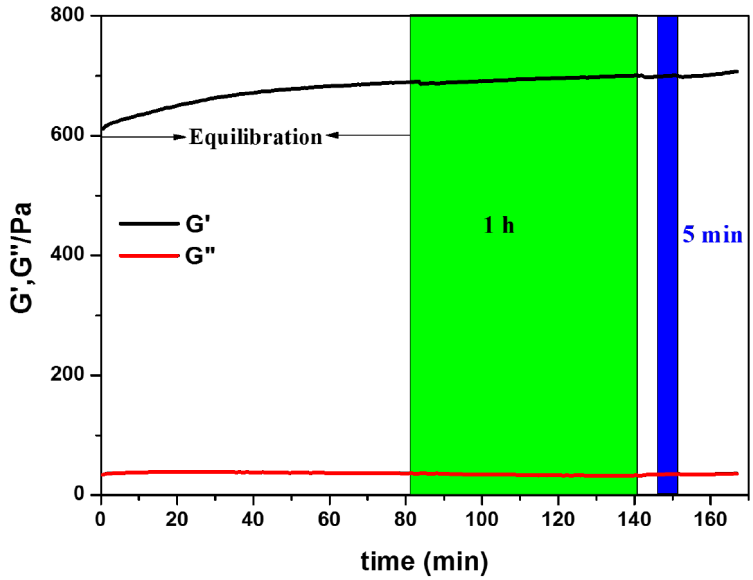

Fig. 4.4 Rheology of CuAAC hydrogel, no modulus change was observed via alternating irradiation with green (> 500 nm, 1 hour) and blue (405 nm, 5 minutes) light.

The reason for the unchangeable G' under light-stimulus in the CuAAC hydrogel is unclear so far. We initially assumed that this might be due to incomplete reaction conversion caused by the easily oxidized Cu(I) as well as its poor dispersion during the process of gelation, which would lower the cross-linking density of the hydrogel network, potentially preventing large photo-modulations of the gel's mechanical properties. Although this hypothesis later proved wrong, at this stage we decided to adopt an alternative method, *i.e.* SPAAC, which does not require the use of a catalyst (see details in section 2.2.2 Huisgen 1, 3-dipolar "click" cycloaddition in hydrogel synthesis).

4.2.2 SPAAC hydrogel

Strain-promoted azide-alkyne cycloaddition reaction was carried out between **tetra-N_3-PEG** and dibenzocyclooctyne (DBCO)-substituted *ortho*-tetrafluoroazobenzene (**F4-azo-bis-DBCO**) with 1: 1 stoichiometry (see scheme 4.2). This reaction is fast, efficient, does not require any catalyst or external stimuli (*e.g.* light), does not produce any byproduct

and the resulting linkage is extremely stable. Gels were prepared in the same mold (diameter: 2 cm, depth: 1 mm) as used for preparation of CuAAC hydrogels. Since **F4-azo-bis-DBCO** is also not water-soluble, the preparation of hydrogels was performed in DMF as well, and water-swollen hydrogels were obtained by solvent-exchange against distilled water for at least three days.

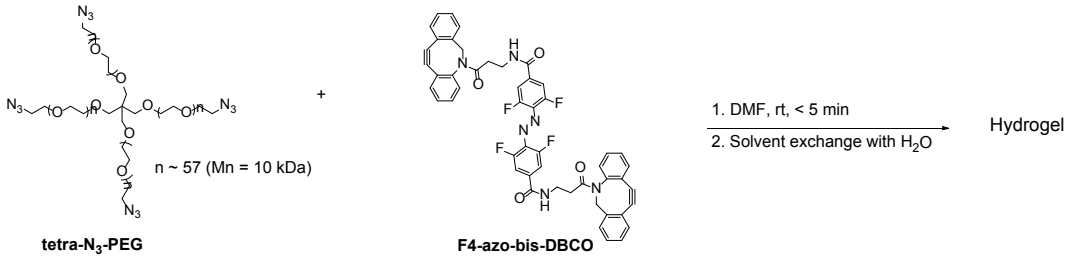

Scheme 4.2 Synthesis of hydrogels using SPAAC reaction.

Gel formation was characterized qualitatively by means of FTIR spectroscopy (see Fig. 4.5). Unwillingly, a small vibration peak of N_3 (2019 cm^{-1}) was detected for the SPAAC gels as well, indicating that full conversion could also not be reached, even after heating at 45 °C for 4 h. Nonetheless, in consideration of the reproducible synthetic method and similar mechanical properties (*vide infra*) observed for each sample, the hydrogels were used as such for the following photo-responsive experiments.

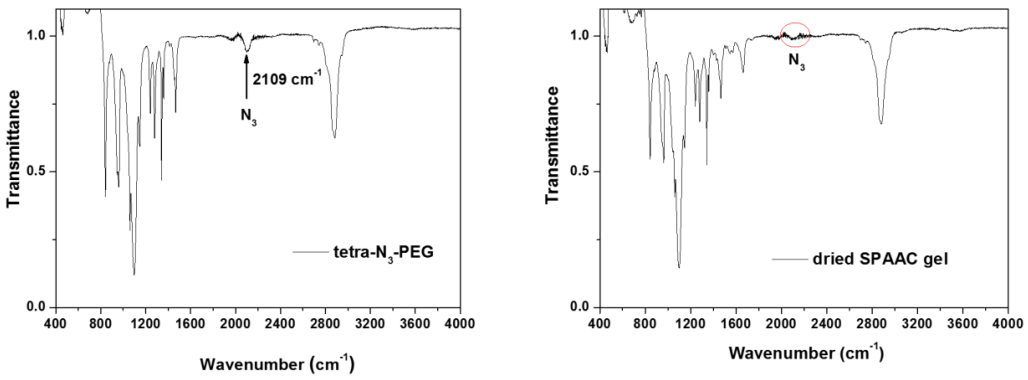

Fig. 4.5 FTIR spectra of **tetra-N_3-PEG** and dried SPAAC hydrogel.

4.2.2.1 Photo-isomerization of F4-azobenzene within the SPAAC hydrogels

The photochemical property of **F4-azo-bis-DBCO** was studied both in solution (acetonitrile) and hydrogel network using UV/vis spectroscopy. Different absorption in the UV region in solution was observed compared to the corresponding spectrum observed in the **alkyne-F4-azo** solution, resulting from the dibenzocyclooctyne moiety in the azo structure. As shown in figure 4.6, the *E* isomer of **F4-azo-bis-DBCO** (see Fig. 4.6 top, black curve) displays several absorption bands in the UV region. Two intense absorption peaks at 293 nm and 311 nm (highlighted in pink) are ascribed to the dibenzocyclooctyne groups,[203] while the shoulder peak overlapping around 330 nm (highlighted in green) results from the $\pi \longrightarrow \pi^*$ transition of the fluorinated azobenzene moiety.[22] The absorption peak in the visible region at 460 nm belongs to the $n \longrightarrow \pi^*$ transition of *E*-azobenzene. Irradiation with green light (> 500 nm) effectively causes the $E \longrightarrow Z$ isomerization, as the typical absorption spectrum of *Z*-fluoroazobenzene was observed, where the absorbance in the UV region decreases while a new blue-shifted $n \longrightarrow \pi^*$ band at 420 nm arises. The *E*-isomer was quickly recovered upon exposure to blue light (405 nm). Therefore, isomerizing **F4-azo-bis-DBCO** with visible light in both directions was achieved, producing PSSs containing 87% of *Z*-isomer with green light and 93% of *E*-isomer with blue light, as determined by UPLC (see 4.4 materials and methods).

The UV/vis spectrum of SPAAC hydrogel shows very similar absorption compared to that in solution (see Fig. 4.6 bottom, only the $n \longrightarrow \pi^*$ absorption bands are shown). A new $n \longrightarrow \pi^*$ band at 420 nm arises upon irradiation with green light, while irradiation with blue light restores the initial spectrum (maximum at 458 nm). This reversible *Z*/*E* isomerization can be repeated for many cycles without obvious decay. Based on the very similar absorption spectra, the composition of PSSs in hydrogel was roughly determined to be 87% for *Z*-isomer (green light) and 93% for *E*-isomer (blue light).

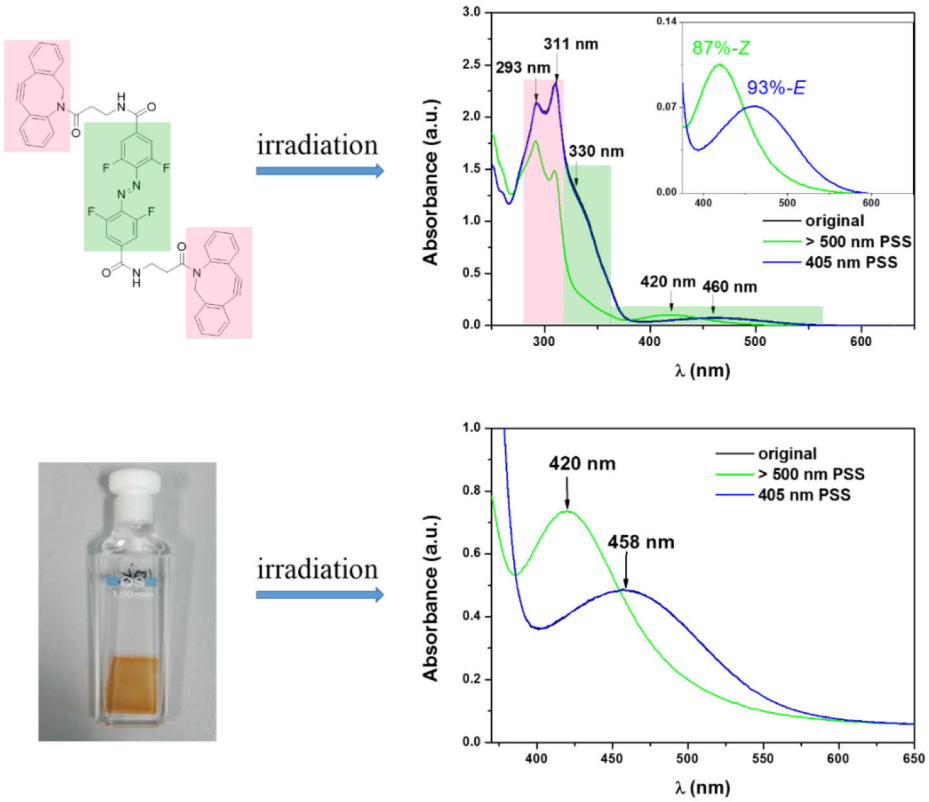

Fig. 4.6 Top: UV/vis spectrum of **F4-azo-bis-DBCO** in acetonitrile at 25 °C, c = 5.5 x 10^{-5} M. Inset shows the n ⟶ π* bands and indicates the compositions (as determined by liquid chromatography) of the PSS mixtures upon irradiation with visible light. Bottom: UV/vis spectrum of cross-linked SPAAC hydrogel (thickness = 0.5 mm) in water at 25 °C.

4.2.2.2 Rheology

Dynamic time sweep rheological experiment was conducted to monitor the response of the SPAAC gel's mechanical property upon exposure to light. The shear moduli were recorded after at least 1.5 hours equilibration in water with the hydrogel loaded into the rheometer. According to the results shown in figure 4.7 a, the storage modulus G' is larger than the loss modulus G" indicating an elastic response. Upon irradiation with green light (> 500 nm, 2 minutes), the gel modulus decreased quickly. After the light was switched off, G' stayed constant for at least 5 minutes. The gel was then subjected to blue light (450 nm, 30 seconds) and consequently G' quickly increased and recovered back to the initial modulus. Again, after removal of the light, G' stayed constant for at least 5 minutes until the next irradiation cycle was performed. An absolute modulation of around 13 Pa (corresponding to

an initial decrease of $\Delta G'/G'_{intial}$ = 3.5%) was achieved upon alternating green and blue light irradiation. Although the magnitude of the change in storage modulus is quite modest, it is larger than the value reported in previous work by the Anseth group, where they demonstrated that a mechanoresponsive cell type can exhibit high level of survival and spread morphology even when encapsulated into a hydrogel network with smaller modulation of the storage modulus ($\Delta G'/G'_{intial}$ = 2%).[159] Most notably, the modulus' change in our work shows good reversibility and reproducibility (see Figure 4.7 b) without using damaging UV light. Although only three cycles are shown here, the hydrogel retained its dynamic switching characteristics over numerous cycles without any photo-degradation.

4.2.2.3 Discussion about the mechanism of G' photo-tuning

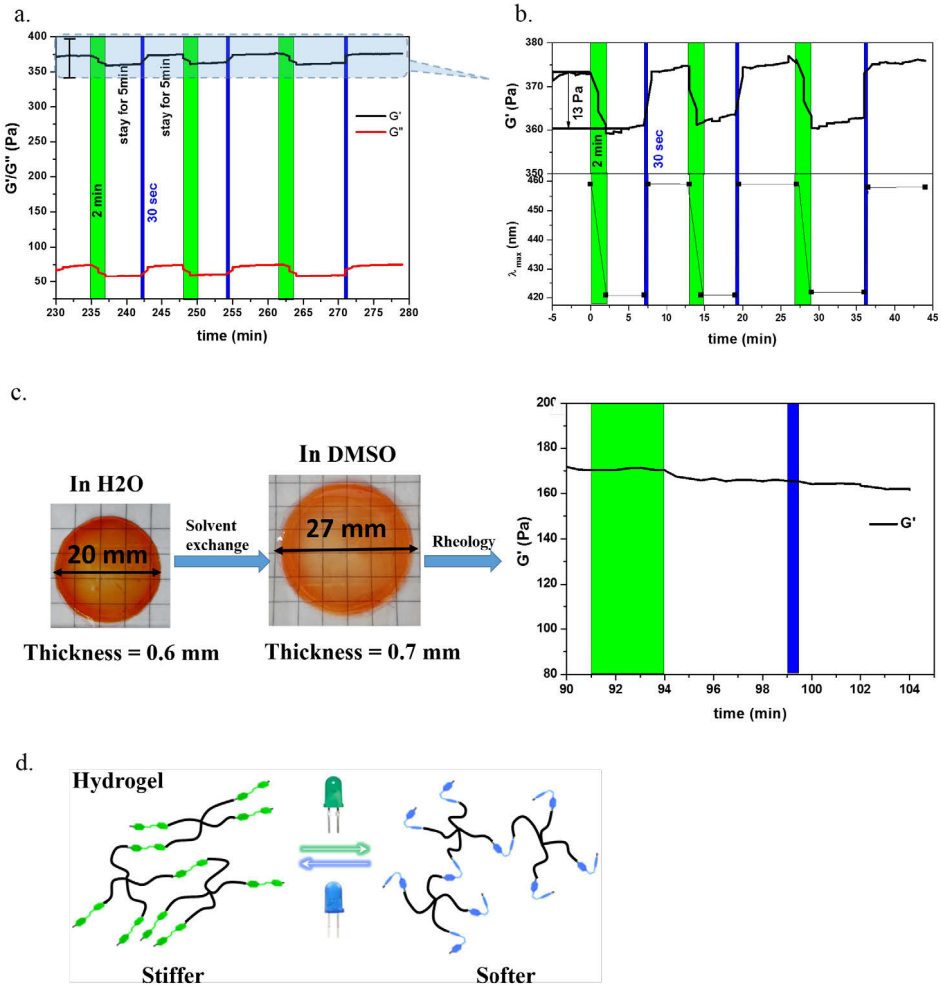

Fig. 4.7 (a) Rheology of SPAAC hydrogel shows a cyclic change in G' upon alternating irradiation with green (> 500 nm, 2 min) and blue (405 nm, 30 s) light. (b) Isolated storage modulus curve (top) and change of λ_{max} in n ⟶ π* absorption band (bottom) upon alternating green (2 min) and blue (30s) light irradiation, indicating a reversible and repeatable change of mechanical gel property and an absolute modulation of around 13 Pa obtained upon irradiation (c) After solvent exchange (water → DMSO), gel samples become bigger while the storage modulus is not affected by light irradiation. (d) Schematic illustration of the mechanism of stiffening–softening in SPAAC hydrogel upon photo-irradiation. The *E*-azo units tend to aggregate to function as cross-linkers, leading to a higher storage modulus (stiffening) as shown in (b). After irradiation with green light, the aggregates dissociate, decreasing the cross-linking density and lowering the gel's storage modulus (softening).

To better understand the mechanism of the modulus change in hydrogel network, the gel's mechanical property was also investigated in an organic solvent (DMSO). The hydrogel was rinsed with DMSO for three days to replace the adsorbed water. As shown in figure 4.7 c, removing the adsorbed water drastically influences the size of the sample, as the diameter increased from 20 mm in water to 27 mm in DMSO, while the thickness increased from 0.6 mm to 0.7 mm. The subsequent rheological experiment, however, showed no obvious change in G' upon irradiation with green or blue light. Moreover, the gel becomes much softer in DMSO (G' of 170 Pa *vs.* 375 Pa in H_2O). In view of the observed results, we presume that the modulus' change most likely arises from the non-covalent interactions of the azobenzene moieties in water (*e.g.* hydrophobic interactions and π-π stacking). The hydrophobic *E*-F4-azo moieties tend to aggregate to function as non-covalent cross-linkers, leading to a stiffer hydrogel (see Fig. 4.7 d). Irradiation with green light causes photo-isomerization from *E*- to *Z*-azo, leading to the disassociation of these physical cross-links. Thus, the cross-linking density decreased, eventually resulting in a softer gel. By contrast, the organogel swollen with DMSO does not exhibit any change in modulus upon irradiation, because the physical cross-links induced by the hydrophobicity of the *E*-azo moiety in water dissociate in DMSO.

It should be mentioned that although the hydrogels developed here display photo-tuned elasticities (stiffening-softening), we did not observe any concomitant macroscopic effects, *i.e.* contraction-expansion, as shown in Harada's work (see figure 4.1). Comparing these two hydrogel systems, very similar components were used in both cases to form the polymer networks: 10 kDa 4-arm-PEG and azobenzene derivatives. They demonstrated that the gel's contraction-expansion effects result from the non-covalent interactions of the azobenzene moiety in water (*e.g.* hydrophobic interactions and π- π stacking) like the mechanism we presumed for our hydrogel system. If the hypotheses are correct, the different resulting effects presented in these two works therefore must be attributed to the difference of the non-covalent interactions between these two azo moieties. In order to better understand it, we computed the dipole moments (μ) of relevant azobenzenes using density functional theory using the B3LYP and a 6-311+G(d,p) basis set. As shown in table 4.1, the $|\Delta\mu|$ (difference in dipole moments of *E* and *Z* isomers) increases with the increase of the fluorine atoms (see compound **1**-**3**), the

largest $|\Delta\mu|$ is found for **3**, with a value of 7.07 D. If we consider **1** ($|\Delta\mu|$= 4.55 D) and **3** ($|\Delta\mu|$= 7.07 D) as the main core who dominates the corresponding hydrogels' mechanical properties, it seems that our hydrogel system containing the fluoroazobenzene should have larger effects. Since it is not the case, the substituents in the *para*-positions of the phenyls ring must also play an important role on $|\Delta\mu|$. As can be seen, the values computed with *para*-amide groups for compound **4** ($|\Delta\mu|$= 0.19 D) and **5** ($|\Delta\mu|$= 1.84 D) are dramatically decreased compared to **3** and **1**, respectively. In particular, the $|\Delta\mu|$of **4** is much smaller compared to **3**, indicating the adverse effect of the polar amide groups for maximizing the $|\Delta\mu|$ of *E*/*Z*-azobenzene. We assume that the difference of the dipole moments between *E*- and *Z*-isomer in the fluoroazobenzene is not sufficient to cause the macro-effects but enough to influence the gel's elasticity, explaining why no visible contraction-expansion were observed in our hydrogel system. Future work should be carried out to focus on maximizing the effect by changing the linkage in the *para*-positions for example with nonpolar alkyl chains to keep the $|\Delta\mu|$ of the fluoroazo.

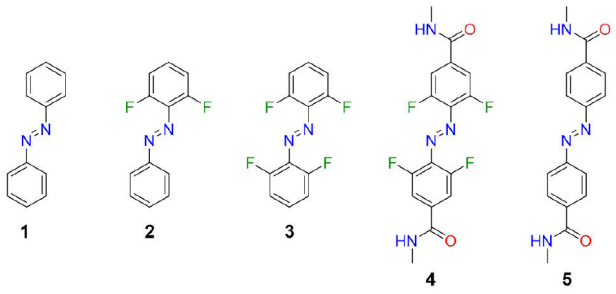

Compound	μ_Z	μ_E	$\lvert\Delta\mu\rvert$
1	4.55	0.00	4.55
2	5.95	1.15	4.80
3	7.44	0.37	7.07
4	8.58	8.39	**0.19**
5	7.89	9.37	**1.84**

Table 4.1 Dipole moments of compounds **1-5,** computed at the B3LYP/6-311+G(d,p) level of theory. Dipole moments (μ) are given in Debye (D).

Comparing the results observed for both CuAAC and SPAAC hydrogels, in particularly

the rheology, we still don't know the reason for the unchangeable storage modulus in the CuAAC hydrogel samples. This could be due to different inner structures resulting from either the different preparation methods or the different molecular structures. In fact, comparing the values of G' and G" in CuAAC hydrogel samples to that observed in SPAAC samples, the former gel is significantly harder (initial value of G' after equilibration: 690 Pa for CuAAC gel *vs.* 375 Pa for SPAAC gel), which could also explain the observed differences in G' photo-tuning. Further experiments using other analytical techniques, such as scanning electron microscopy (SEM), might help gaining deeper insight into the mechanism.

4.2.2.4 Relaxation behavior

The kinetics of the thermal *Z*-to-*E* isomerization process of the hydrogel network was investigated by means of UV/vis spectroscopy. Keeping in mind the potential of hydrogels to act as biomaterials, the thermal relaxation behavior of the photo-responsive hydrogel was investigated at 37 °C. After irradiation to the PSS with green light (> 500 nm, 2 min), the gel was kept in the dark and monitored over 60 h. The peak at 420 nm (λ_{max}) decreased very slowly (see Figure 4.8), as typically observed for fluoroazobenzens.[23] Almost no change occurred within 24 hours (see inset in Figure 4.8), whereas only a slight difference was observed within 60 hours (15 nm, which would correspond to a PSS of 53 % of *Z*-azo in solution).

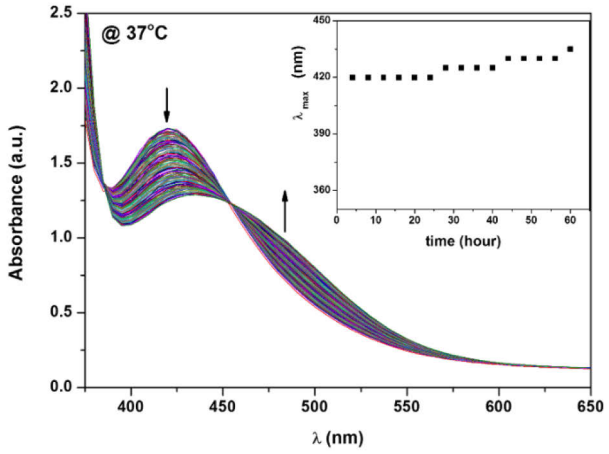

Fig. 4.8 Thermal *Z* ⟶ *E* isomerization of SPAAC hydrogel at 37 °C.

4.3 Conclusion

Prior work has demonstrated diverse strategies for fabricating stimuli-responsive hydrogels with tunable elastic modulus to mimic bio-environments such as the extra-cellular matrix (ECM). In particular, photoreactions have shown their potential to control ECM elasticity, which offer spatial and temporal control in a noninvasive manner. The group of Anseth,[204] for example, reported that the modulus of a hydrogel can be decreased over several kPa via incorporation of a photo-degradable moiety. Photo-cleavage reactions decrease the cross-linking density and hence the gel's elasticity. However, in most cases the reported strategies either make use of damaging UV light and/or are irreversible. In this study, we followed an alternative way to achieve reversible changes without using hazardous UV light, by introducing "*all visible*" fluoroazobenzenes into a PEG-based polymer network. Hydrogel's mechanical properties could be controlled on demand upon irradiation with green and blue light.

We found that the amount of the isomer obtained in each direction (*i.e.* $E \longrightarrow Z$ and $Z \longrightarrow E$) after short irradiation times within the hydrogel network is nearly the same as that obtained in solution owing to the good penetration of high intensity visible light. A photo-modulation of 13 Pa ($\Delta G'$) was obtained reversibly accompanying the isomerization of the switches. In addition, the *Z* isomer of the azo moiety showed (unsurprisingly) great thermal stability. Thus, our hydrogel networks offer a promising platform with potential applications as extra-cellular matrix environment. To that end, however, the gels should be functionalized with *e.g.* adhesion peptides.

Nevertheless, some limitations are worth noting. Although the azo moiety shows good photo-responses, the modulus change of the gel is limited as discussed above. The little change of the shear modulus is most likely due to the small differences in aggregation tendency of *E*- and *Z*-isomer. Future work should therefore focus on maximizing the change in modulus via larger difference in dipole moments of the *E*-*Z* isomers, or by modifying the network design, for example linking the azo moiety into the network as pendant groups. Pendant azo groups would be more flexible and potentially better function as cross-linkers compared to that directly attached into the polymer backbone. Higher reaction conversions could also make a difference.

4.4 Materials and methods

Materials

4-arm poly(ethylene glycol) (PGE, Mn = 10 kDa) was purchased from JenKem USA. All other chemicals were purchased from commercial suppliers and used without further purification. The same materials, methods and instruments (such as TLC, NMR and UPLC *etc.*) as described in the experimental part in chapter 3 were used in this work for the synthesis, reaction monitoring, purification and characterization of involved intermediates and products, unless otherwise specified.

Synthesis of macromonomer tetra-N_3-PEG

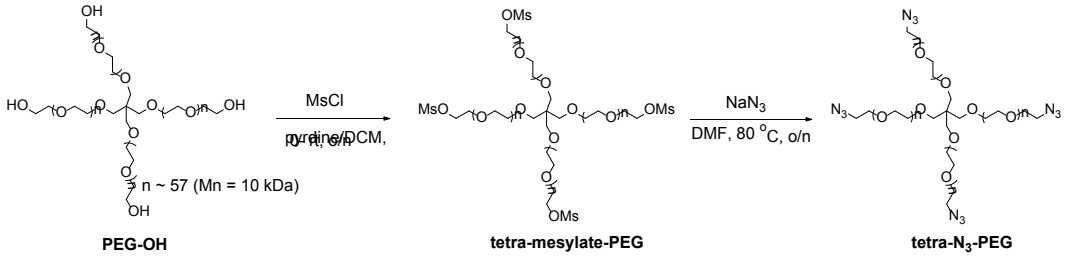

Scheme 4.3 Synthetic protocol for synthesizing macromonomer tetra-N_3-PEG.

The synthesis of **tetra-N_3-PEG** is shown in scheme 4.3. It was prepared starting from purchased PEG-OH according to a procedure reported previously.[205] Briefly, 10 kDa 4-arm poly(ethylene glycol) (2.0 g, 0.2 mmol) was dissolved in a mixture of dry pyridine/dichloromethane (2:3 mL) under argon. After cooling to 0 °C, mesyl chloride (0.3 mL, 4 mmol) was added dropwise. The solution was allowed to warm to room temperature and stirred overnight under argon. The solution was concentrated under reduced pressure, and the residue was quenched by saturated $NaHCO_3$ solution and extracted with dichloromethane. The combined organic phase was dried over Mg_2SO_4, filtered and evaporated under vacuum to afford a viscous liquid. The viscous liquid was then precipitated via treatment with diethyl ether overnight in the fridge, filtered, and the precipitate was dried under vacuum to yield tetra-mesylate-PEG as a white solid (1.6 g, 80%). ^{1}H NMR (DMSO d_6):

4.32 – 4.29 (m, 8H, MsO**CH₂**-), 3.70 – 3.64 (m, 8H, MsOCH₂-**CH₂**-), 3.51 (s, 914H, [**CH₂CH₂**O]$_n$), 3.18 (s, 12H, 4 x **CH₃**SO₂O-).

Afterwards, a mixture of tetra-mesylate-PEG (1.6 g, 0.16 mmol) and sodium azide (0.2 g, 3.2 mmol) in dry DMF (20 mL) was allowed to react at 80 °C under argon for 24 hours. After cooling down, the unreacted sodium azide was removed via filtration through celite, and the filtrate was concentrated via evaporation. The polymer was recovered via precipitation with diethyl ether and filtration. The precipitate was then dissolved in distilled water and dialyzed against water for 2 days, then against methanol for 1 day. The dialyzed solution was evaporated under vacuum to yield the desired product (0.8 g, 50%). ^{1}H NMR ($CDCl_3$): 3.62 (s, 907H, [**CH₂CH₂**O]$_n$), 3.38 – 3.50 (m, 8H, 4 x **CH₂**N₃-).

Synthesis of alkyne-F4-azo

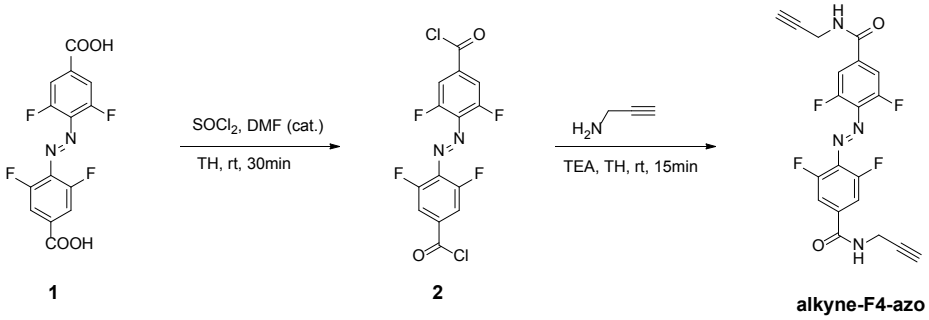

1 **2** **alkyne-F4-azo**

Scheme 4.4 Synthetic protocol for synthesizing alkyne-F4-azo.

alkyne-F4-azo was synthesized via two steps as shown in scheme 4.4. All reactions were carried out under anhydrous anaerobic conditions. Starting compound **1** was used as obtained from our previous work.[23] In brief, to a suspension of **1** (113 mg, 0.33 mmol) in DMF (5 mg, 0.07 mmol) and dry THF (2 mL) was added dropwise thionyl chloride (157 mg, 1.32 mmol) at room temperature under argon atmosphere. The suspension gradually turned to a clear red solution and was stirred for another 30 minutes. The resulting solution was then carefully concentrated under reduced pressure and the residue was further dried under vacuum to yield **2** as a red solid, which was used as such in the next step. To a solution of **2** in dry THF (1 mL) was added dry triethylamine (60 mg, 0.59 mmol) at room temperature in the presence of argon, followed by the addition of a prop-2-yn-1-amine (33 mg, 0.59 mmol) solution in 1 mL

dry THF. The clear solution precipitated with the addition of amine. After stirring for 15 minutes, to the suspension was added a 10% Na_2CO_3 solution and stirring was prolonged for 5 minutes. The precipitate was collected by filtration and washed with water and methanol. The product was dried under vacuum to yield **alkyne-F4-azo** as a light red solid (90 mg, 73%). ^{1}H NMR (300 MHz, DMSO *d*6) δ ppm 9.31 (t, *J* = 5.4 Hz, 2H), 7.83 (d, *J* = 10.2 Hz, 4H), 4.10 (q, *J* = 2.4 Hz, 4H), 3.21 (t, *J* = 2.4 Hz, 2H). ^{13}C NMR (75 MHz, CD_2Cl_2) δ ppm 163.10, 153.60, 138.16, 112.91, 112.61, 81.00, 7.97, 29.34. HRMS-ESI: *m/z* = 417.0988 (calcd for $[M + H]^+$, 417.0975).

Synthesis of F4-azo-bis-DBCO

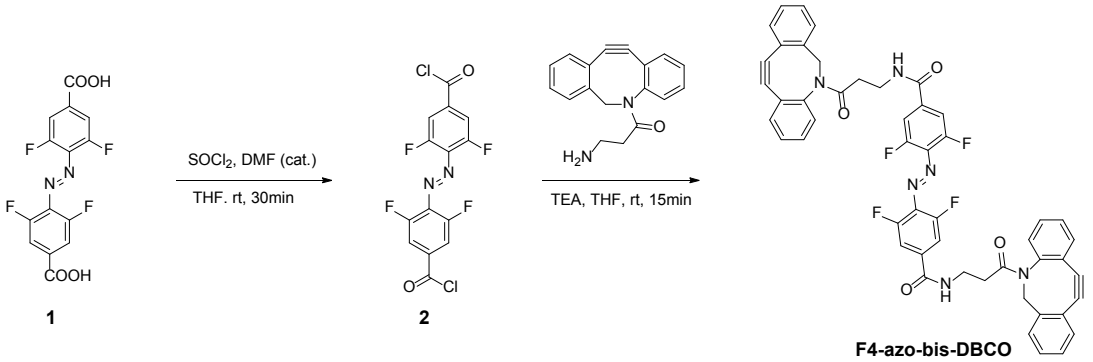

Scheme 4.5. Synthetic protocol for synthesizing **F4-azo-bis-DBCO**.

The procedure used for preparation of this compound is the same as that used for **alkyne-F4-azo**. When the reaction completed, the resulting mixture was concentrated under vacuum and purified by column chromatography (dichloromethane/methanol: 20/1) to yield **F4-azo-bis-DBCO** as a red solid. Yield, 71%. ^{1}H NMR (300 MHz, CD_2Cl_2) δ ppm 7.70 (d, *J* = 7.5 Hz, 2H), 7.43 - 7.19 (m, 16H), 6.87 (t, *J* = 5.4 Hz, 2H), 5.16 (d, *J* = 13.8 Hz, 2H), 3.72 (d, *J* = 13.8 Hz, 2H), 3.54 - 3.38 (m, 4H), 2.59 - 2.50 (m, 2H), 2.16 - 2.07 (m, 2H), 1.64 (br s, 2H). ^{13}C NMR (75 MHz, CD_2Cl_2) δ ppm 172.31, 151.49, 148.58, 132.66, 129.50, 129.05, 128.81, 128.42, 128.25, 127.59, 125.91, 123.26, 122.85, 114.96, 111.94, 111.64, 110.39, 108.16, 55.88, 36.52, 34.73. HRMS-ESI: *m/z* = 859.2698 (calcd for $[M + H]^+$, 859.2656).

CuAAC Hydrogel formation

In a discotic mold (height: 1 mm, diameter: 2 cm) **tetra-N_3-PEG** (12.5 mg, 0.00125 mmol) was dissolved in degassed dry DMF (0.125 ml), to the solution was added CuBr (1.8 mg, 0.0125 mmol) followed by the addition of **alkyne-F4-azo** (1.0 mg, 0.0025 mmol). The resulting mixture was stirred intensively for 5 minutes at room temperature. In order to get a flat uniform sample, the stirring bar was taken out before adding the ligand. Afterwards, PMDETA (2.2 mg, 0.0125 mmol) was carefully added to the mixture and gelation occurred within 10 seconds. The sample was kept as such overnight at room temperature to afford maximal conversion. The hydrogel was removed gently from the mold and washed intensively with saturated ethylene-diamine-tetraacetic acid (EDTA) solution, water, and finally a red transparent gel was obtained. The gels were immersed in distilled water for at least 3 days before performing further experiments.

SPAAC hydrogel formation:

In a discotic mold (height: 1 mm, diameter: 2 cm) **F4-azo-bis-DBCO** (2.1 mg, 2.5 x 10^{-3} mmol) was added to a solution of **tetra-N_3-PEG** (12.5 mg, 1.25 x 10^{-3} mmol) in dry DMF (0.125 ml). The resulting mixture was stirred carefully at room temperature for ca. 3 minutes, after which the solution became viscous. At this stage, in order to get a flat uniform sample, the stirring bar was taken out before complete gelation. The gel was kept as such at room temperature for another 1 h, then distilled water was added to cover the gel and the sample was heated at 45 °C for 4 h to afford maximal conversion. After cooling down, solvent-exchange with distilled water was done at room temperature for 3 days to obtain a fully swollen hydrogel.

UV/vis spectroscopy

UV/vis absorption spectra were recorded using the same spectrophotometer (Cary 50) as described in chapter 3. The solvents used were of spectrophotometric grade. Two light-emitting diodes (LEDs, THORLABS, USA) equipped with an adjustable collimation adapter with AR-Coated lens (ACP2520-A, for 350-700 nm, THORLABS) were used for irradiation experiments: M530L3, 530 nm, 350 mW (minimum value) and M405L2, 405 nm,

410 mW (minimum value). Moreover, to extract a specific wavelength, a band-pass filter (> 500 nm) was placed on the 530 nm-LED lamp, and the distance between the sample and the lamp was around 10 cm.

Rheology

Dynamic viscoelasticities of hydrogels were measured in situ on an Anton Paar MCR301 rheometer. The experimental set-up is shown in figure 4.9. A disposable parallel-plate geometry (25 mm) with a light guide accessory was used for the operation. A constant deformation of 1% shear strain at a frequency of 10 Hz was applied for all experiments, and the environment was maintained at 25 °C using a Peltier temperature control stage. The starting normal force applied for all measurements was between 0.1 and 0.2 N. Two LED lamps (530 nm with > 500 nm band-pass filter and 405 nm) were manually and alternatively switched at the desired time points while measuring the modulus of the gel, and the distance between the sample and the lamps was around 10 cm. All the experiments were performed with the gel surrounded with water to maintain their maximum swollen state and to avoid drying at the gel-air interface.

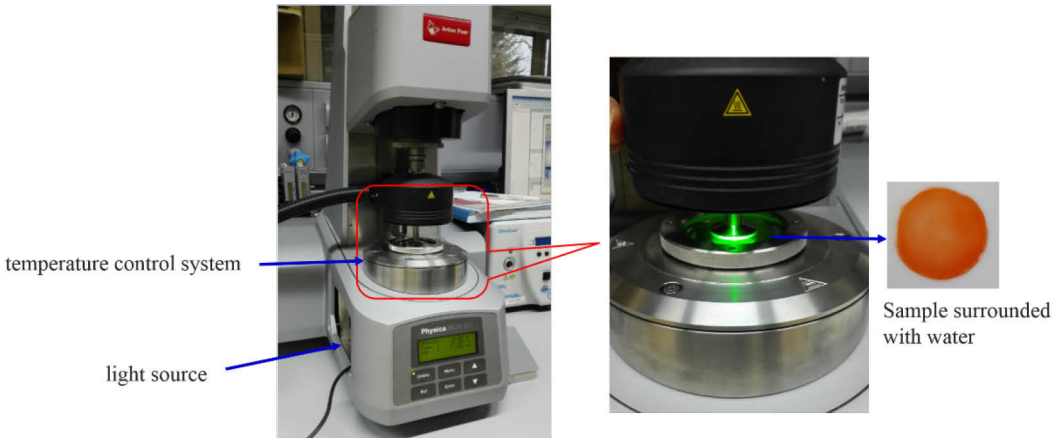

Fig. 4.9 Set-up for the rheology measurements.

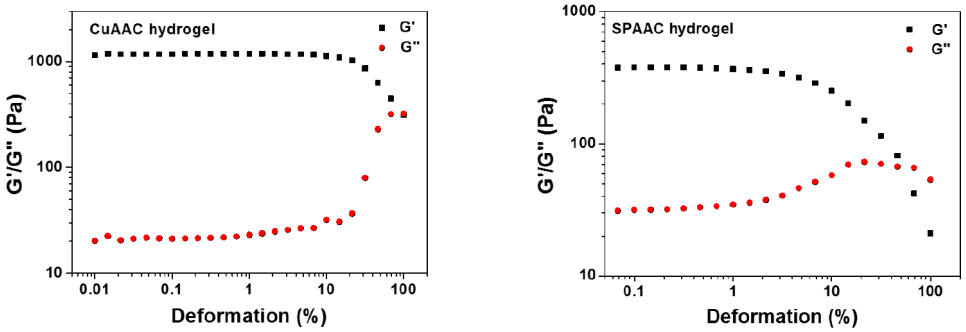

Fig. 4.10 Amplitude sweep of CuAAC hydrogel and SPAAC hydrogel (T = 25 °C).

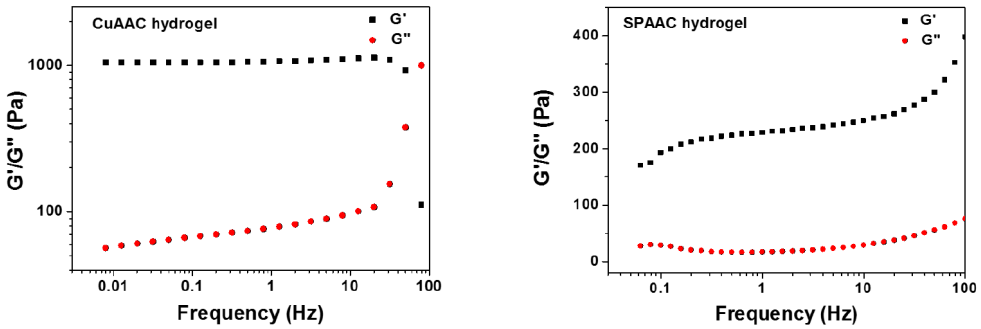

Fig. 4.11 Frequency sweep of CuAAC hydrogel and SPAAC hydrogel (T = 25 °C, shear strain = 1 %).

Fourier-transform infrared spectroscopy (FTIR) was carried out on a Bruker Vertex 70v equipped with a Specac Golden Gate single reflection diamond ATR sample holder. Scans (number of scans: 100) were collected with a resolution of 1 cm^{-1} from 4000 to 400 cm^{-1}. Baseline correction was performed using spline interpolation in OriginPro 9.1, OriginLab Corp., Northampton, USA.

UPLC was performed to determine the PSSs compositions for the azo solutions using the same conditions as described in the experimental part in chapter 3.

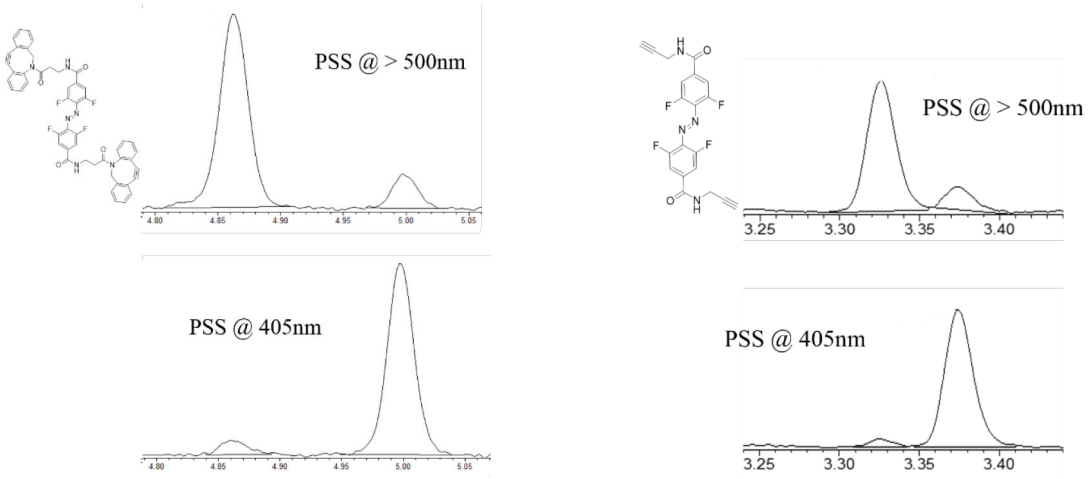

Fig. 4.10 UPLC traces (recorded at the corresponding isosbestic points) of **F4-azo-bis-DBCO** and **alkyne-F4-azo** PSS mixtures in acetonitrile.

Computational models

The calculations have been performed with the Gaussian 09 Rev. C01 suite of programs and used GaussView v.5.0.8 for the graphic representation of the results.[206] Geometry optimization of the target structures has been performed by means of Density Functional Theory (DFT); B3LYP functional,[207] 6-311+G(d,p) Pople basis set[208] have been used for all the calculations. The nature of the critical points was checked by vibrational analysis. Solvent effects (acetonitrile) have been introduced by the Polarizable Continuum Model (IEF-PCM).[209]

5. Conclusion

The ability to influence key properties of molecular systems by using light holds much promise for the fields of materials science and life sciences. In particular, synthetic photo-switchable systems that respond primarily to visible and near-infrared (NIR) light tremendously extend the scope of photo-sensitive systems for future applications and technologies. The benefits of visible light comprise its predominance in the portion of the solar spectrum reaching the surface of the earth, a large window of available wavelengths, its harmless character and often times good penetration depth. In this context, the thesis provided the utilization of *all-visible ortho*-tetrafluoroazobenzenes in two different contexts.

We have shown four-state mixed dimers consisting of classical azobenzenes and *ortho*-tetrafluoroazbenzenes, in which all the isomers can be orthogonally addressed with good to quantitative selectivity using three different wavelengths of light and electrons. Such azobenzene-based multi-photochromes with full addressability will allow to precisely control the isomerization of each unit on demand. Ester groups in *para* position enables them to be further functionalized and incorporated into more complex systems, in order to *e.g.* perform directional motions. The control of motion on the molecular scale is still one of the most fascinating challenges in nanoscience. Further work will aim to construct a molecular machine incorporating the dimer within a molecular ring (crown ether or cucurbiturils) to obtain rotaxanes able to perform directional linear motions. A system of this kind would act as an artificial molecular pump.

We have also successfully synthesized an *ortho*-tetrafluoroazbenzene-containing hydrogel network using strain-promoted “click” chemistry. Fluoroazobenzene was covalently attached into the hydrogel network allowing to control hydrogels’ mechanical properties by using visible light only. Upon alternating irradiation with green and blue light, hydrogels showed reversible changes of shear modulus, which could be repeated over many cycles without photo-degradation. The retained superior thermo-stability of *Z*-fluoroazobenzenes further brightens its utility as a photo-controllable biomaterial. Owing to the widespread application of hydrogels in tissue engineering, cell cultures and *in vitro*/*vivo* biological studies, we

believe the present system, due to its ease of synthesis and visible-light-tunable mechanics, will benefit the realization of practical light-responsive biomaterials.

References:

[1] R. G. Hafsa Ahmad, Sakshi Sehgal, Anurag Mishra, *Pharmacogn Rev* **2012**, *6*, 115–124.

[2] T. Traut, *Allosteric Regulatory Enzymes* **2008**, *Springer*.

[3] J. M. Requena, Stress Response in Microbiology **2012**, *Caister Acad. Press*.

[4] G. M. and A. Heckel, *Angew. Chem., Int. Ed.* **2006**, *45*, 4900.

[5] C. Brieke, F. Rohrbach, A. Gottschalk, G. Mayer, A. Heckel, *Angew. Chem., Int. Ed.* **2012**, *51*, 8446–8476.

[6] M. M. Russew, S. Hecht, *Adv. Mater.* **2010**, *22*, 3348–3360.

[7] M. Irie, *Chem. Rev.* **2000**, *100*, 1683–1890.

[8] H. B.-L. Heinz Dürr, Photochromism: Molecules and Systems **2003**, *Elsevier, Amsterdam*.

[9] W. R. B. and B. L. Feringa, Molecular Switches **2011**, *Wiley-VCH Verlag GmbH Co. KGaA*.

[10] S. K. and T. Y. M. Itoh, K. Harada, *Jpn. J. Appl. Phys.* **2004**, *43*, 4968–4971.

[11] P. Várhegyi, A. Kerekes, S. Sajti, F. Ujhelyi, P. Koppa, G. Szarvas, E. Lorincz, *Appl. Phys. B Lasers Opt.* **2003**, *76*, 397–402.

[12] X. L. Jiang, L. Li, J. Kumar, D. Y. Kim, S. K. Tripathy, *Appl. Phys. Lett.* **1998**, *72*, 2502–2504.

[13] F. Puntoriero, P. Ceroni, V. Balzani, G. Bergamini, F. Vögtle, *J. Am. Chem. Soc.* **2007**, *129*, 10714–10719.

[14] C. U. Bang, A. Shishido, T. Ikeda, *Macromol. Rapid Commun.* **2007**, *28*, 1040–1044.

[15] R. M. Parker, J. C. Gates, H. L. Rogers, P. G. R. Smith, M. C. Grossel, *J. Mater. Chem.* **2010**, *20*, 9118–25.

[16] M. Dong, A. Babalhavaeji, S. Samanta, A. A. Beharry, G. A. Woolley, *Acc. Chem. Res.* **2015**, *48*, 2662–2670.

[17] R. Siewertsen, H. Neumann, B. Buchheim-Stehn, R. Herges, C. Nä, F. Renth, F. Temps, *J. Am. Chem. Soc.* **2009**, *131*, 15594–15595.

[18] A. A. Beharry, O. Sadovski, G. A. Woolley, *J. Am. Chem. Soc.* **2011**, *133*, 19684–19687.

[19] S. Samanta, A. A. Beharry, O. Sadovski, T. M. Mccormick, A. Babalhavaeji, V. Tropepe, G. A. Woolley, *JACS* **2013**, *135*, 9777–9784.

[20] S. Samanta, T. M. Mccormick, S. K. Schmidt, D. S. Seferos, G. A. Woolley, *Chem. Commun.* **2013**, *49*, 10314–10316.

[21] S. Samanta, A. Babalhavaeji, M. X. Dong, G. A. Woolley, *Angew. Chem., Int. Ed.* **2013**, *52*, 14127–14130.

[22] D. Bléger, J. Schwarz, A. M. Brouwer, S. Hecht, *J. Am. Chem. Soc* **2012**, *134*, 20597–20600.

[23] C. Knie, M. Utecht, F. Zhao, H. Kulla, S. Kovalenko, A. M. Brouwer, P. Saalfrank, S. Hecht, D. Bléger, *Chem. - A Eur. J.* **2014**, *20*, 16492–16501.

[24] A. Goulet-Hanssens, M. Utecht, D. Mutruc, E. Titov, J. Schwarz, L. Grubert, D. Bleer, P. Saalfrank, S. Hecht, *J. Am. Chem. Soc.* **2017**, *139*, 335–341.

[25] J. Moreno, M. Gerecke, L. Grubert, S. A. Kovalenko, S. Hecht, *Angew. Chem., Int. Ed.* **2016**, *55*, 1544–1547.

[26] S. Castellanos, A. Goulet-Hanssens, F. Zhao, A. Dikhtiarenko, A. Pustovarenko, S. Hecht, J. Gascon, F. Kapteijn, D. Bléger, *Chem. - A Eur. J.* **2016**, *22*, 746–752.

[27] K. Kumar, C. Knie, D. Bléger, M. A. Peletier, H. Friedrich, S. Hecht, D. J. Broer, M. G. Debije, A. P. H. J. Schenning, *Nat. Commun.* **2016**, *7*, 11975.

[28] S. Iamsaard, E. Anger, S. J. Aßhoff, A. Depauw, S. P. Fletcher, N. Katsonis, *Angew. Chem., Int. Ed.* **2016**, *55*, 9908–9912.

[29] C. Hoppmann, I. Maslennikov, S. Choe, L. Wang, *J. Am. Chem. Soc.* **2015**, *137*, 11218–11221.

[30] J. B. Trads, J. Burgstaller, L. Laprell, D. B. Konrad, L. de la Osa de la Rosa, C. D. Weaver, H. Baier, D. Trauner, D. M. Barber, *Org. Biomol. Chem.* **2017**, 76–81.

[31] G. S. Hartley, *Nature* **1937**, *140*, 281–281.

[32] A. A. Beharry, G. A. Woolley, *Chem Soc Rev* **2011**, *40*, 4422–4437.

[33] B. G. C Hampson, J. Monteath Robertson, *J. Chem. Soc.* **1941**.

[34] E. Merino, M. Ribagorda, *Beilstein J. Org. Chem.* **2012**, *8*, 1071–1090.

[35] X. Liang, H. Asanuma, M. Komiyama, *J. Am. Chem. Soc.* **2002**, *124*, 1877–1883.

[36] O. Pieroni, A. Fissi, N. Angelini, F. Lenci, *Acc. Chem. Res.* **2001**, *34*, 9–17.

[37] S. Iamsaard, S. J. Aßhoff, B. Matt, T. Kudernac, J. J. L. M. Cornelissen, S. P. Fletcher, N. Katsonis, *Nat. Chem.* **2014**, *6*, 229–235.

[38] O. S. Bushuyev, A. Tomberg, T. Friščić, C. J. Barrett, *J. Am. Chem. Soc.* **2013**, *135*, 12556–12559.

[39] S. K. M. Nalluri, J. Voskuhl, J. B. Bultema, E. J. Boekema, B. J. Ravoo, *Angew. Chem., Int. Ed.* **2011**, *50*, 9747–9751.

[40] A. M. Smith, M. C. Mancini, S. Nie, *Nat. Nanotechnol.* **2009**, *4*, 710–711.

[41] J. García -Amorós, D. Velasco, *Beilstein J. Org. Chem.* **2012**, *8*, 1003–1017.

[42] S. Samanta, C. Qin, A. J. Lough, G. A. Woolley, *Angew. Chem., Int. Ed.* **2012**, *51*, 6452–6455.

[43] M. Hammerich, C. Schütt, C. Stähler, P. Lentes, F. Röhricht, R. Höppner, R. Herges, *J. Am. Chem. Soc* **2016**, *138*, 13111–13114.

[44] A. Rullo, A. Reiner, A. Reiter, D. Trauner, E. Y. Isacoff, G. A. Woolley, *Chem. Commun.* **2014**, *50*, 14613–14615.

[45] S. Samanta, T. M. McCormick, S. K. Schmidt, D. S. Seferos, G. A. Woolley, *Chem. Commun. (Camb).* **2013**, *49*, 10314–10316.

[46] M. Dong, A. Babalhavaeji, M. J. Hansen, L. Kálmán, G. A. Woolley, *Chem. Commun.* **2015**, *51*, 12981–12984.

[47] Á. Moneo, G. C. Justino, M. F. N. N. Carvalho, M. C. Oliveira, A. M. M. Antunes, D. Bléger, S. Hecht, J. P. Telo, *J. Phys. Chem. A* **2013**, *117*, 14056–14064.

[48] H. M. D. Bandara, S. C. Burdette, *Chem. Soc. Rev.* **2012**, *41*, 1809–1825.

[49] Y. Yang, R. P. Hughes, I. Aprahamian, *J. Am. Chem. Soc* **2012**, *134*, 15221–15224.

[50] Y. Yang, R. P. Hughes, I. Aprahamian, *J. Am. Chem. Soc.* **2014**, *136*, 13190–13193.

[51] D. Bléger, J. Dokić, M. V. Peters, L. Grubert, P. Saalfrank, S. Hecht, *J. Phys. Chem. B* **2011**, *115*, 9930–9940.

[52] X. Zhang, L. Hou, P. Samorì, *Nat. Commun.* **2016**, *7*, 11118.

[53] T. Leydecker, M. Herder, E. Pavlica, G. Bratina, S. Hecht, E. Orgiu, P. Samorì, *Nat. Nanotechnol.* **2016**, 769–776.

[54] M. Suda, R. Kato, H. M. Yamamoto, *Science* **2015**, *347*, 743–746.

[55] J. P. Stradins, V. T. Glezer, In Encyclopedia of Electrochemistry of the Elements, Volume XIII; A. J.Bard, H. Lund, Eds.; Dekker: New York, 1979; p 163.

[56] P. Neta, H. Levanon, H. Levanon, *J. Phys. Chem.* **1977**, *81*, 2288–2292.

[57] E. Laviron, Y. Mugnier, *J. Electroanal. Chem.* **1978**, *93*, 69–73.

[58] E. Laviron, Y. Mugnier, *J. Electroanal. Chem.* **1980**, *111*, 337–344.

[59] N. Klopman, G.; Doddapaneni, *J. Phys. Chem.* **1974**, *78*, 1825− 1828.

[60] Z. F. Liu, K. Hashimoto, A. Fujishima, *Nature* **1990**, *347*, 658–660.

[61] G. Grampp, C. Mureşanu, S. Landgraf, *J. Electroanal. Chem.* **2005**, *582*, 171–178.

[62] J. L. Sadler, A. J. Bard, *J. Am. Chem. Soc.* **1968**, *90*, 1979–1989.

[63] K. L. Shantha, P. Ravichandran, K. P. Rao, *Biomaterials* **1995**, *16*, 1313–1318.

[64] X. Liao, G. Chen, M. Jiang, *Polym. Chem.* **2013**, *4*, 1733–1745.

[65] S. Dong, B. Zheng, D. Xu, X. Yan, M. Zhang, F. Huang, *Adv. Mater.* **2012**, *24*, 3191–3195.

[66] M. Zhang, D. Xu, X. Yan, J. Chen, S. Dong, B. Zheng, F. Huang, *Angew. Chem., Int. Ed.* **2012**, *51*, 7011–7015.

[67] J. M. Urueña, A. A. Pitenis, R. M. Nixon, K. D. Schulze, T. E. Angelini, W. G. Sawyer, *Biotribology* **2015**, *1–2*, 24–29.

[68] I. R. and M. N. Gupta, *Chem. Biol.* **2003**, *10*, 1161–1171.

[69] J. Kopeček, *Biomaterials* **2007**, *28*, 5185–5192.

[70] S. Van Vlierberghe, P. Dubruel, E. Schacht, *Biomacromolecules* **2010**, *12*, 1387–1408.

[71] I. Tomatsu, K. Peng, A. Kros, *Adv. Drug Deliv. Rev.* **2011**, *63*, 1257–1266.

[72] A. M. Rosales, K. S. Anseth, *Nat. Rev. materals* **2016**, *1*, 1–16.

[73] D A. Ossipov, J. Hilborn, *Macromolecules* **2006**, *39*, 1709–1718.

[74] Y. Jiang, J. Chen, C. Deng, E. J. Suuronen, Z. Zhong, *Biomaterials* **2014**, *35*, 4969–4985.

[75] X. Zhang, S. Malhotra, M. Molina, R. Haag, *Chem. Soc. Rev.* **2015**, *44*, 1948–1973.

[76] A. Uliniuc, M. Popa, T. Hamaide, M. Dobromir, *Cellul. Chem. Technol.* **2012**, *46*, 1–11.

[77] D. D. Díaz, S. Punna, P. Holzer, A. K. Mcpherson, K. B. Sharpless, V. V. Fokin, M. G. Finn, *J. Polym. Sci. Part A Polym. Chem.* **2004**, *42*, 4392–4403.

[78] B. Parrish, R. B. Breitenkamp, T. Emrick, *J. Am. Chem. Soc.* **2005**, *127*, 7404–7410.

[79] W. H. Zhan, H. N. Barnhill, K. Sivakumar, H. Tian, Q. Wang, *Tetrahedron Lett.* **2005**, *46*, 1691–1695.

[80] P.-Y. Liu, N. Jiang, J. Zhang, X. Wei, H.-H. Lin, X.-Q. Yu, *Chem. Biodivers.* **2006**, *3*, 958–966.

[81] P. Natarajan, G. Ferraudi, *Inorg. Chem* **1981**, *20*, 3708–3712.

[82] V. O. Rodionov, V. V. Fokin, M. G. Finn, *Angew. Chem., Int. Ed.* **2005**, *44*, 2210–2215.

[83] F. Himo, T. Lovell, R. Hilgraf, V. V. Rostovtsev, L. Noodleman, K. B. Sharpless, V. V. Fokin, *J. Am. Chem. Soc.* **2005**, *127*, 210–216.

[84] B. F. Straub, *Chem. Commun. (Camb).* **2007**, 3868–3870.

[85] L. Jin, D. R. Tolentino, M. Melaimi, G. Bertrand, *Sci. Adv.* **2015**, *1*, 1–5.

[86] E. Lallana, R. Riguera, E. Fernandez-Megia, *Angew. Chem., Int. Ed.* **2011**, *50*, 8794–8804.

[87] W. Song, Y. Wang, J. Qu, M. M. Madden, Q. Lin, *Angew. Chem., Int. Ed.* **2008**, *47*, 2832–2835.

[88] Y. Wang, W. Song, W. J. Hu, Q. Lin, *Angew. Chemie - Int. Ed.* **2009**, *48*, 5330–5333.

[89] N. J. Agard, C. R. Bertozzi, *Acc. Chem. Res.* **2009**, *42*, 788–797.

[90] S. S. Van Berkel, A. J. Dirks, M. F. Debets, F. L. Van Delft, J. J. L. M. Cornelissen, R. J. M. Nolte, F. P. J. T. Rutjes, *ChemBioChem* **2007**, *8*, 1504–1508.

[91] M. Arseneault, I. Levesque, J. F. Morin, *Macromolecules* **2012**, *45*, 3687–3694.

[92] J. C. Jewett, C. R. Bertozzi, *Chem. Soc. Rev.* **2010**, *39*, 1272–1279.

[93] N. J. Agard, J. A. Prescher, C. R. Bertozzi, *J. Am. Chem. Soc.* **2004**, *126*, 15046–15047.

[94] N. J. Agard, J. M. Baskin, J. A. Prescher, A. Lo, C. R. Bertozzi, *ACS Chem. Biol.* **2006**, *1*, 644–648.

[95] J. M. Baskin, J. A. Prescher, S. T. Laughlin, N. J. Agard, P. V. Chang, I. A. Miller, A. Lo, J. A. Codelli, C. R. Bertozzi, *Proc. Natl. Acad. Sci. U. S. A.* **2007**, *104*, 16793–16797.

[96] X. Ning, J. Guo, M. A. Wolfert, G. J. Boons, *Angew. Chem., Int. Ed.* **2008**, *47*, 2253–2255.

[97] N. E. Mbua, J. Guo, M. A. Wolfert, R. Steet, G. J. Boons, *ChemBioChem* **2011**, *12*, 1912–1921.

[98] M. F. Debets, S. S. van Berkel, S. Schoffelen, F. P. J. T. Rutjes, J. C. M. van Hest, F. L. van Delft, *Chem. Commun. (Camb).* **2010**, *46*, 97–99.

[99] J. C. Jewett, E. M. Sletten, C. R. Bertozzi, *J. Am. Chem. Soc.* **2010**, *132*, 3688–3690.

[100] C. G. Gordon, J. L. MacKey, J. C. Jewett, E. M. Sletten, K. N. Houk, C. R. Bertozzi, *J. Am. Chem. Soc.* **2012**, *134*, 9199–9208.

[101] D. Zeng, N. S. Lee, Y. Liu, D. Zhou, C. S. Dence, K. L. Wooley, J. A. Katzenellenbogen, M. J. Welch, *ACS Nano* **2012**, *6*, 5209–5219.

[102] C.-X. Song, K. E. Szulwach, Y. Fu, Q. Dai, C. Yi, X. Li, Y. Li, C.-H. Chen, W. Zhang, X. Jian, et al., *Nat. Biotechnol.* **2011**, *29*, 68–72.

[103] A. A. Poloukhtine, N. E. Mbua, M. A. Wolfert, G. J. Boons, V. V. Popik, *J. Am. Chem. Soc.* **2009**, *131*, 15769–15776.

[104] M. Shelbourne, X. Chen, T. Brown, A. H. El-Sagheer, *Chem. Commun. (Camb).* **2011**, *47*, 6257–6259.

[105] R. Manova, T. A. Vanbeek, H. Zuilhof, *Angew. Chem., Int. Ed.* **2011**, *50*, 5428–5430.

[106] J. Dommerholt, S. Schmidt, R. Temming, L. J. A. Hendriks, F. P. J. T. Rutjes, J. C. M. Van Hest, D. J. Lefeber, P. Friedl, F. L. Van Delft, *Angew. Chem., Int. Ed.* **2010**, *49*, 9422–9425.

[107] C. A. DeForest, B. D. Polizzotti, K. S. Anseth, *Nat Mater* **2009**, *8*, 659–664.

[108] O. Wichterle, D. Lím, *Nature* **1960**, *185*, 117–118.

[109] T. R. Hoare, D. S. Kohane, *Polymer (Guildf).* **2008**, *49*, 1993–2007.

[110] Biancamaria Baroli, *J. Pharm. Sci.* **2007**, *96*, 2197–2223.

[111] A. S. Hoffman, *J. Control. Release* **1987**, *6*, 297–305.

[112] M. A. Cole, N. H. Voelcker, H. Thissen, H. J. Griesser, *Biomaterials* **2009**, *30*, 1827–1850.

[113] J. Zhang, N. A. Peppas, *Macromolecules* **2000**, *33*, 102–107.

[114] A. M. Lowman, M. Morishita, M. Kajita, T. Nagai, N. A. Peppas, *J. Pharm. Sci.* **1999**, *88*, 933–937.

[115] W. S. Yeo, M. N. Yousaf, M. Mrksich, *J. Am. Chem. Soc.* **2003**, *125*, 14994–14995.

[116] M. Zrinyi, *Colloid Polym. Sci.* **2000**, *278*, 98–103.

[117] A. M. Kloxin, C. J. Kloxin, C. N. Bowman, K. S. Anseth, *Adv. Mater.* **2010**, *22*, 3484–3494.

[118] D. Y. Wong, D. R. Griffin, J. Reed, A. M. Kasko, *Macromolecules* **2010**, *43*, 2824–2831.

[119] D. R. Griffin, A. M. Kasko, *J. Am. Chem. Soc.* **2012**, *134*, 13103–13107.

[120] A. Deiters, *ChemBioChem* **2010**, *11*, 47–53.

[121] C. P. Holmes, *J. Org. Chem.* **1997**, *62*, 2370–2380.

[122] Y. Luo, M. S. Shoichet, *Nat. Mater.* **2004**, *3*, 249–53.

[123] Y. Ohmuro-Matsuyama, Y. Tatsu, *Angew. Chem., Int. Ed.* **2008**, *47*, 7527–7529.

[124] A. M. Kloxin, A. M. Kasko, C. N. Salinas, K. S. Anseth, *Science* **2009**, *324*, 59–63.

[125] Y. Jiang, P. Wan, H. Xu, Z. Wang, X. Zhang, M. Smet, *Langmuir* **2009**, *25*, 10134–10138.

[126] M. Bradley, B. Vincent, N. Warren, J. Eastoe, A. Vesperinas, *Langmuir* **2006**, *22*, 101–105.

[127] J. Jiang, X. Tong, Y. Zhao, *J. Am. Chem. Soc.* **2005**, *127*, 8290–8291.

[128] M. Nagata, Y. Yamamoto, *React. ad Funct. Polym.* **2008**, *68*, 915–921.

[129] S. H. Kim, Y. Sun, J. A. Kaplan, M. W. Grinstaff, J. R. Parquette, *New J. Chem.* **2015**, *39*, 3225–3228.

[130] M. A. Azagarsamy, D. D. Mckinnon, D. L. Alge, K. S. Anseth, *Macroletters* **2014**, *3*, 515–519.

[131] Y. Sako, Y. Takaguchi, *Org. Biomol. Chem* **2008**, *6*, 3843–3847.

[132] K. Tanaka, *Molecules* **2012**, *17*, 1408–1418.

[133] Y. Chujo, K. Sada, *Macromoleculs* **1990**, *23*, 2693–2697.

[134] E. R. Draper, T. O. Mcdonald, D. J. Adams, *Chem. Commun.* **2015**, *51*, 12827–12830.

[135] F. M. Andreopoulos, E. J. Beckman, A. J. Russell, *J. Polym. Sci. Part A Polym. Chem.* **2000**, *38*, 1466–1476.

[136] Y. Zheng, M. Micic, S. V. Mello, M. Mabrouki, F. M. Andreopoulos, V. Konka, S. M. Pham, R. M. Leblanc, *Macromolecules* **2002**, *35*, 5228–5234.

[137] B. Y. Zheng, F. M. Andreopoulos, M. Micic, Q. Huo, S. M. Pham, R. M. Leblanc, *Adv. Funct. Mater.* **2001**, *11*, 37–40.

[138] F. M. Andreopoulos, I. Persaud, *Biomaterials* **2006**, *27*, 2468–2476.

[139] D. Shi, M. Matsusaki, M. Akashi, *Bioconjug. Chem.* **2009**, *20*, 1917–1923.

[140] O. Pieroni, A. Fissi, A. Viegi, D. Fabbri, F. Ciardelli, *J. Am. Chem. Soc* **1992**, *114*, 2734–2736.

[141] C. Konak, R. Rathi, P. Kopeckova, J. Kopecek, *Macromolecules* **1997**, *30*, 5553–5556.

[142] S. Z. Qiu, H. Yu, J. Li, Y. Wang, Y. Zhang, Z. Qiu, *Chem. Commun.* **2009**, 3342–3344.

[143] R. Klajn, *Chem. Soc. Rev.* **2014**, *43*, 148–184.

[144] G. Berkovic, V. Krongauz, V. Weiss, *Chem. Rev.* **2000**, *100*, 1741–1754.

[145] N. Tamai, H. Miyasaka, *Chem. Rev.* **2000**, *100*, 1875–1890.

[146] B.-H. Tan, M. Yoshio, T. Ichikawa, T. Mukai, H. Ohno, T. Kato, *Chem. Commun.* **2006**, 4703–4705.

[147] J. Ter Schiphorst, S. Coleman, J. E. Stumpel, A. Ben Azouz, D. Diamond, A. P. H. J. Schenning, *Chem. Mater.* **2015**, *27*, 5925–5931.

[148] K. Ishihara, N. Hamada, S. Kato, I. Shinohara, *J. Polym. Sci. Polym. Chem. Ed.* **1984**, *22*, 121–128.

[149] M. Moniruzzaman, G. F. Fernando, J. D. R. Talbot, *J. Polym. Sci. Part A Polym. Chem.* **2004**, *42*, 2886–2896.

[150] K. Iwaso, Y. Takashima, A. Harada, *Nat. Chem.* **2016**, *8*, 625–632.

[151] Y. Takashima, S. Hatanaka, M. Otsubo, M. Nakahata, T. Kakuta, A. Hashidzume, H. Yamaguchi, A. Harada, *Nat. Commun.* **2012**, *3*, 2280.

[152] Y.-L. Zhao, J. F. Stoddart, *Langmuir* **2009**, *25*, 8442–8446.

[153] K. Peng, I. Tomatsu, A. Kros, *Chem. Commun.* **2010**, *46*, 4094–4096.

[154] R. Yang, S. Peng, W. Wan, T. C. Hughes, *J. Mater. Chem. C* **2014**, *2*, 9122–9131.

[155] Y. Huang, Z. Qiu, Y. Xu, J. Shi, H. Lin, Y. Zhang, *Org. Biomol. Chem* **2011**, *9*, 2149–2155.

[156] W. A. Velema, M. C. A. Stuart, W. Szymanski, B. L. Feringa, *Chem. Commun.* **2013**, *49*, 5001–5003.

[157] Y. Ogawa, C. Yoshiyama, T. Kitaoka, *Langmuir* **2012**, *28*, 4404–4412.

[158] S. Peng, Q. Guo, T. C. Hughes, P. G. Hartley, *Langmuir* **2013**, *30*, 866–872.

[159] A. M. Rosales, K. M. Mabry, E. M. Nehls, K. S. Anseth, *Biomacromolecules* **2015**, *16*, 798–806.

[160] H. Meier, *Angew. Chem., Int. Ed. Engl.* **1992**, *31*, 1399–1420.

[161] S. Matsumoto, S. Yamaguchi, S. Ueno, H. Komatsu, M. Ikeda, K. Ishizuka, Y. Iko, K. V. Tabata, H. Aoki, S. Ito, et al., *Chem. - A Eur. J.* **2008**, *14*, 3977–3986.

[162] C. B. McArdle, Applied Photochromic Polymer Systems **1992**, *Springer*.

[163] A. Prestel, H. M. Möller, *Chem. Commun.* **2015**, *52*, 701–704.

[164] T. Fukaminato, T. Doi, N. Tamaoki, K. Okuno, Y. Ishibashi, H. Miyasaka, M. Irie, *J. Am. Chem. Soc* **2011**, *133*, 4984–4990.

[165] T. K. Masahiro Irie, Tuyoshi Fukaminato, Takatoshi Sasaki, Naoto Tamai, *Nature* **2002**, *420*, 759–760.

[166] S. Erbas-Cakmak, D. A. Leigh, C. T. McTernan, A. L. Nussbaumer, *Chem. Rev.* **2015**, *115*, 10081–10206.

[167] A. Coskun, M. Banaszak, R. D. Astumian, J. F. Stoddart, B. a. Grzybowski, *Chem. Soc. Rev.* **2012**, *41*, 19–30.

[168] A. J. Myles, T. J. Wigglesworth, N. R. Branda, *Adv. Mater.* **2003**, *15*, 745–748.

[169] K. Higashiguchi, K. Matsuda, N. Tanifuji, M. Irie, *J. Am. Chem. Soc.* **2005**, *127*, 8922–8923.

[170] A. Kanaya, Y. Takashima, A. Harada, *J. Org. Chem.* **2011**, *76*, 492–499.

[171] K. Fukushima, A. J. Vandenbos, T. Fujiwara, *Chem. Mater.* **2007**, *19*, 644–646.

[172] S. Kumar, D. L. Watkins, T. Fujiwara, *Chem. Commun. (Camb).* **2009**, *1*, 4369–4371.

[173] R. H. Mitchell, T. R. Ward, Y. Wang, P. W. Dibble, *J. Am. Chem. Soc* **1999**, *121*, 2601–2602.

[174] R. H. Mitchell, S. Bandyopadhyay, *Org. Lett.* **2004**, *6*, 1729–1732.

[175] C. Tie, J. C. Gallucci, J. R. Parquette, *J. Am. Chem. Soc.* **2006**, *128*, 1162–1171.

[176] A. Natansohn, P. Rochon, *Chem. Rev.* **2002**, *102*, 4139–4175.

[177] Y. Yu, M. Nakano, T. Ikeda, *Nature* **2003**, *425*, 145–145.

[178] C. L. van Oosten, C. W. M. Bastiaansen, D. J. Broer, *Nat. Mater.* **2009**, *8*, 677–682.

[179] A. Fihey, A. Perrier, W. R. Browne, D. Jacquemin, *Chem. Soc. Rev.* **2015**, *44*, 3719–3759.

[180] F. Cisnetti, R. Ballardini, A. Credi, M. T. Gandolfi, S. Masiero, F. Negri, S. Pieraccini, G. P. Spada, *Chem. - A Eur. J.* **2004**, *10*, 2011–2021.

[181] K. N. and M. I. K. Uchida, G. Masuda, Y. Aoi, *Chem. Lett.* **1999**, 1071–1072.

[182] A. Peters and N. R. Branda, *Adv. Mater. Opt. Electron.* **2000**, *10*, 245–249.

[183] S. Kobatake, S. Kuma, M. Irie, *J. Phys. Org. Chem.* **2007**, *20*, 960–967.

[184] M. M. Lerch, M. J. Hansen, W. a Velema, W. Szymanski, B. L. Feringa, *Nat. Commun.* **2016**, *7*, 12054.

[185] Y. Norikane, N. Tamaoki, *European J. Org. Chem.* **2006**, 1296–1302.

[186] J. Robertus, S. F. Reker, T. C. Pijper, A. Deuzeman, W. R. Browne, B. L. Feringa, *Phys. Chem. Chem. Phys.* **2012**, *14*, 4374–4382.

[187] D. B. Konrad, J. A. Frank, D. Trauner, *Chem. - A Eur. J.* **2016**, *22*, 4364–4368.

[188] D. Bléger, Z. Yu, S. Hecht, *Chem. Commun.* **2011**, *47*, 12260–12266.

[189] P. K. Kundu, R. Klajn, *ACS Nano* **2014**, *8*, 11913–11916.

[190] C. Li, J. H. Yun, H. Kim, M. Cho, *Macromolecules* **2016**, *49*, 6012–6020.

[191] D. Seliktar, *Science* **2012**, *336*, 1124–1129.

[192] M. Zhong, R. Wang, K. Kawamoto, B. D. Olsen, J. A. Johnson, *Science* **2016**, *353*, 1264–1268.

[193] A. J. Engler, S. Sen, H. L. Sweeney, D. E. Discher, *Cell* **2006**, *126*, 677–689.

[194] S. Chaterji, I. K. Kwon, K. Park, *Prog. Polym. Sci.* **2007**, *32*, 1083–1122.

[195] W. A. Petka, *Science* **1998**, *281*, 389–392.

[196] Y. H. Bae, T. Okano, S. W. Kim, *J. Polym. Sci. Part B Polym. Phys.* **1990**, *28*, 923–936.

[197] K. Sumaru, M. Kameda, T. Kanamori, T. Shinbo, *Macromolecules* **2004**, *37*, 4949–4955.

[198] M. Irie, D. Kunwatchakun, *Macromolecules* **1986**, *2480*, 2476–2480.

[199] T. Ikeda, M. Nakano, Y. Yu, O. Tsutsumi, A. Kanazawa, *Adv. Mater.* **2003**, *15*, 201–204.

[200] N. Hosono, M. Yoshikawa, H. Furukawa, K. Totani, K. Yamada, T. Watanabe, K. Horie, *Macromolecules* **2013**, *46*, 1017–1026.

[201] Q. Li, G. Fuks, E. Moulin, M. Maaloum, M. Rawiso, I. Kulic, J. T. Foy, N. Giuseppone, *Nat. Nanotechnol.* **2015**, *10*, 161–165.

[202] J. T. Foy, Q. Li, A. Goujon, J.-R. Colard-Itté, G. Fuks, E. Moulin, O. Schiffmann, D. Dattler, D. P. Funeriu, N. Giuseppone, *Nat. Nanotechnol.* **2017**, *12*, 540–545.

[203] S. M. Hodgson, E. Bakaic, S. A. Stewart, T. Hoare, A. Adronov, *Biomacromolecules* **2016**, *17*, 1093–1100.

[204] A. M. Kloxin, A. M. Kasko, C. N. Salinas, K. S. Anseth, *Science* **2009**, *324*, 59–63.

[205] B. D. Polizzotti, B. D. Fairbanks, K. S. Anseth, *Biomacromolecules* **2008**, *9*, 1084–1087.

[206] M. J. Frisch, G. W. Trucks, H. B. Schlegel, G. E. Scuseria, M. A. Robb *et al.* Gaussian,Inc., Wallingford, CT, USA, **2009**.

[207] a) A. D. Becke, *The Journal of Chemical Physics* **1993**, *98*, 5648-5652.;
b) P. J. Stephens, F. J. Devlin, C. F. Chabalowski, M. J. Frisch, *The Journal of Physical Chemistry* **1994**, *98*, 11623-11627.

[208] R. Ditchfield, W. J. Hehre, J. A. Pople, *The Journal of Chemical Physics* **1971**, *54*, 724-728.

[209] J. Tomasi, B. Mennucci, R. Cammi, *Chem. Rev.* **2005**, *105*, 2999-3094.

Curriculum Vitae

Name: Fangli Zhao

Date and place of birth: 16-12-1985 in Henan, China

Education

Since Dec. 2013 Ph.D. candidate at Humboldt Universität zu Berlin, Germany.
Advisor: Dr. David Bléger and Professor Dr. Stefan Hecht
Thesis: Optical Control of "*All Visible*" Fluoroazobenzene-Containing Architectures: From Small Molecules to 3D Networks

Sep. 2008–Jun. 2011 M.S. (Honors), Pharmaceutical College of Henan University, China.
Advisor: Professor Zhiyong Jiang
Thesis: Highly Enantioselective Sulfa-Michael Addition (SMA) of 1,4-Dicarbonyl but-2-enes

Sep. 2003–Jun. 2007 B.S., Pharmaceutical College of Henan University, China.

Work Experience

Feb. 2012–Sep. 2013 Chemist, Pharmaron Ltd (Beijing China)
Synthesis and characterization of medicine intermediates

Nov. 2010- Nov. 2011 Research assistant, Singapore Polytechnic
Design and synthesis of small molecular organic photovoltaic (OPV) materials

....

Date Fangli Zhao

Publications

[1] **F. Zhao**, L. Grubert, S. Hecht, D. Bléger*: "Orthogonal switching in four-state azobenzene mixed-dimers" *Chem. Commun.* **2017**, *53*, 3323-3326.

[2] S. Castellanos,* A. Goulet-Hanssens, **F. Zhao**, A. Dikhtiarenko, A. Pustovarenko, S. Hecht, J. Gascon, F. Kapteijn, D. Bléger*: "Structural Effects in Visible-Light-Responsive Metal-Organic Frameworks Incorporating *ortho*-Fluoroazobenzenes" *Chem. Eur. J.* **2016**, *22*, 746-752.

[3] C. Knie, M. Utecht, **F. Zhao**, H. Kulla, S. Kovalenko, A. M. Brouwer,* P. Saalfrank,* S. Hecht,* D. Bléger*: "*ortho*-Fluoroazobenzenes: Visible-light switches with very long-lived *Z* isomers" *Chem. Eur. J.* **2014**, *20*, 16492-16501.

[4] S. Lam, X. Liu, **F. Zhao**, W. Kwan* *et al.*: "Manipulating open-circuit voltage in an organic photovoltaic device *via* a phenylalkyl side chain" *Chem. Commun.* **2013**, *49*, 4543-4545.

[5] Y. Lu, R. Peh, **F. Zhao**, W. Kwan* *et al.*: "Vacuum-free processed transparent inverted organic solar cell with spray-coated PEDOT : PSS anode" *Solar Energy Material and Solar Cells* **2011***, 95*, 3579-3584.

[6] **F. Zhao**, Z. Jiang* *et al.*: "Highly Enantioselective Sulfur-Michael Addition (SMA) of 1,4-Dicarbonyl but-2-enes" *Adv. Synth. Catal.* **2011**, *353*, 2624 - 2630.

....

Date Fangli Zhao

I declare that I have completed the thesis independently using only the aids and tools specified. I have not applied for a doctor's degree in the doctoral subject elsewhere and do not hold a corresponding doctor's degree. I have taken due note of the Faculty of Mathematics and Natural Sciences PhD Regulations, published in the Official Gazette of Humboldt-Universität zu Berlin no. 126/2014 on 18/11/2014.

....

Date Fangli Zhao